

CHES Lab Bulletin

2018
Vol.1 No.1

To cite the contents:

Mochamad Riam Badriana (2018). Surface wind validation for wave climate modelling in the Western North Pacific, *CHES Lab Bulletin*, 1(1), 6-13.

CHES Lab

Coastal Hazards and Energy System Science Lab
Graduate School for International Development and Cooperation (IDEC)
Hiroshima University
Copyright © CHES Lab, IDEC, Hiroshima University

Contents

1. CHESS Lab Members.....	3
2. Surface wind validation for wave climate modelling in the Western North Pacific.....	7
3. Evaluation of optimal location of wastewater treatment plant in Ger areas of Ulaanbaatar city using multi-criteria decision making (MCDM) analysis.....	14
4. Climate Change Impact on Species Distribution of <i>Styrax sumatrana</i> in North Sumatra using Maximum Entropy Modeling Approach.....	26
5. Quantitative Assessment of Climate Change Impacts on Flood-Prone Areas in Davao Oriental, Philippines.....	42
6. ArcSWAT Modeling: Study on Sustainable Management for Water and Energy Environment in Mindanao.....	65
7. Method for calculating snow losses on solar photovoltaic system production in Yamagata prefecture, Japan.....	72
8. Semester research activity summary.....	76
9. An Investigational Approach to the 1993 Tsunami Run-up Model on the Built-in Monai Beach used in GERRIS.....	77

CHES Lab members

Staff (教員)

	Status	Associate Professor
	Home country	Korea (South)
	Research interests	Coastal hazards and mitigation strategy, Sustainable energy strategy in developing countries

Doctoral course (博士課程後期)

None

Master course (博士課程前期)

	Name	Jonathan CABRERA (M2)
	Home country	Philippines
	Research Topic	A multi-criteria approach for flood risk and coastal erosion mapping: A case study of Davao region in Philippines
	Name	Chantheaphar KHATTIYAVONG (M2)
	Home country	Laos

	Research Topic	Assessment and improvement of sanitation and wastewater treatment in densely-populated residential area in Vientiane
	Name	Ariuntuya BYAMBADORJ (M2)
	Home country	Mongolia
	Research Topic	Study on sustainable methodology for safe water supply and waste water treatment in mainline-disconnected Ger areas of Ulaanbaatar City
	Name	Muhammad Hadi Saputra (M2)
	Home country	Indonesia
	Research Topic	Climate change impacts on the suitability of tree species in Lake Toba catchment area (LTCA), Indonesia
	Name	Guiamel Ismail Adal (M1)
	Home country	Philippines
	Research Topic	Access to Quality Waters and Energy in Mindanao, Philippines
	Name	Md Morshed Bin Shiraj (M1)
	Home country	Bangladesh
	Research Topic	Storm surge and flood modeling with adaptive mesh refinement (AMR) in coastal zones and built-in environment

	Name	Alex Bunodiére (M1)
	Home country	South Africa
	Research Topic	Offshore wind power in Japan
	Name	Mochamad Riam Badriana (M1)
	Home country	Indonesia
	Research Topic	Multi-model ensemble projection of future wave climate in the western North Pacific using CMIP5 dataset

Undergraduate course (学部)

	Name	Kotaro NAKATSUKA (B4)
	Home country	Japan
	Research Topic	CMIP5 データ解析による日本における風力エネルギー資源の将来予測
	Name	Yukiya KOJIMA (B4)
	Home country	Japan
	Research Topic	波浪中を低速航行する船舶に働く流体力と運動に関する研究

Visiting Students (University of Graz)

	Name	Thomas Hocking (M1)
	Home country	Sweden
	Research Topic	TBD
	Name	Nicholas Denegre (M1)
	Home country	USA
	Research Topic	Photovoltaic systems

Surface wind validation for wave climate modelling in the Western North Pacific

Mochamad Riam Badriana¹

¹Graduate School for International Development and Cooperation, Hiroshima University, 1-5-1 Kagamiyama, Higashi-Hiroshima 739-8592, Hiroshima, Japan

Abstract

Validation is necessary to be sure of wind data utilization for model and analysis. CMIP5 consist ensembles data which beneficial for predicting future wave climate and ocean-atmospheric phenomenon. Wind data is processed using simple statistical approach to observe the uncertainty of ensemble and wind distribution. Seasonal wind distribution is contrast due to obstacle, coarse grid, and ensemble setting. Ensemble data near Wakkanai and Hachijojima have a good correlation with 55-70% correlation using moving average method. Standard deviation range is between 1-1.6 m. Wind measurement need to be corrected by factor 1.45 due to its underestimate value than ensemble data.

Keywords: wind surface, CMIP5, ensemble data

1. Introduction

Future changes in surface wind have implication for ocean-atmosphere phenomenon, particularly wind waves, storm surges and typhoons. The increasing trend of emission and sea-level rise is evidence for a possibility of different wind behavior in the following decades. CMIP5 provides several scenarios for historical and future condition adopted by IPCC Assessment Report (AR5).

CMIP5 data have more comprehensive and better documentation other than previous phases. Through gateways to modeling and data centers worldwide, the dataset could be archived freely (Taylor et al., 2012). Many researchers dealing CMIP5 data for ocean-atmospheric modeling. Shimura et al. (2013) used CMIP5 to predict wave climate pattern and compare with teleconnection pattern index, Hemer et al. (2013) calculated wave parameter in summer and winter use multi-model ensemble, Bennet et al. (2016) observed future wave climate in UK sea, and Shimura et al (2016) found the future decreases in wave heights correspond to positive changes in the WP pattern using CMIP5 scenario.

The reliability of ocean-atmospheric modeling depends on the quality of wind data itself. Since wind is the source which generates wind waves, the improper wind data will produce low quality of output model. Furthermore, it will lead to incorrect analysis and comprehension in using provided CMIP5 data. A good agreement in validation is necessary to convince the utility of ensemble data, otherwise it will be just random model with more uncertainty.

2. Objectives

CMIP5 data consist many kind data that can be useful for environmental modeling and analysis. However due to uncertainty of many ensemble models provided, validation is necessary. There is increasing study in term of wind wave. Some study done by Hemer et al. (2013) and Bennet et al. (2016) which correlated significant wave height between ensembles and satellite data or observation measurement. Those study applied wind from coupled general circulation model (GCMs) to ocean model to obtain the wave height. In other words, the quality of produced wind wave depends on wind input. Consequently, each ensemble wind needs to be observed further.

This study seeks the uncertainty of each ensemble through surface wind validation for each ensemble. To narrow the vast possibility of future condition, the uncertainty must be avoided as many as possible. Thereupon, it is important to verified first the past ensemble data then future dataset can be implemented. Therefore, we derive historical data of wind surface which is obtained between 1979 and 2008. This study stands as preliminary study before using CMIP5 wind surface data for wind wave, cyclone, and another atmospheric-ocean event. Ensemble data will be observed using simple statistical approach and be compared with observation data.

3. Data and methodology

3.1 Data

The National Climatic Data Center (NCDC) developed integrated global database of hourly land surface climatological data. Approximately 20,000 stations has data from early 1900 to the latest data can be used by varied applications (Lott, 2004). Numerous stations appear in Western Northern Pacific, however in this study only the

station located near the coast or open sea is chosen among other. The reason of avoiding some obstacle / building is reasonable since the ensemble model is coarse in term of topography. Three station ID of 450070, 474010, 476780 is Hongkong Airport, Wakkanai, and Hachijojima, respectively. NCDC provided 3-hourly data in general and the time space become finer nowadays (1-hourly in several point). However, data absence cannot be avoided and most data are missing in early 1980.

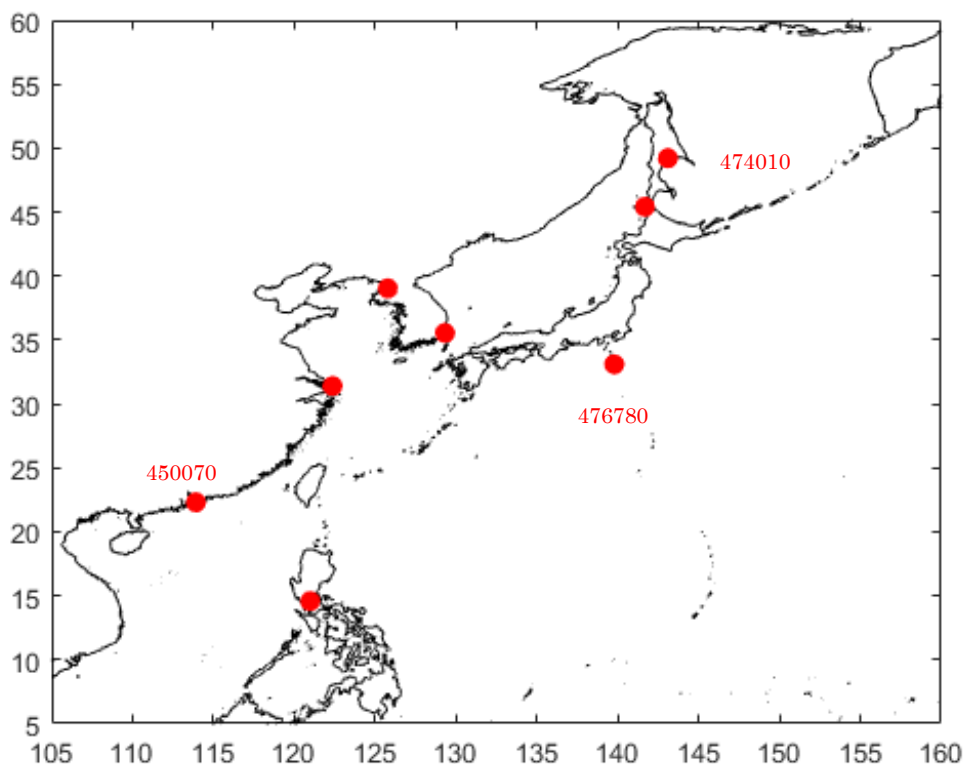


Figure 1. Location of observation station

Ensemble data (Table 1) has similar length of data (around 30 years) but the resolution of each ensemble is different. The Experiment of AMIP is chosen. Historical data in CMIP5 database includes changing conditions of atmospheric composition (anthropogenic and volcanic influence), solar forcing, emission, and land use. In AMIP experiment, sea surface temperature & sea ice (from observations) are imposed in addition to historical experiment (Taylor et al., 2009). Ensemble variances in one GCM model indicates the different initial condition, parameterization, and physical parameter. Most of the data do not overlap with observation point, thus nearest data is elected as the representative ensemble. The 3-hourly u and v component of surface wind, the finest temporal resolution, is retrieved.

Table 1. Model ensemble resolution. Number inside bracket indicates the total model ensemble

Model ensemble	Resolution	
	Latitude	Longitude
ACCESS1.0	1.25 ⁰	1.875 ⁰
ACCESS1.3 (ii)		
INM-CM4	1.5 ⁰	2 ⁰
GFDL-CM3 (ii)	2 ⁰	2.5 ⁰
CNRM-CM5	1.4008 ⁰	1.40625 ⁰
CanAM4 (iv)	1.7906 ⁰	2.8125 ⁰
MIROC-ESM		
IPSL-CM5A-LR	1.8947 ⁰	3.75 ⁰
IPSL-CM5A-MR	1.2676 ⁰	2.5 ⁰
MRI-CGCM3	1.121 ⁰	1.125 ⁰
GISS-E2-R (ii)	2 ⁰	2.5 ⁰

3.2 Methodology

Observation wind data consists wind speed and wind direction in degree, while CMIP5 generally produce wind as wind component of u and v (above surface at 10-m height). To be compared well, each ensemble's wind component is simply calculated to find

Wind magnitude. Using simple statistical approach as maximum, minimum, and mean can be discovered the uncertainty of ensemble data. Thus, correlation and standard deviation of each ensemble can be obtained. Wind rose is used to inspect wind distribution and wind direction. Result, analysis, and comparison have been made to be able answer the aim of preliminary study so we can keep going for future projection (CMIP5 scenario) and make sure the wind input for ocean-atmospheric field.

Ensemble data is taken only the nearest data between the global data and the observation point. There is no ensemble which intersect the measurement location. Even though, the location is surrounding by 4 points-box shaped of each CMIP5 ensemble, we avoid the interpolation between due to uncertainty occurrence of many interpolation method. Missing wind data at certain time and on a leap year is treated as blank data so it can be compared.

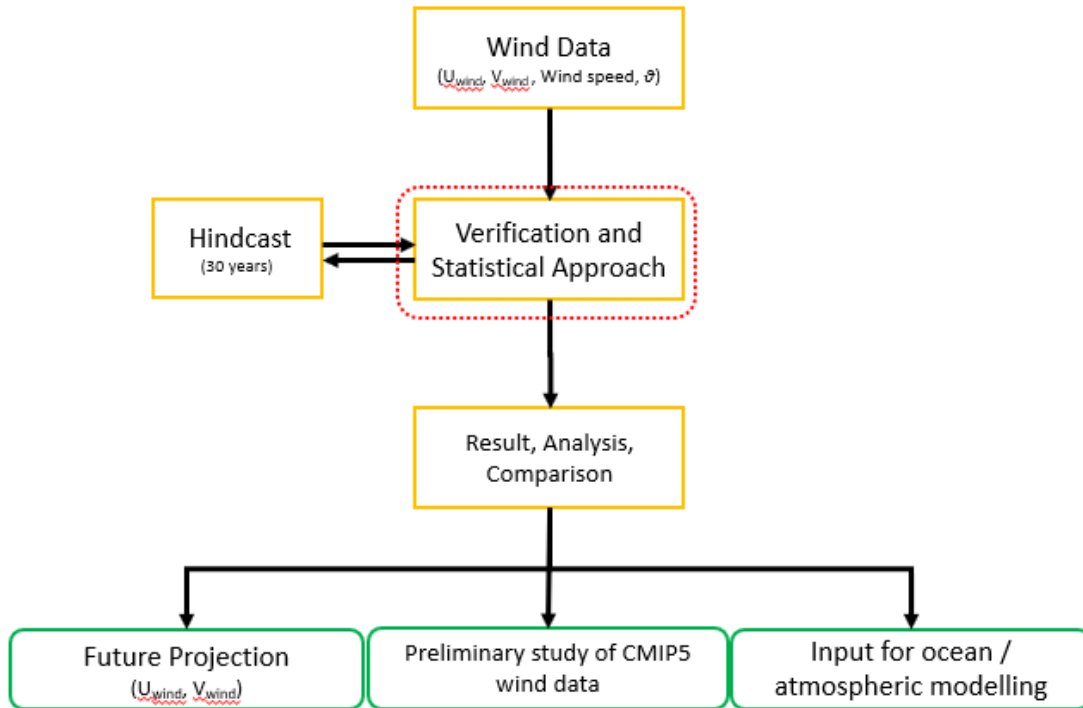


Figure 2. Research methodology structure

Moving Average

Wind pattern in the field commonly is not trivial to be observed. Many aspects influence wind in term of local wind, typhoon, and variance frequency of wind. However, it is likely to have sinusoidal pattern if the high frequency is withdrawn. Model (ensemble) use some limitation and simplification in their simulation setting so the model could not yet reconstruct wind as real wind which occurred in field. Therefore, moving average (m.a.) method is taken to inspect the pattern lies on real wind data. Moving average (eq.1) calculates data points by creating series of averages of different subsets of the full dataset. This subset will be averaged by shifting forward to the end of data. Smoother wind data is produced then longer-term trends/cycle can be highlighted. For this study, monthly and seasonal simple m.a. is applied.

$$S_i = \frac{1}{n} \sum_{j=1}^{i+n-1} a_j \quad (eq. 1)$$

with a_j as data and n for total data.

Wind correction

Common wind data can be underestimated or overestimated compare to data measurement. The differences between them caused by several factor, particularly different surface height, existed obstacle, quality of data, measurement instruments and surface roughness due to terrain type. Correcting the wind use log wind profile or wind power law could solve the lower wind value matter. Estimated mean wind speed (u_z) at height z (m) above the ground

can be written in eq.2. Holmes (2015), rearranged the formula into eq.3.

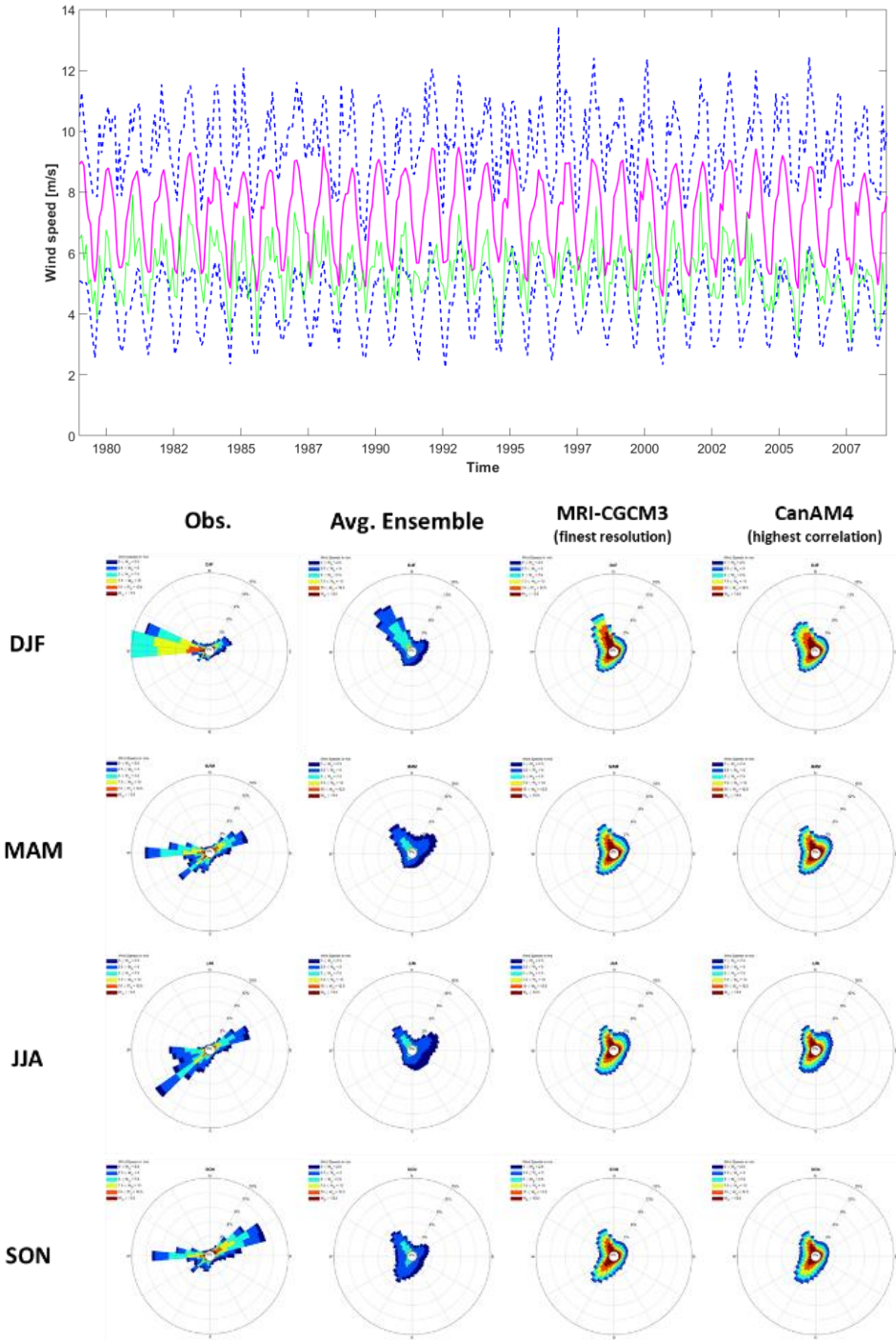


Figure 3. Monthly m.a. time series of observation (green) and mean ensemble (purple) in station 3. Blue dashed line indicates uncertainty (maximum and minimum) of ensemble. (left). Seasonal wind rose for observation, average ensemble, MRI-CGCM3 (finest resolution), and CanAM4 (highest resolution) in station 3 (right)

$$u_z = \frac{u_*}{\kappa} \left[\ln \left(\frac{z-d}{z_0} \right) \right] \quad (eq. 2)$$

$$u(z_2) = u(z_1) * \frac{\ln((z_2 - d) / z_0)}{\ln((z_1 - d) / z_0)} \quad (eq. 3)$$

where u_* is the friction velocity (m/s), κ is the Von Karman constant (~ 0.41), d is zero displacement which is the height above ground at which zero wind speed is archived and can be approximated as $2/3$ or $3/4$. Roughness

length (z_0) is an effect of surface roughness of surface and wind flow. The roughness value depends on the terrain and each type has each own value which is described by Holmes (2015). Since the global area is consist of forest and urban, the z_0 of 1 is arbitrary chosen.

4. Results

Wind time series for whole 30 years of CMIP5 data tends to have similar pattern with observation time series, particularly in station 2 and 3 while station 1 does not. Without m.a. method, it is hardly to see the relation since measurement have more fluctuation compare to ensemble. The correlation increases as long the increases subset time in those method. However, if yearly m.a. is taken, the correlation become less. There is no correlation changing in station 1, almost no relation at all due to unordinary pattern. Correlation in station 2 (station 3) are 0.05 (0.07), 0.56 (0.57), and 0.69 (0.72) for no m.a., monthly m.a., and seasonal m.a. respectively. Standard deviation is calculated separately due to mean observation and mean ensemble. Clearly, standard deviation due to mean ensemble is lower compare to mean observation. Standard deviation range is between 1 – 1.6 meter (with m.a. method). Result both from time series and deviation show the ensemble overestimate measurement. However, the measurement is still inside ensemble’s uncertainty area.

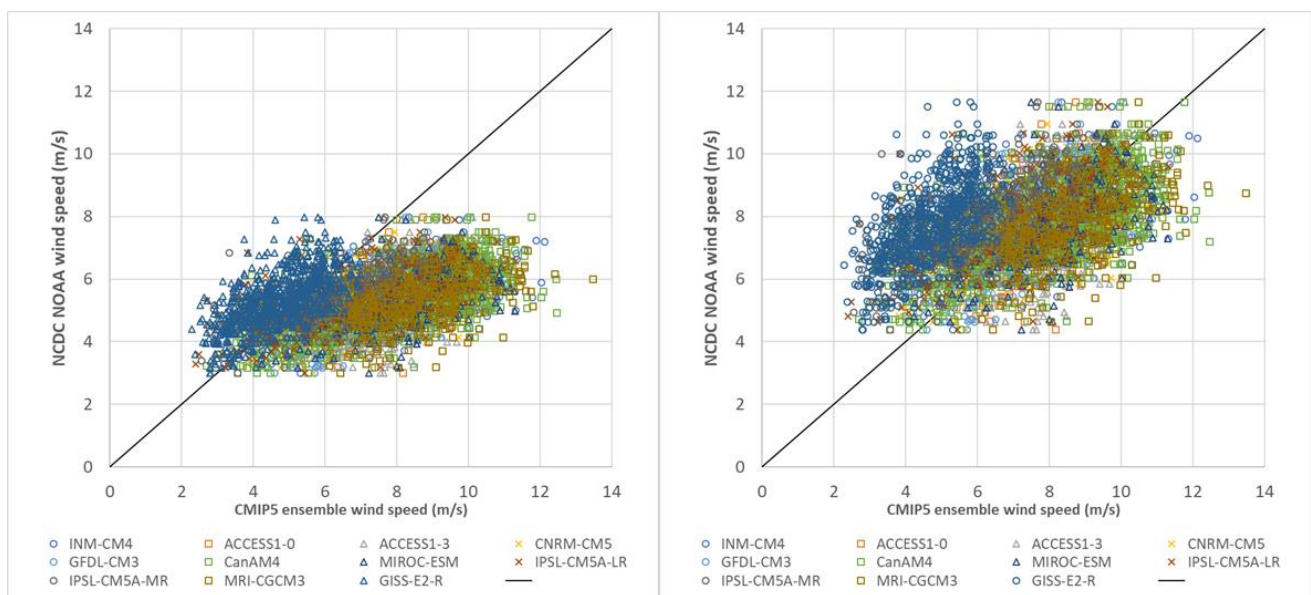


Figure 4. Validation of monthly m.a. between each CMIP5 ensemble and NCDC NOAA wind speed. The left figure is validation without any correction while in the right figure wind has been corrected by factor 1.45.

Wind direction and wind distribution shows from wind rose has different result between ensemble and observation. Generally, each station has majority of wind which blow from slightly east and west while in ensemble wind comes from northeast, southwest, and strong wind from northwest direction. To see further this peculiarity, wind rose is plotted seasonally. Wind distribution from observation, average ensemble, finest resolution ensemble, and highest correlation ensemble are compared. The pattern can be recognized differently, but still the pattern is not identical. Wind commonly blow from east direction in station 1 in each season. For station 2, majority wind comes from west and northwest in winter while in summer wind come from southwest and east. In station 3, the wind direction is relative stable with constant direction from northeast and southwest for entire season, only difference in term of speed and frequency of distribution.

Wind correction is shown in Figure 4. Wind measurement have been modified using log wind profile. Ensemble wind surface stated as wind in 10 m height above surface while there is no detail information from NCDC source. Therefore, we assume wind observation is measured slightly below (around 2.5 m) the ensemble wind height. Wind observation then multiplied by factor 1.45 as obtained from calculation of eq.3. The correlation is not changing, but the distribution between ensemble and measurement become closer to middle line. This factor can be applied in station 2 and 3, but in station 1 the ensemble still overestimates.

The index of DPO and WP pattern had been compared with ensemble time series. However, it is not trivial to see the index relation with monthly and seasonal m.a.. However, if the DPO index is adjusted with yearly m.a. wind time series, there are certain periods which have relation with the index. For a moment, we cannot pronounce the relation between index and wind surface time series.

5. Discussion and Limitation

The calculation of ensemble is still limited due to matter of time and huge data to be archived and kept in storage. Dealing huge data means consume much computer memory and sometimes it is problematic when the machine stop function properly. Ensemble time series needs to be inspected carefully since some of ensemble do not include leap year. Thus, the value of one day in a leap year is blanked manually in some ensemble. Some ensemble cannot be archived due to protection and an ensemble does not have full data only for wind parameter. To be considered that ensemble is done by many institutions then it is not trivial to ensure one by one.

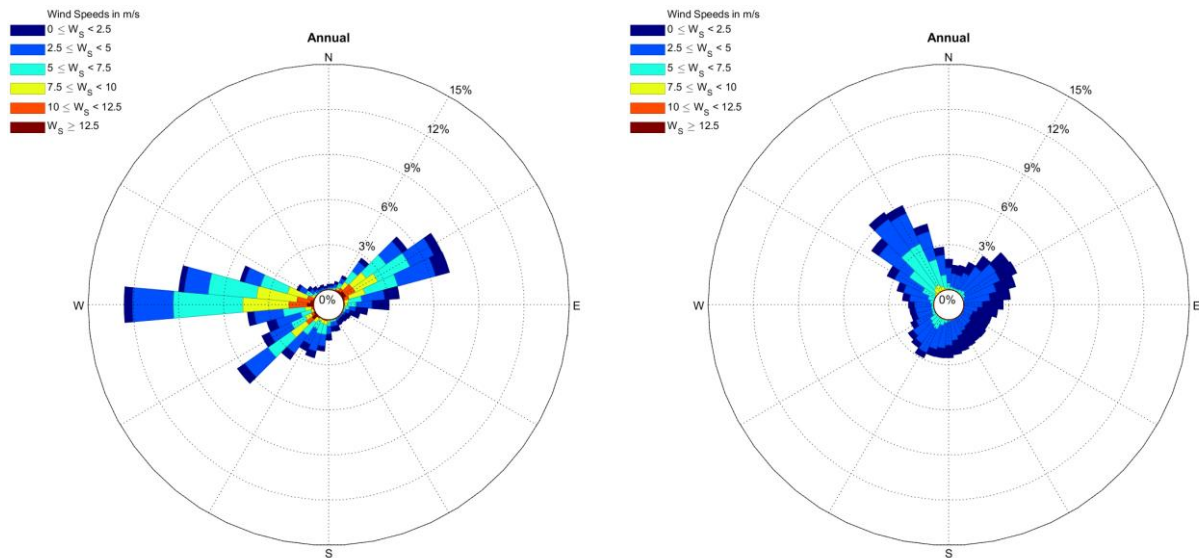


Figure 5. Annual wind rose of observation (left) and ensemble (right) in station 3.

It is assumed that obstacle around observation point, such as mountain and tall building, affect the distribution of wind rose. The wind distributes in every direction in station 2. Concerning the station 2 is almost no obstacle, except in southwest part which is mainland. Ensemble also have less wind come from southeast. In station 3, the wind distributes mainly in northeast, east, and southeast direction. The mountain actually exist in north and southwest part of Hachijojima Island. On other hand, ensemble model does not include this condition due to coarse grid or even the island is neglected. Also, to be considered that averaging all of ensemble can reduce speed and distribution (see Figure 3). This can be seen in seasonal wind rose Thus, it reasonable to say that wind model cannot precisely identical with observation in term of direction.

Even wind correction has succeeded in increasing wind speed, however the assumption need more convincing. The height of wind measurement ($z_1 = 7.5m$) and height displacement ($d = 3/4$) is chosen without basis foundation. After the multiplied factor is obtained, then other wind data is simply multiplied by this number. Certainly, it worked for station 2 and 3, but station 1 still underestimate, meaning that factor have different value concerning to height. This study still lacks information due to measurement height and the reason behind low value of wind speed.

6. Things to be done further

CMIP5 AMIP wind surface data provided 57 ensembles in the source, it should be considering all of the ensemble to observed total uncertainty in wind study. More than a hundred stations are available around WNP region. However, it should be investigated more which one is representative enough for study, examined observation area due to mountain or any obstacle, and certainly checked the quality of data. Many indexes have been made, thus can be compared with monthly or seasonal wind and see the relation and observed what is going on in certain period. Linear trend can be inspected also using many method, thus for further study, EDM, EEDM, etc. method will be applied.

Carry out the future scenario of CMIP5 and wind input modeling is not part of this study but it can be next step for upcoming research.

References

Bennett, W., Karunarathna, H., Mori, N., & Reeve, D. (2016). Climate Change Impacts on Future Wave Climate around the UK. *Journal of Marine Science and Engineering*, 4(4), 78. <https://doi.org/10.3390/jmse4040078>

- Hemer, M. A., Fan, Y., Mori, N., Semedo, A., & Wang, X. L. (2013). Projected changes in wave climate from a multi-model ensemble. *Nature Climate Change*, 3(5), 471–476. <https://doi.org/10.1038/nclimate1791>
- Holmes, J. D. (2015). *Wind loading of structures* (3rd ed). CRC. Retrieved from <http://ci.nii.ac.jp/ncid/BB19758031.bib>
- Shimura, T., Mori, N., & Mase, H. (2013). Ocean waves and teleconnection patterns in the northern hemisphere. *Journal of Climate*, 26(21), 8654–8670. <https://doi.org/10.1175/JCLI-D-12-00397.1>
- Shimura, T., Mori, N., & Hemer, M. A. (2016). Variability and future decreases in winter wave heights in the Western North Pacific. *Geophysical Research Letters*, 43(6), 2716–2722. <https://doi.org/10.1002/2016GL067924>
- Taylor, K. E., Stouffer, R. J., & Meehl, G. a. (2007). A Summary of the CMIP5 Experiment Design. *World*, 4(January 2011), 1–33. <https://doi.org/10.1175/BAMS-D-11-00094.1>

Evaluation of optimal location of wastewater treatment plant in Ger areas of Ulaanbaatar city using multi-criteria decision making (MCDM) analysis.

BYAMBADORJ ARIUNTUYA^{1,2}

¹ Graduate School for International Development and Cooperation, Hiroshima University, 1-5-1 Kagamiyama, Higashi-Hiroshima 739-8529, Hiroshima, Japan. E-mail: ariunaa0710@yahoo.com

² Property Relations Department, Ulaanbaatar City, Mongolia

ABSTRACT

The objective of this research was to assess the willingness to pay (WTP) for improvements in the water supply and wastewater treatment system's capital cost and operation & management of Ulaanbaatar city residents and land suitability for Decentralized Wastewater Treatment plant in Ger area of Ulaanbaatar city. In addition to define decentralized wastewater treatment plant (DWWTP) locations in target area (Damba Planning Unit) and prioritize defined DWWTPs. The results of this research can encourage public participation in the urban decision-making process and assist various planners and authorities to formulate a suitable plan for ger area development.

To assess household WTP of residents for improved domestic water service, a random sampling process was run in Damba area to select households to be interviewed. The survey team contacted 300 households. A total of 298 questionnaire were completed with a response rate of 99 %. Among the 298 observations, 14 outliers were excluded from the analyses; the remaining 285 observations were kept in the sample. The questionnaire included five sections: (1) respondent's identification; (2) Household information; (3) household water supply and consumption; (4) wastewater sanitation; (5) Willingness to pay. Of the 285 responses included in analysis, 101 (35.4%) indicate a zero WTP for water supply and waste water treatment.

In this study two main analysis was done: 1. WTP for Wastewater treatment condition in Ulaanbaatar city is analyzed by Contingent valuation method (CVM): Tobit model, 2. land Suitability for Decentralized Wastewater treatment plant (DWWTP), High potential area for DWWTP and priority of DWWTP locations are analyzed by Multi-Criteria Decision Making (MCDM) method with GIS analysis. In MCDM analysis 1. Geographically weighted regression (GWR) used for analyzing WTP, 2. Weighted overlay analysis used for Suitability map for DWWTP, 3. GIS analysis used for creating population density map. 4. Grouping analysis used for define DWWTP locations by using GWR analysis result. 5. Weighted sum analysis done in high potential map analyze by using WTP map, Population density Suitability map for DWWTP. 6. TOPSIS and Fuzzy TOPSIS method used for to rank the selected location of DWWTP.

Visualization of the WTP surfaces clearly indicates that the relative magnitudes of the WTP for maintenance (F2) values appear to be higher in the close area of sewer system and new settlement areas. In the main, highest values are found in center of Damba area and west side, WTP for O&M (F8) values appear to be higher in the close area of city center and new settlement areas. In the main, highest values are found in south of Damba area and east side. An average total WTP for water supply and wastewater treatment facility installation was 1000.0 (thous.MNT), An average total WTP for operation and management was 6.0 (thous.MNT). People who lives in own build house, higher than high school educated people willing to pay more.

In the suitability result, 0.05% very high suitable, 4% high suitable for DWWTP for ger area in Ulaanbaatar city but in the Damba study area 4% very high suitable, 69% was high suitable for DWWTP for ger area.

Grouping analysis used for defining 40 DWWTP locations by predicted WTP and Slope data. Analysis done by Grouping analysis tool, method with 200 neighbors. The lowest elevation location from each group selected for DWWTP location.

AHP TOPSIS analysis result shows, WWTP location number 12, 39, 25, 26 was high priority and Fuzzy TOPSIS analysis, WWTP location number 6, 35, 2, 32 was high priority. The potential value of Location 12 which defined first rank by Topsis was 10, Location 6 which defined first rank by Fuzzy Topsis was 11.

1. Introduction

Ulaanbaatar is the capital of Mongolia, and also as its largest city serves as the economic and cultural center of the country. Ulaanbaatar is experiencing many environmental, health and socio-economic problems. Sixty

percent of the total population of Ulaanbaatar reside in peri-urban informal settlements, called Ger areas. A lack of safe water supply and unimproved sanitation have been found to be the key issues in the Ger areas of Mongolia. Simple, unimproved and unventilated pit latrines and soak pits are generally used for on-site sanitation and household greywater, resulting in unhygienic living conditions. Ger area sanitation practice has significant and cumulative impacts on the soil and groundwater. Although pathogens from human waste eventually degrade in the ground, these processes are slowed by the cold climate and the large amounts of waste going into the soil can be transported by ground water and by surface water during spring thaw and summer rains. Other impacts are to the health of the residents due to the lack of hygienic sanitation, likely contributing directly to higher disease rates. The lack of adequate wastewater disposal systems is one barrier to increasing the quantity of water supplied to the residents. The lack of basic urban services and infrastructure in Ger area settlements has become a source of urban environmental issues such as air, water and soil pollution.

In this study 4 type of literature review was done. 1. Ulaanbaatar city development and Wastewater treatment study in Mongolia, 2. Analysis of willingness to pay (WTP), Tobit model, 3. MCDM, Suitability analysis, AHP, TOPSIS, Fuzzy-AHP, Fuzzy-TOPSIS studies, 4. Geographical autocorrelation and geographically weighted regression study,

1. Several studies in decentralized Wastewater treatment plant done in Mongolia which is underground (UG-), greenhouse (GH-) and ice-hole greywater treatment unit (IH-GWTU) for graywater reuse. (Uddin, Li, Mang, et al., 2014). Laboratory analysis showed a high chemical oxygen demand, $N-NH_4^+$, PO_4^- and total suspended solids values exceeding the WHO guidelines and much higher than in any other country: low water consumption combined with traditional diet might be major reasons. Odorless and colorless water after treatment in a UG-GWTU lead to more acceptance than a GH-GWTU.

City Environment and Development Review (UN-Habitat, 2010a), Service Distribution and Infrastructure Review (UN-Habitat, 2010c), Citywide Pro-Poor Ger Area Upgrading Strategy of Ulaanbaatar City (UN-Habitat, 2010b) are the reviews of reports prepared for the development of Ger Area Upgrading Strategy of Ulaanbaatar City. The review assessing growth prospects, land requirements, environmental issues and development constraints, profiling opportunities and constraints in all service and infrastructure areas (water supply, sanitation, solid waste management, heating, electricity, street lighting, roads and footpaths, transportation services, flood control and drainage, health services, emergency services, education, and greening), assesses the growth of Ger areas, sets out the legal and institutional structure of land management and planning, and identifies the specific issues related to the Ger areas.

2. Contingent valuation method used broadly used to assess public goods. (Goodwin, Offenbach, Cable, & Cook, 1993), Goodwin, Offenbach, Cable, & Cook used Tobit model to estimate WTP for private hunting access in Kansas.

3. The problems of Multi-Criteria Decision Making (MCDM) appear and are intensely applied in many domains, such as Economics, Social Sciences, Medical Sciences etc. (Nădăban, Dzitac, & Dzitac, 2016), Nădăban, Dzitac, & Dzitac offered a general view of the developments of fuzzy TOPSIS methods. They explored different fuzzy models that have been applied to the decision-making field. Seker, Dursun Zafer, Yuçel, Ugur (Seker & Yuçel, 2017), Mansouri, Zeinab, Hafezi Moghaddas, Naser, Dahrazma, Behnaz (Mansouri, Hafezi Moghaddas, & Dahrazma, 2013) are used MCDM method to find optimal site for Waste water treatment plant.

4. Geographically weighted regression (GWR) has been established as a flexible framework for modelling spatially varying relationships between predictor variables and an outcome variable. Campbell, Danny, Hutchinson, W George (Campbell & Hutchinson, 2009), Zhang, Honglei, Zhang, Jie, Lu, Shaojing, Cheng, Shaowen, Zhang, Jinhe, (Zhang, Zhang, Lu, Cheng, & Zhang, 2011), Dong, Guanpeng, Nakaya, Tomoki, Brunson, Chris (Dong, Nakaya, & Brunson, 2018) are used geographically weighted regression to estimate WTP, hotel room price and life satisfaction. The researchers used kriging to interpolate GWR map.

2. Objectives

The objective of this research was to assess the willingness to pay for improvements in the water supply and wastewater treatment system's capital cost and operation & management of Ulaanbaatar city residents and land suitability for Decentralized Wastewater Treatment plant in Ger area of Ulaanbaatar city. In addition to define decentralized wastewater treatment plant (DWWTP) locations in target area (Damba Planning Unit) and prioritize defined DWWTPs.

The results of this research can encourage public participation in the urban decision-making process and assist various planners and authorities to formulate a suitable plan for ger area development.

3. Data and methodology

3.1 Data 3.1.1 Field survey

To estimate the willingness to pay for improving water supply and wastewater treatment system, a field survey conducted in Damba planning unit which is defined by Urban Development Trend 2030 (Fig. 1). It is locating in north east part of the Ulaanbaatar city and residents all live in ger and owner-built house housing. The population of the Damba area was 32.1 thousand and household number was 8.7 thousand in 2010 (Urban Development Trend 2030, 2013).

To assess household willingness to pay of residents for improved domestic water service, a random sampling process was run in Damba area to select households to be interviewed. The survey team contacted 300 households. A total of 298 questionnaire were completed with a response rate of 99 %. Among the 298 observations, 14 outliers were excluded from the analyses; the remaining 285 observations were kept in the sample. The questionnaire included five sections: (1) respondent's identification; (2) Household information; (3) household water supply and consumption; (4) wastewater sanitation; (5) Willingness to pay. Of the 285 responses included in analysis, 101(35.4%) indicate a zero willingness to pay for water supply and waste water treatment.

The consumer's willingness to pay was elicited through the following two-part questioning framework:

a) Would you be willing to pay an _____ fee to access WS WWT facilities? (Yes or No)

b) If yes, how much would you be willing to pay for installation (capital cost)? (0=0, 1=less than 1000.0, 2=1000.0-1500.0, 3=1500.0-2000.0, 4=higher than 2000.0 (thousand MNT).

A "No" response to part (a) implied a zero willing to pay in part (b).

3.1.2 Dataset

Table3.1 shows the data set list used in this study.

Table 3.1. Dataset used in the analysis

	Data	Type	Data type	Figure
1	Land use plan	.shp	Polygon	Figure 3.2
2	Elevation	Raster	30m resolution	Figure 3.3
3	Population density	Table	Text	Figure 3.4
4	Soil	.shp	Polygon	Figure 3.5
5	River	.shp	Polygon	Figure 3.5
6	Road	.shp	Polygon	Figure 3.6
7	Power station	.shp	polygon	Figure 3.7
8	Sewerage	.shp	Line	Figure 3.8
9	Drainage	.shp	Line	Figure 3.9
10	Ger area settlement	.shp	Polygon	Figure 3.10
11	Land evaluation zone	.shp	Polygon	Figure 3.11
12	Planned DWWTP location	.shp	Point	Figure 3.12

3.2 Methodology

In this study two main analysis was done: 1. Willingness to pay (WTP) for Wastewater treatment condition in Ulaanbaatar city is analyzed by Contingent valuation method (CVM): Tobit model, 2. land Suitability for Decentralized Wastewater treatment plant (DWWTP), High potential area for DWWTP and priority of DWWTP locations are analyzed by Multi-Criteria Decision Making (MCDM) method with GIS analysis. In MCDM analysis 1. Geographically weighted regression (GWR) used for analyzing WTP, 2. Weighted overlay analysis used for Suitability map for DWWTP, 3. GIS analysis used for creating population density map. 4. Grouping analysis used for define DWWTP locations by using GWR analysis result. 5. Weighted sum analysis done in high potential map analyze by using WTP map, Population density Suitability map for DWWTP. 6. TOPSIS and Fuzzy TOPSIS method used for to rank the selected location of DWWTP.

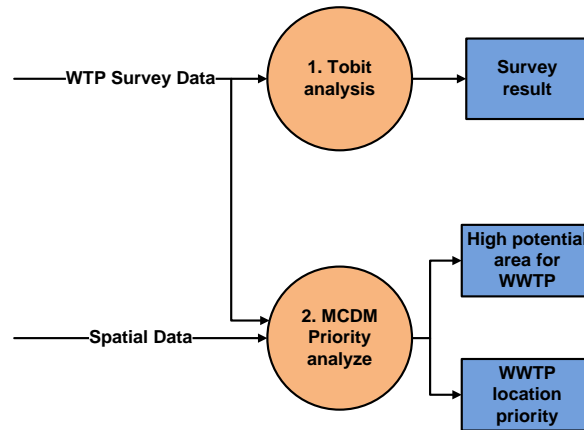


Figure 1: Analyze main flow chart

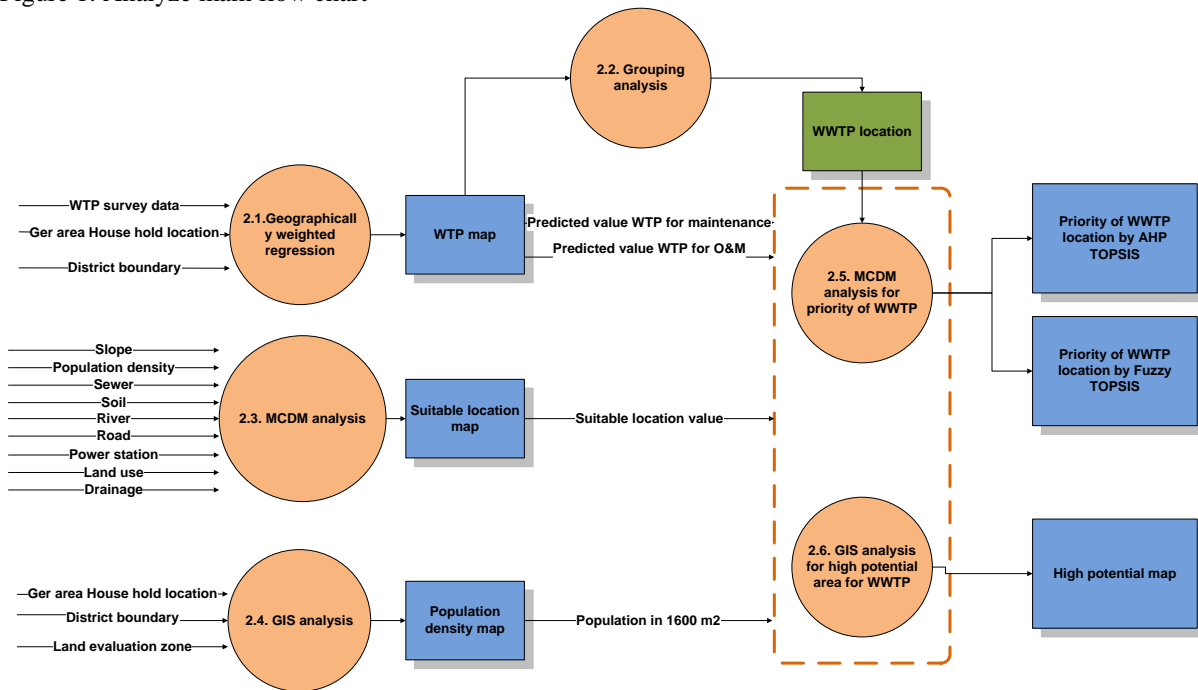


Figure 2: MCDM analyze flow chart.

This work aims at identifying potential sites for DWWT for ger area of Ulaanbaatar city by GIS-based multi-criteria analysis. GIS (ArcGIS) techniques were used and integrated in a multi-criteria analysis to benefit of its capacity to elaborate and to analyze spatial data. A GIS flowchart of the entire process is shown in Figure 4.3.

First of all, process OLS and Moran's I analysis done for make sure that WTP spatially autocorrelated. In the red rectangle shows WTP prediction map analysis flow chart. First step was data preparation by connecting survey data to house hold location by address and 400mx400m grid was prepared for next step. After data preparation Geographical weighted regression used for predicting WTP (point map) by house hold settlement period, distance from water supply station and population density. Then predicted point map joined by average value with 400x400 grid. Then it is converted to point. To interpolating WTP prediction map Kriging was used.

In the green rectangle shows land suitability map analysis flow chart. It is starting from defining criteria weight. Weighted overlay tool used for suitable location analysis. For detailed explanation research accomplished in this analysis is found in next chapter.

Suitability map generalized from 10m to 100m by average value and converted to point. Point map joined by average value of suitability value with 400x400 grid. To interpolating aggregated suitability map kriging was used.

In the blue rectangle shows population density map analysis flow chart. In this analysis ger area house hold location 266280 sample point joined and counted with 400x400 grid. To interpolating population density map kriging was used.

After these 3-analysis weighted sum tool used for analysing high potential area for DWWT in ger area of Ulaanbaatar city.

For defining 40 DWWT locations Grouping analysis used by predicted WTP and Slope.

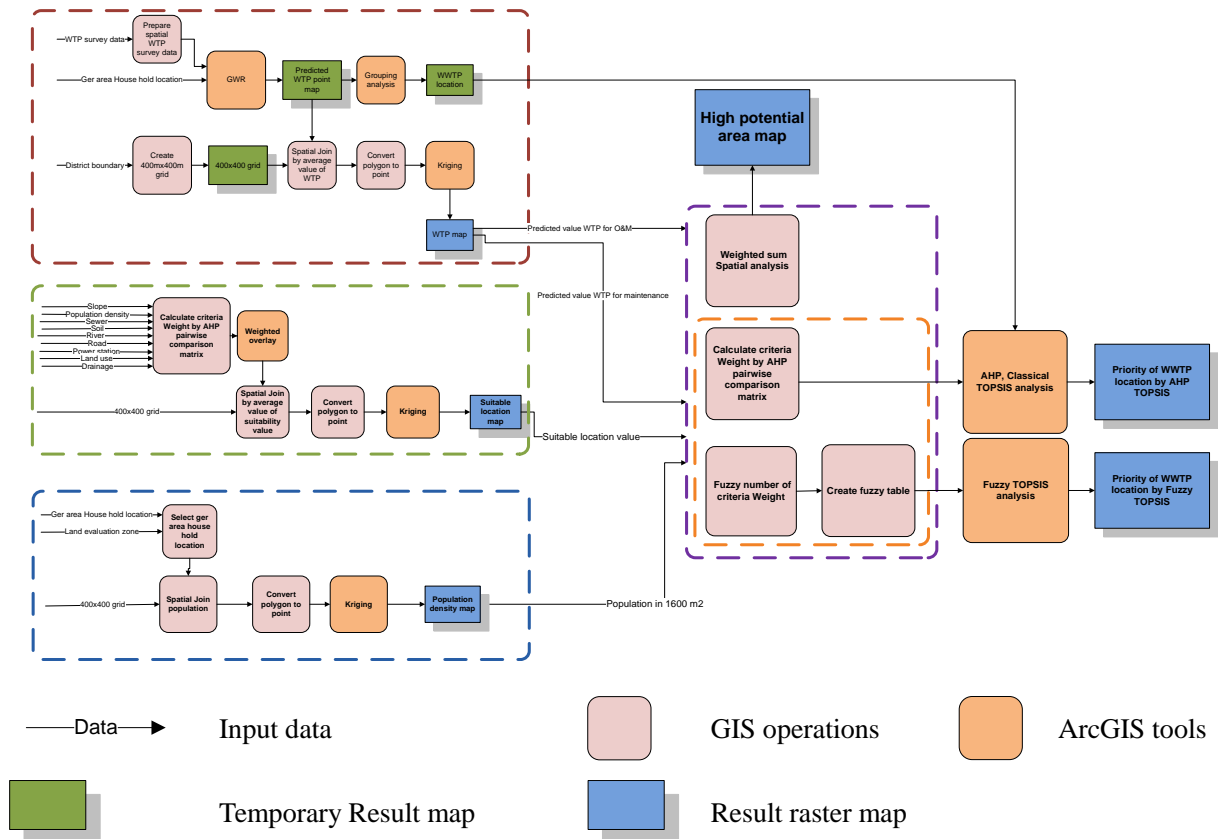


Figure 3. Analyze flow chart

3. Results

Survey result shows: Average Household in fence 1.5, Average Household member 3.72, Average income 700.0 thous.MNT, 88% of respondents could access improved Water supply source, 91% of respondents don't have improved wastewater, sanitation facility, 62% of respondents was Willingness to improve Water supply and wastewater discharge condition, 71% of respondents willing to pay monthly for fee for O&M, An average WTP for maintenance is 1000.0 (thous.MNT), An average WTP for maintenance is O&M 6.0 (thous.MNT).

Table 1. Summary statistics of variable relevant to willingness to pay for Water supply and wastewater treatment.

	Total sample		Willingness to pay maintenance				Willingness to pay Operation and management			
			Yes		No		Yes		No	
			Mean	Std Dev	Mean	Std Dev	Mean	Std Dev	Mean	Std Dev
Agreement of WS and WWT facility improvement (installation) payment	0.639	0.481	-	-	-	-	0.840	0.367	0.208	0.408
Willingness to pay WS and WWT facility installation (thousand MNT)	0.827	0.785	1.206	0.663	-	-	1.044	0.766	0.258	0.510
Agreement of WS and WWT facility operation and management (monthly) fee	0.708	0.456	0.908	0.290	0.330	0.473	-	-	-	-
Willingness to pay WS and WWT facility operation and management fee (monthly) (thousand MNT)	1.708	1.546	2.260	1.432	0.728	1.241	2.437	1.286	-	-
Education	0.599	0.491	0.634	0.483	0.525	0.502	0.661	0.475	0.434	0.499
Family size	3.489	1.586	3.598	1.691	3.343	1.379	3.587	1.617	3.224	1.457

Income level 1 (thousand MNT in Month)	0.151	0.359	0.089	0.286	0.257	0.439	0.116	0.322	0.231	0.424
Income level 2 (thousand MNT in Month)	0.372	0.484	0.408	0.493	0.307	0.464	0.365	0.483	0.372	0.486
Income level 3 (thousand MNT in Month)	0.067	0.250	0.084	0.278	0.040	0.196	0.079	0.271	0.038	0.194
Income level 4 (thousand MNT in Month)	0.021	0.144	0.034	0.180	0	0	0.026	0.161	0.013	0.113
Housing	0.668	0.472	0.713	0.453	0.590	0.494	0.690	0.464	0.590	0.495
Time for water access	0.853	0.355	0.886	0.319	0.810	0.394	0.866	0.342	0.813	0.392
Water consumption (HH)	298	276	301	283	290	262	306	297	281	231
Person who bring water	0.192	0.395	0.158	0.366	0.250	0.435	0.160	0.367	0.276	0.450
Current monthly payment of water supply (thousand MNT)	1.919	1.215	2.096	1.173	1.554	1.189	1.978	1.156	1.795	1.354

Table 2. Result of Tobit model

	WTP installation		WTP operation and management	
	Tobit coefficient		Tobit coefficient	
(Intercept)		-3.496e-01		-0.1418798
Education		2.698e-01	.	0.4087174
Family size		3.544e-02		0.2996797 ***
Income level 1 (thousand MNT in Month)		-6.862e-01 *		-1.0849575 **
Income level 2 (thousand MNT in Month)		-1.322e-0		-0.7623613 **
Income level 3 (thousand MNT in Month)		-1.384e-02		-0.2187766
Income level 4 (thousand MNT in Month)		3.942e-01		-0.4980350
Housing		4.075e-01 *		0.4015222
Time for water access		2.856e-01		0.5543989
Water consumption (HH)		-7.242e-05		-0.0003210
Person who bring water		-3.518e-01 .		-0.4455065
Current monthly payment of water supply		1.848e-01 **		0.0932675
Logsigma		3.017e-02		0.5807389 ***
Log-likelihood:		-277.9653 on 13 Df		-398.3712 on 12 DF

Signif. codes: 0 '***' 0.001 '**' 0.01 '*' 0.05 '.' 0.1 ' ' 1

Tobit result shows: Education was statistically positive significant in F2, Family size was positive statistically strong significant in F8, Income level 1, Income level 2 statistically negative significant in both F2 and F8, Housing who lives in detached house statistically positively significant in F2, Current monthly payment statistically positively strong significant, To elucidate the geographical dimension of WTP, the individual 219 house hold WTP estimates.

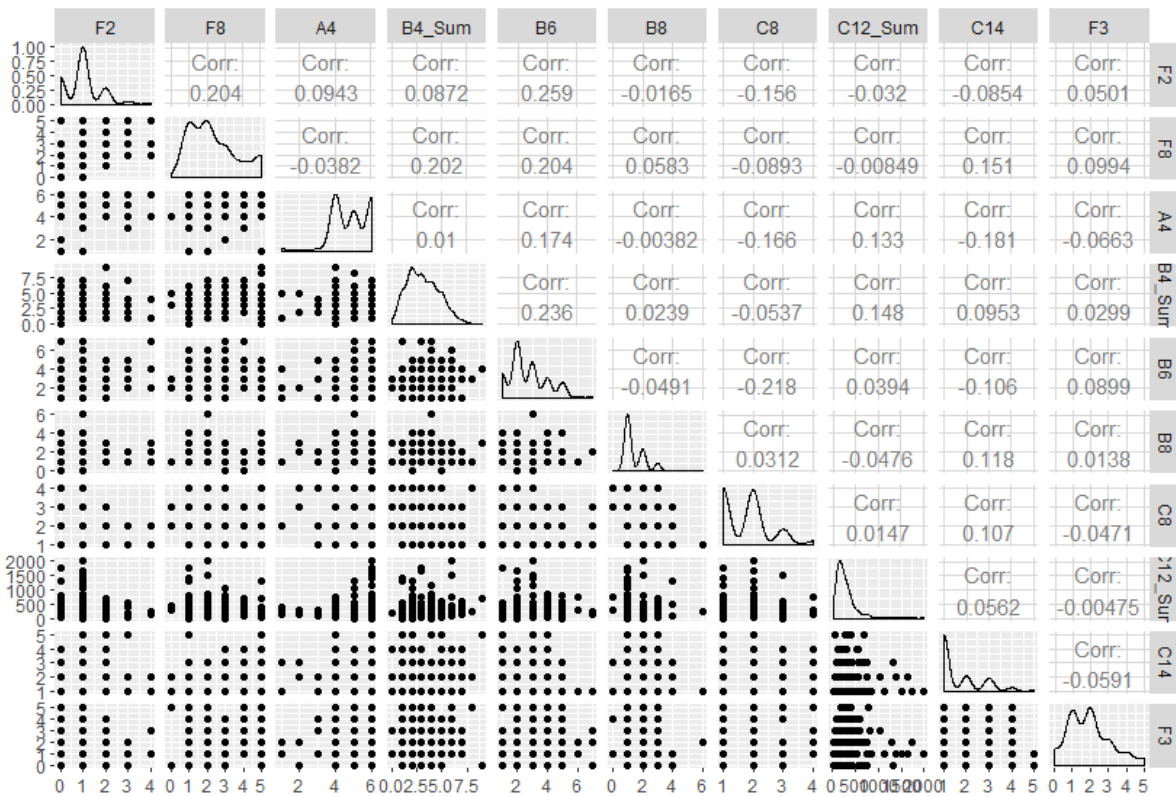


Figure 4. Correlation matrix

Prediction of WTP by geographical weighted regression for 10210 sampling points across the Damba planning unit. Visualization of the kriged surfaces clearly indicates that the relative magnitudes of the WTP for maintenance (F2) values appear to be higher in the close area of sewer system and new settlement areas. In the main, highest values are found in center of Damba area and west side, WTP for O&M (F8) values appear to be higher in the close area of city center and new settlement areas. In the main, highest values are found in south of Damba area and east side. An average total willingness to pay for water supply and wastewater treatment facility installation was 1000.0 (thous.MNT), An average total willingness to pay for operation and management was 6.0 (thous.MNT). People who lives in own build house, higher than high school educated people willing to pay more.

Multi-Criteria Evaluation technique used to evaluate the land suitability of Decentralized Wastewater Treatment Plant (DWWTP). The individual class weights and map scores were determined through AHP technique. A pairwise comparison matrix was prepared for the nine criteria (Slope, population density, soil, river, road, sewerage, land use plan, drainage) for the study area of Ulaanbaatar city. The final suitability for DWWTP map were produced by overlapping the 9 data layers in GIS system. The final scores vary from 1 to 9 and they are classified into five classes of very suitable (scores of 7 and 8), suitable (scores of 5 and 6), medium suitable (score 4), low suitable (scores of 2 and 3) and unsuitable (score 1). Based on the final map, 0.05% very high suitable, 4% high suitable for DWWTP for ger area in Ulaanbaatar city but in the Damba study area 4% very high suitable, 69% was high suitable for DWWTP for ger area.

Grouping analysis used for defining 40 DWWTP locations by predicted WTP and Slope data. Analysis done by Grouping analysis tool, method with 200 neighbors. The lowest elevation location from each group selected for DWWTP location.

According to high potential map 27% of total area was very high, 69% of total area was high potential for decentralized wastewater treatment plant in Damba planning unit.

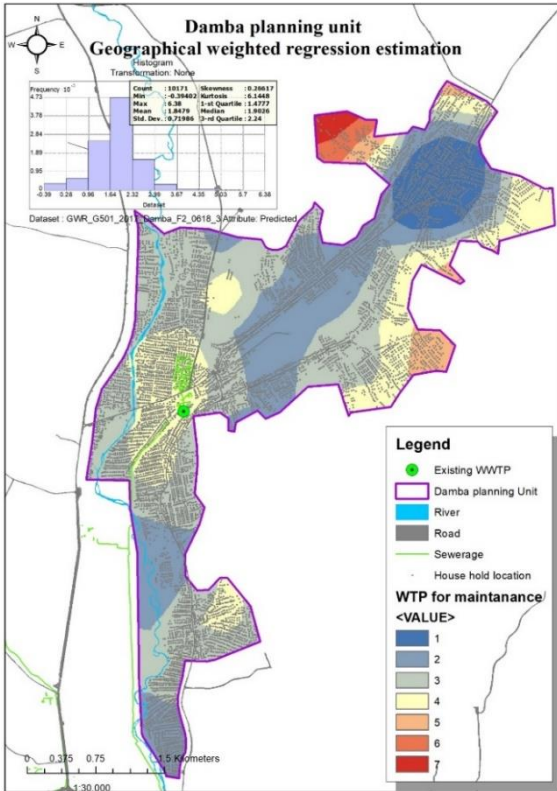


Figure 5. Spatial distribution WTP for maintenance by equidistant.

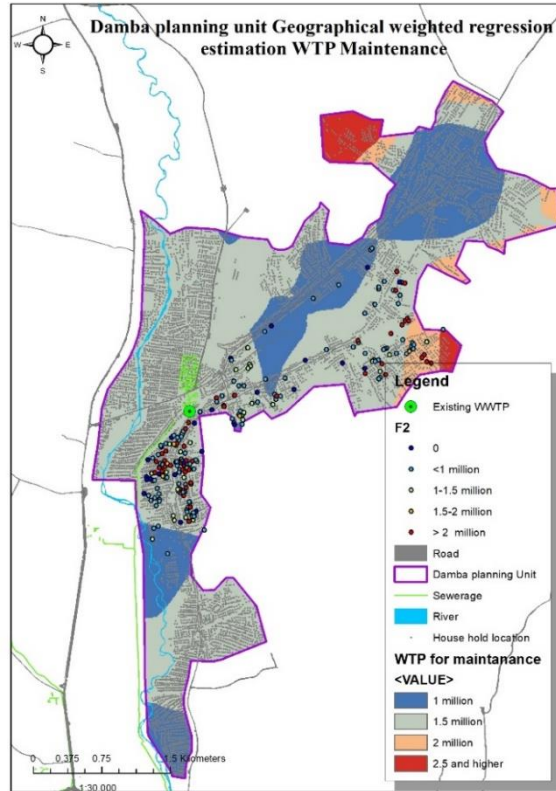


Figure 6 Spatial distribution WTP for maintenance by amount of WTP

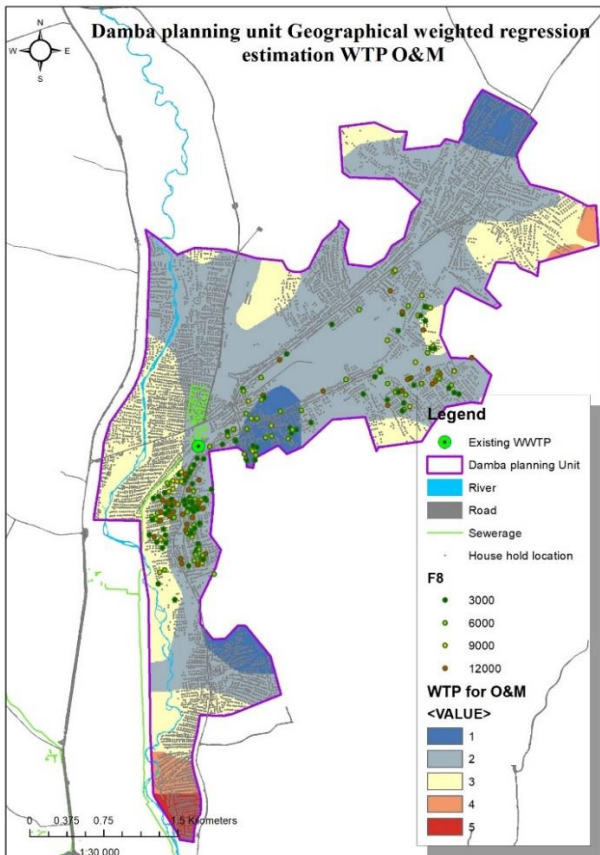


Figure 7 Spatial distribution WTP for O&M by equidistant.

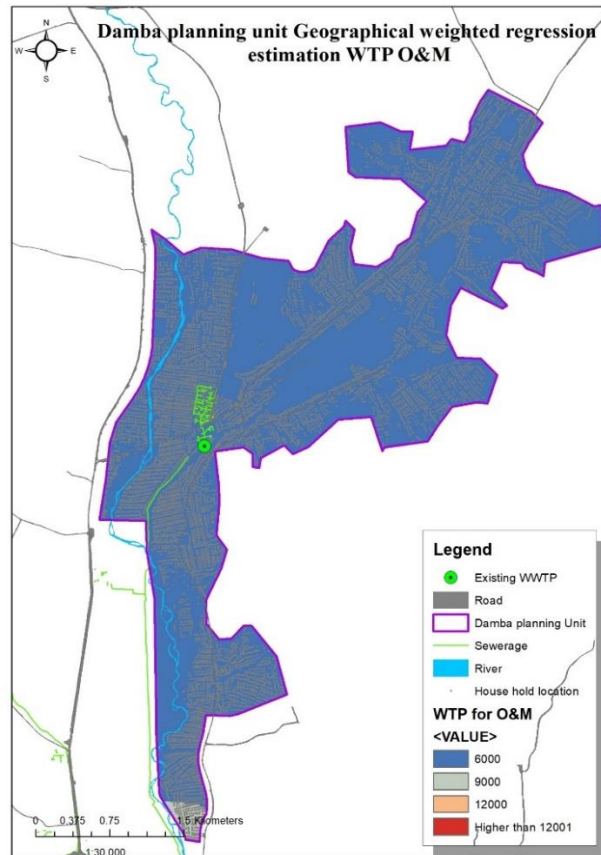


Figure 8 Spatial distribution WTP for O&M by amount of WTP

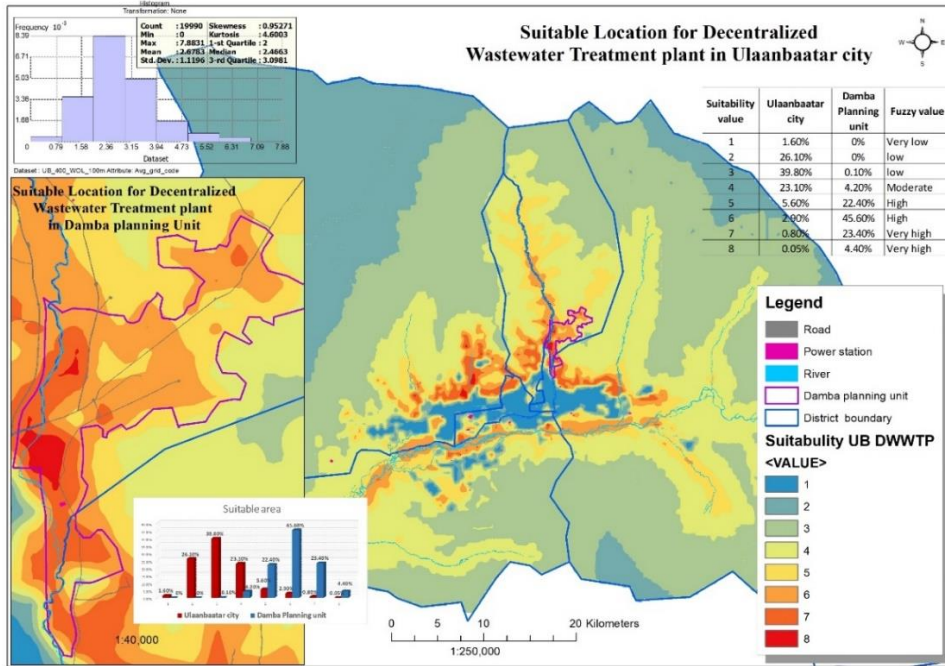


Figure 7 Suitability map (DWWTP)

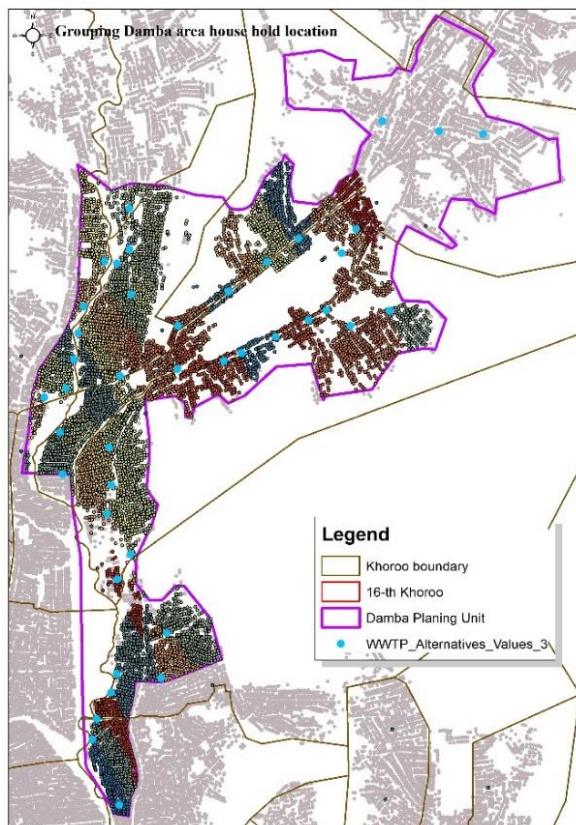


Figure 8 Selected DWWTP location

Four parameters which is WTP maintenance (F2), WTP O&M (F8), Suitability value, Population density are used in TOPSIS analysis. Based on the AHP TOPSIS analysis, WWTP location number 12, 39, 25, 26 was high priority and Fuzzy TOPSIS analysis, WWTP location number 6, 35, 2, 32 was high priority. The potential value of Location 12 which defined first rank by Topsis was 10, Location 6 which defined first rank by Fuzzy Topsis was 11.

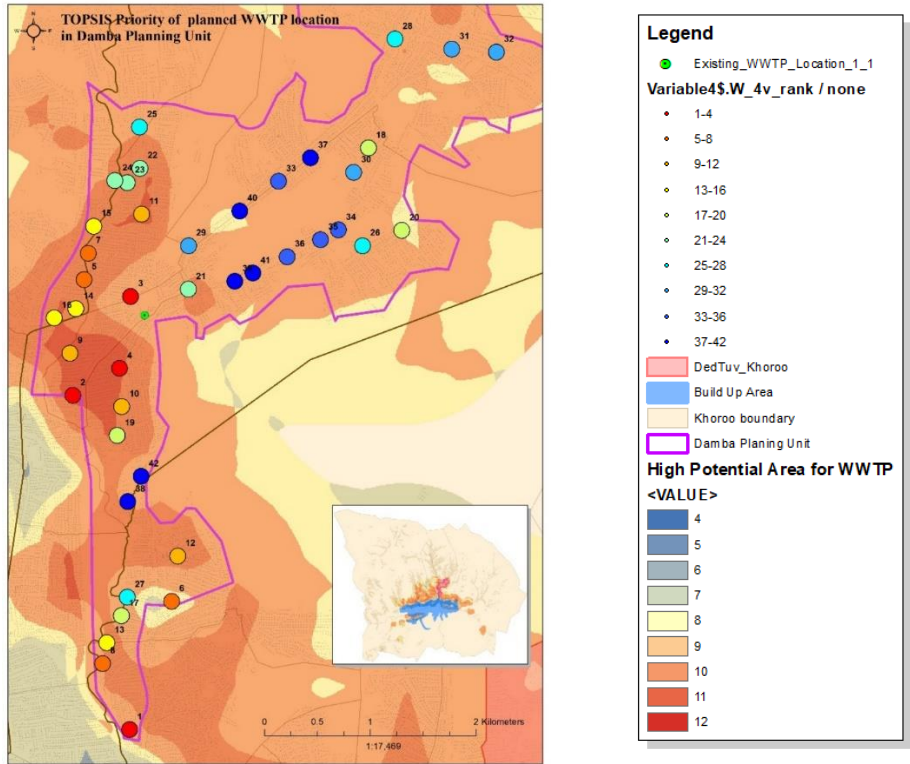


Figure 9 Topsis Rank of DWWTP

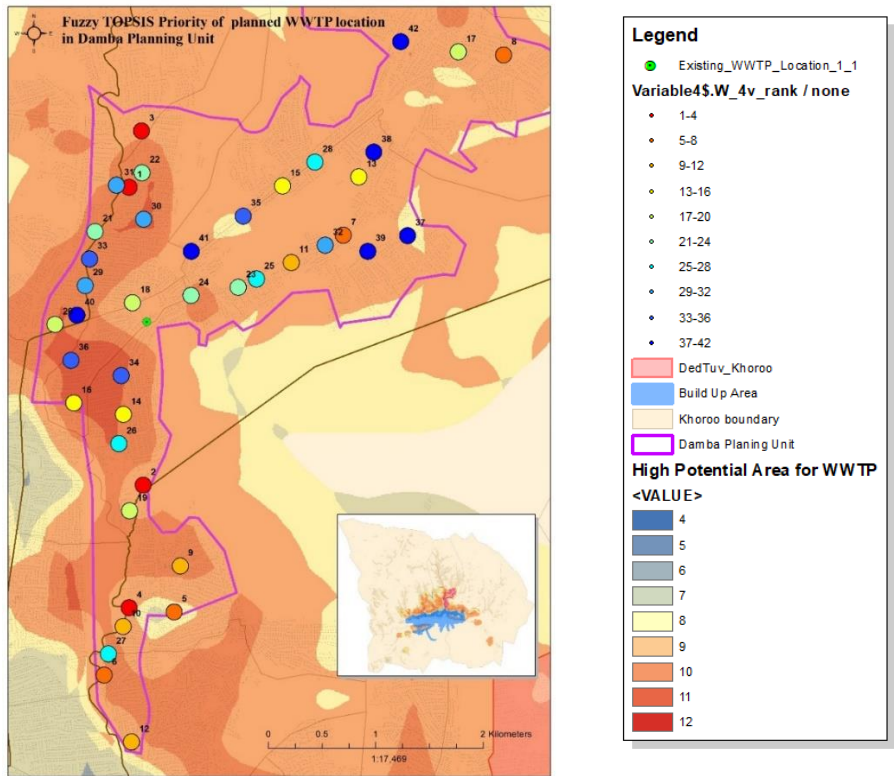


Figure 6.23. Fuzzy-Topsis Rank of DWWTP

According to estimation WTP by using high priority locations of DWWTP, WTP for maintenance (F2) will increase 1.14%, WTP O&M will 0.33% by Fuzzy Topsis analysis and F2 will 0.0079%, F8 will 1.43% increase by AHP-Topsis analysis.

5. Conclusion

This study aims to estimate the willingness to pay for improvements in the water supply and wastewater treatment system's capital cost and operation & management of Ulaanbaatar city residents, using the CVM's Tobit model and find high potential location for DWWTP.

An average total willingness to pay for water supply and wastewater treatment facility installation was 1000.0 (thous.MNT), An average total willingness to pay for operation and management was 6.0 (thous.MNT). People who lives in own build house, higher than high school educated people willing to pay more.

Population density, Settlement period, distance from water supply station used by criteria In Geographically weighted regression(GWR and result interpolated by kriging. Visualization of the kriged surfaces clearly indicates that the relative magnitudes of the WTP for maintenance (F2) values appear to be higher in the close area of sewer system and new settlement areas. In the main, highest values are found in center of Damba area and west side, WTP for O&M (F8) values appear to be higher in the close area of city center and new settlement areas. In the main, highest values are found in south of Damba area and east side.

In the present study, 9 criteria were used as main and exclusive parameters in suitable location analysis. Each criterion has been converted to numerical values and weighted using AHP method.

The suitability map was prepared and classified by reclassify tool and Weighted overlay method. 28% of total area was very high, 68% of total area was high potential for decentralized wastewater treatment plant in Damba planning unit.

High potential area map was prepared by weighted sum method. 27% of total area was very high, 69% of total area was high potential for decentralized wastewater treatment plant.

Based on the AHP TOPSIS analysis, WWTP location number 12, 39, 25, 26 was high priority and Fuzzy TOPSIS analysis, WWTP location number 6, 35, 2, 32 was high priority. The potential value of Location 12 which defined first rank by Topsis was 10, Location 6 which defined first rank by Fuzzy Topsis was 11.

According to estimation WTP by using high priority locations of DWWTP, WTP for maintenance (F2) will increase 1.14%, WTP O&M will 0.33% by Fuzzy TOPSIS analysis and F2 will 0.0079%, F8 will 1.43% increase by AHP-TOPSIS analysis.

Reference

- 30-Meter SRTM Tile Downloader. (n.d.). Retrieved from <http://dwtkns.com/srtm30m/>
- Blanca, A., Martin, A. C., Blanca, M., & Martin, A. C. (2016). Package ' FuzzyMCDM ,' 1–8.
- Çalışkan, H., Kurşuncu, B., Kurbanoğlu, C., & Güven, Şevki Y. (2013). Material selection for the tool holder working under hard milling conditions using different multi criteria decision making methods. *Materials and Design*, 45, 473–479. <https://doi.org/10.1016/j.matdes.2012.09.042>
- Campbell, D., & Hutchinson, W. G. (2009). Using choice experiments to explore the spatial distribution of willingness to pay for rural landscape improvements, 41(2001), 97–112. <https://doi.org/10.1068/a4038>
- Castro, D. M., & Parreiras, F. S. (2018). A Review on Multi-Criteria Decision-Making for Energy Efficiency in Automotive Engineering. *Applied Computing and Informatics*. <https://doi.org/10.1016/j.aci.2018.04.004>
- Chen, C. T. (2000). Extensions of the TOPSIS for group decision-making under fuzzy environment. *Fuzzy Sets and Systems*, 114(1), 1–9. [https://doi.org/10.1016/S0165-0114\(97\)00377-1](https://doi.org/10.1016/S0165-0114(97)00377-1)
- Ching-Lai Hwang, K. Y. (1981). *Multi-attribute Decision making Methods and application*. Berlin Heidelberg New York: Springer-Verlag.
- Deepa, K. (2012). Suitable Site Selection of Decentralised Treatment Plants Using Multicriteria Approach in GIS. *Journal of Geographic Information System*, 04(03), 254–260. <https://doi.org/10.4236/jgis.2012.43030>
- Dong, G., Nakaya, T., & Brunson, C. (2018). Geographically weighted regression models for ordinal categorical response variables: An application to geo-referenced life satisfaction data. *Computers, Environment and Urban Systems*, 70(February), 35–42. <https://doi.org/10.1016/j.compenvurbsys.2018.01.012>
- ESRI. (n.d.-a). Analyzing 911 response data using Regression.
- ESRI. (n.d.-b). ArcGIS Desktop web help. Retrieved from <http://desktop.arcgis.com/en/arcmap/>
- Goodwin, B. K., Offenbach, L. A., Cable, T. T., & Cook, P. S. (1993). Discrete/Continuous Contingent Valuation of Private Hunting Access in Kansas. *Journal of Environmental Management*. <https://doi.org/10.1006/jema.1993.1049>
- Henningesen, A. (2010). Estimating Censored Regression Models in R using the censReg Package. *R Package Vignettes Collection*, 5(2), 12.
- Jan Caha, A. D. (n.d.). Examples of FuzzyAHP package application (ver. 0.9.1). Retrieved from <https://cran.r-project.org/web/packages/FuzzyAHP/vignettes/examples.html>
- Libralato, G., Ghirardini, A. V., & Avezù, F. (2012). To centralise or to decentralise : An overview of the most recent trends in wastewater treatment management. *Journal of Environmental Management*, 94(1), 61–68.

<https://doi.org/10.1016/j.jenvman.2011.07.010>

- Mansouri, Z., Hafezi Moghaddas, N., & Dahrazma, B. (2013). Wastewater treatment plant site selection using AHP and GIS: a case study in Falavarjan, Esfahan. *Geopersia*, 3(2), 63–72.
- McDonald, J. F., & Moffitt, R. A. (2018). The Uses of Tobit Analysis Author (s): John F. McDonald and Robert A. Moffitt Source: The Review of Economics and Statistics, Vol. 62, No. 2 (May, 1980), pp. 318–321 Published by: The MIT Press Stable URL: <http://www.jstor.org/stable/192476>, 62(2), 318–321.
- Mosalman Yazdi, M. (2015). Package TOPSIS for R, (Mcdm), 1–3.
- NAdÄban, S., Dzitac, S., & Dzitac, I. (2016). Fuzzy TOPSIS: A General View. *Procedia Computer Science*, 91(Itqm), 823–831. <https://doi.org/10.1016/j.procs.2016.07.088>
- National registration and statistics office. (2015). *Mongolian statistical year book*. Ulaanbaatar, Mongolia: National registration and statistics office.
- Office, N. registration and statistic. (n.d.). National registration and statistic office. Retrieved from www.1212.mn
- R.Qasim, S. (2000). *Wastewater Treatment Plants – Planning, design and operation*. (Second edi). Florida: CRC press.
- Saaty, T. L. (1990). How to make a decision: The analytic hierarchy process. *European Journal of Operational Research*, 48(1), 9–26. [https://doi.org/10.1016/0377-2217\(90\)90057-I](https://doi.org/10.1016/0377-2217(90)90057-I)
- Seker, D. Z., & Yucel, U. (2017). Gis Based Multi-Criteria Decision Analysis for Site Selection of a Wastewater Treatment Plant. *Fresenius Environmental Bulletin*, 26(1), 399–404. Retrieved from http://apps.webofknowledge.com/full_record.do?product=WOS&search_mode=GeneralSearch&qid=6&SID=F2kB6x1T1vwMbHdzcch&page=1&doc=1
- Seyedmohammadi, J., Sarmadian, F., Jafarzadeh, A. A., Ghorbani, M. A., & Shahbazi, F. (2018). Application of SAW, TOPSIS and fuzzy TOPSIS models in cultivation priority planning for maize, rapeseed and soybean crops. *Geoderma*, 310(September 2017), 178–190. <https://doi.org/10.1016/j.geoderma.2017.09.012>
- Uddin, S. M. N., Li, Z., Adamowski, J. F., Ulbrich, T., Mang, H. P., Ryndin, R., ... Cheng, S. (2016). Feasibility of a “greenhouse system” for household greywater treatment in nomadic-cultured communities in peri-urban Ger areas of Ulaanbaatar, Mongolia: An approach to reduce greywater-borne hazards and vulnerability. *Journal of Cleaner Production*, 114, 431–442. <https://doi.org/10.1016/j.jclepro.2015.07.149>
- Uddin, S. M. N., Li, Z., Gaillard, J. C., Tedoff, P. F., Mang, H. P., Lapegue, J., ... Rheinstein, E. (2014). Exposure to WASH-borne hazards: A scoping study on peri-urban Ger areas in Ulaanbaatar, Mongolia. *Habitat International*, 44, 403–411. <https://doi.org/10.1016/j.habitatint.2014.08.006>
- Uddin, S. M. N., Li, Z., Mang, H.-P., Schübler, A., Ulbrich, T., Huba, E. M., ... Lapegue, J. (2014). Opportunities and challenges for greywater treatment and reuse in Mongolia: lessons learnt from piloted systems. *Journal of Water Reuse and Desalination*, 4(3), 182. <https://doi.org/10.2166/wrd.2014.008>
- Uddin, S. M. N., Li, Z., Ulbrich, T., Mang, H.-P., Adamowski, J. F., & Ryndin, R. (2016). Household greywater treatment in water-stressed regions in cold climates using an ‘Ice-Block Unit’: Perspective from the coldest capital in the world. *Journal of Cleaner Production*, 133, 1312–1317. <https://doi.org/10.1016/j.jclepro.2016.06.063>
- UN-Habitat. (2010a). *City Environment and Development Review*, 32.
- UN-Habitat. (2010b). *Citywide Pro-Poor Ger Area Upgrading Strategy of Ulaanbaatar*. Washington DC, USA. Retrieved from http://www.citiesalliance.org/sites/citiesalliance.org/files/CAFiles/Projects/GUSIP_Output_1.6_-_Citywide_Pro-poor_Ger-area_Upgrading_Strategy_December2010reduced.pdf
- UN-Habitat. (2010c). *Service Distribution and Infrastructure Review*. Washington DC, USA.
- Urban Development Trend 2030. (2013). The Ministry of Construction and Urban Development, City Governor’s Office.
- Wikipedia. (n.d.-a). Contingent valuation. Retrieved from https://en.wikipedia.org/wiki/Contingent_valuation#Current_status
- Wikipedia. (n.d.-b). Moran’s I. Retrieved from https://en.wikipedia.org/wiki/Moran%27s_I
- Wikipedia. (n.d.-c). Regression analysis. Retrieved from https://en.wikipedia.org/w/index.php?title=Regression_analysis&oldid=845907644
- Zhang, H., Zhang, J., Lu, S., Cheng, S., & Zhang, J. (2011). Modeling hotel room price with geographically weighted regression. *International Journal of Hospitality Management*, 30(4), 1036–1043. <https://doi.org/10.1016/j.ijhm.2011.03.010>

Climate Change Impact on Species Distribution of *Styrax sumatrana* in North Sumatra using Maximum Entropy Modeling Approach

Muhammad Hadi Saputra¹

¹ Graduate School for International Development and Cooperation, Hiroshima University, 1-5-1 Kagamiyama, Higashi-Hiroshima 739-8529, Hiroshima, Japan

Abstract

The impact of climate change shown by the ecosystem changing such as in aquatic, land and the forest area. Forest as the larger terrestrial ecosystem senses the impact of climate due to the changes in temperature and precipitation. The changes in climate and land use and land cover affected the suitable area for the tree to distribute in the specific condition. The *Styrax sumatrana* as one of the tree species that has a higher value in North Sumatra region has threatened by the changes of climate as well as the human activities. The objectives are to identify the environment variable that contributed to *Styrax sumatrana* distribution in North Sumatra region and forecast the future potential distribution by considering the climate changes scenario and land use and land cover changes. Four models and two scenarios from CMIP5 implemented in this research followed by the model of land use and land cover changes to predict the distribution of *Styrax sumatrana* in the year of 2050 and 2070. Maximum Entropy (MaxEnt) model produced present and future potential distribution with 63 presences of *Styrax sumatrana* as the sample and bioclimatic, biophysical, and anthropogenic as environmental data. The result shows the mean temperature of the coldest quarter give the higher contribution to the model followed by elevation and land use and land cover changes. The suitable area in the year 2050 reduces to 3.87% and decline to 3.54% in 2070 by 4.5 scenario. The 8.5 scenario shows the suitable area below 3.04% and drops to 1.365 in the year 2050 and 2070 respectively. The changes in land use and land cover shows that tree distribution in forest and crop classification will reduce while nearest with shrub and garden and rice field increase the probability for *Styrax sumatrana* to distribute with small changes

Keywords: Climate change, CMIP5, land use land cover, *Styrax sumatrana*, North Sumatra, SDMs, MaxEnt

1. Introduction

Climate change is the important issue that influences human activities in the world. This condition has the impact not only on the human, but also for the nature such as plant, animal, and microbiological species over the whole earth. The impact of this condition can be seen in the aquatic environment (Dove-Thompson et al. 2011), in agriculture plant (Dait 2015), and also in forestry as well by fluctuating the intensity, frequency, timing or duration any kind of disaster such as fire, drought and many more (Dale 2001). In another place, it may occur in pathogen outbreaks (Ray et al. 2008).

Recently the impact of climate change directly or indirectly affected the tree species. In term of tree growths, the climate change impact notes significantly. The research shows that the circular ring of the tree in Thailand decrease as the result of long-term climate change (Vlam et al. 2014). In China, tropical acacias that have been planted were destroyed by cold damage in inland areas and typhoon damage in coastal areas (Booth, Jovanovic, and Harwood 2014). The pines species in Southeast Asia will face the threat from the increasing temperature in the lowland area (Zonneveld et al. 2009). This fact gives the preliminary sight that climate change will give the impact to the tree species that spreading around the tropical area such as Indonesia with the vast biodiversity threatened.

Indonesia as one of the tropical country experience the climate change for centuries. Mostly in the developed area where many trees have been cutting and land conversion increase rapidly. After a decade, the climate change in Indonesia gives the significant impact in every sector such as the economy, poor population, human health, and the environment and biodiversity. In environment and biodiversity aspect, the forest fire that occurs as El Nino create 2 million hectares of peat swamp forests were burned, warming temperatures and precipitation changes will affect the phenology of fruit trees, and treat the orangutan live as the result (Measey 2010). North Sumatra was known as one of the province in Indonesia that has the enormous amount of forest area. Based on Ministry Decree No. 579/Menhut-II/2014 the total area of Terrestrial Forest Area in North Sumatra is 3,055,794Ha in 2014. However, the cover decreasing for the year. Nowadays, the total amount of forest cover area is only 26.1% of the total of land area. Most of the area converted into plantation and crop area. This condition leads to biodiversity lost especially the indigenous one. One of the valuable trees that has a traditional identity for North Sumatra ethnic like Batak tribe is *Styrax sumatrana*. This tree has a long history for indigenous people in North Sumatra.

Styrax sumatrana as one of the valuable trees in North Sumatra has known since 17th century. The Sumatra benzoin mostly uses in many aspects such as pharmacy, food, industry and also traditional ceremony (Jayusman 2014; García-Fernández, Casado, and Ruiz Pérez 2003; Silalahi and Sunandar 2017). The area of this species distributed along the North Sumatra mostly founded around Lake Toba Catchment Area (LTCA) (Sunandar 2012). However, this species be threatened by the land use changes and the climate condition that might shift the distribution of the species in the future as well as the reducing the quality of its gum (Anas and Kholibrina 2017; Kholibrina, Anas, and Susilowati 2018; Anas and Kholibrina 2018).

Although many activities that have been conducted by the government, local people, an even non-government organization to rehabilitate this area, the degradation of biodiversity and land still exists and increase gradually. Most of the rehabilitation trees are not suitable due to the land use and community interest. The income value for the trees not matched compare with the other crop plantation (Affandi and Harianja 2008). Moreover, the climate change involves this condition by affected the tree growth in the rehabilitation program. Most of the trees are burned by the fire and drought by the long-term dry season (Utomo, Dalimunthe, and Hutagalung 2015).

Many research have been done to analyze the impact of climate change to species distribution that show the changes in future condition (Zonneveld et al. 2009; Soheli et al. 2017; Rodrigues et al. 2015). Another research using the GIS model to predict the suitable area for species distribution in current condition by considering the climate condition (Sunandar 2012; Nimasow et al. 2016). However, the anthropogenic factor still limited in those research. One of the research try to include the land use land cover (LULC) changes as the anthropogenic factors in the species distribution model (Benítez-Badillo et al. 2018). Yet, this research limited in the future and climate model.

Regarding the condition of *Styrax sumatrana* in North Sumatra and previous research, the understanding about species distribution of *Styrax sumatrana*, as one of the valuable trees and ecologically beneficial for rehabilitation and reforestation, and the threat in future condition need to consider. This information will be used to formulate the best management to protect the species and at the same time plan the future scenario that will suit regarding the rehabilitation and reforestation of the North Sumatra region.

2. Objectives

The problem that faced by Indonesia as the country with huge biodiversity is the shifting of tree suitability that occurs as the result of climate change. This impact will be affected the important species like *Styrax sumatrana* that need to notice in the future. Considering the background, several questions that need to be answered:

1. What variable that contributed to the distribution of *Styrax sumatrana* in North Sumatra?
2. How the climate change impact the distribution of *Styrax sumatrana* in the future scenario?

The objective conducted as the result of research problems which systematically address the issue into some research activities. According to several problems that are noticed in this research several objectives need to achieve. This research aims

1. To Identify the variable that contributed to *Styrax sumatrana* distribution in North Sumatra
2. To predict the distribution of *Styrax sumatrana* in future scenario due to the climate change

3. Data and methodology

3.1 Data

Species Distribution models were used to predict the distribution of *Styrax sumatrana* form the presence data that collected from observation as primary and literature for secondary data. The presence record for *Styrax sumatrana* in North Sumatrana collected from two regencies which are Humbanghasundutan and Tapanuli Utara, meanwhile the others were collected from book with title “Flora Sumatera Utara Eksotik dan Berpotensi” that published by The Indonesian Institute of Sciences or Lembaga Ilmu Pengetahuan Indonesia (LIPI) (Hartini and Dwi Murti Puspitaningtyas 2005). Total occurrence data that collected are 63 data (34 observation and 29 secondary data) that consists of the name and geographical latitude and longitude coordinate of the trees. Several data that important to predict the species distribution using maximum entropy modeling is presented in table 1.

Table 1. Datasets for MaxEnt modeling approach

No	Data	source	Year	Type
1	Elevation	www.earthexplorer.usgs.gov	2017	.tif
2	Aspect	spatial analysis from DEM data	2017	.tif
3	Slope	spatial analysis from DEM data	2017	.tif
4	Land use and land cover	www.appgis.dephut.go.id	1990,2000,2010, 2050, 2070	.kml
5	Presence data of trees	Primary data and literature	2012	.csv

6	Climate package	www.worldclimate.org	1990,2050,2070	.bil
7	Soil Type	http://www.fao.org/soils-portal	2000	.asc

The aspect and slope raster map were developed from elevation data using Spatial Analysis Tools in ArcGIS program. Elevation was generated from Aster Global Digital Elevation Model (DEM) as 18 tiles in total by 30 arc-second resolutions to cover North Sumatra Region. Furthermore, soil type was downloaded as the global map with 30 arc-resolution in raster data. The soil type refers to the Food and Agriculture Organization (FAO) soil type classification.

Climate package consists of 19 bio-climate data that delivered from the monthly temperature and rainfall values. It is used to generate more biologically meaningful variables. The bioclimatic variables represent annual trends (e.g., the mean annual temperature, annual precipitation) seasonality (e.g., the annual range in temperature and precipitation) and extreme or limiting environmental factors (e.g., the temperature of the coldest and warmest month, and precipitation of the wet and dry quarters). The climate data that was use consists of present data delivered from the year 1990 arranged from 1960-1990, 2050 arranged from 2040-2060 and 2070 that provided 2061-2080 climate data. This data was included in the Bioclimate explanation provided in the appendix (O'Donnell and Ignizio 2012).

Land use land cover data are collected from three different years which are 1990, 2000 and 2010. The data was presented by Ministry of Environment and Forestry of Indonesia and converted to raster data using ArcGIS program. The resolution in 30 arc-second with 25 categories of land cover. According to the purpose of this research, we reduce the number of class by regrouping several categories into 12 classifications.

In term of future prediction, we used four models to forecast the future climate condition in 2050 and 2070. Four models that we used are CCSM4, CNRM-CM5, MIROC5 and MRI-CGCM3 model which are presented as the bioclimate package. Every model has the bioclimate data that different with other models. Every bioclimate packages will be used separately in the MaxEnt input for projection analysis. The result will combine the four models result for each year and scenarios using the overlay process in ArcGIS after the MaxEnt modeling applied. Moreover, for the future scenario of LULC changes, we generated the cellular automata model by using Artificial Neuron Network (ANN) that installed in open source program QGIS called MOLUSCE. The program used 2 different year input data from 1990 as a started year and 2000 for an ended year followed by two variables in raster data which are road distance and elevation as variable factors. Afterward, the ANN model was chosen to produce the land use changes followed by run the cellular-automata simulation to project the changes in LULC for 2010, 2050 and 2070. Those data were used as the environmental input layer in the projection folder in MaxEnt program.

3.2 Methodology

In this research, we used 3 software to produce the appropriate data for analyzing procedures. They are ArcGIS version 10.3.1, QGIS version 2.18.21 with the plugin which is MOLUSCE (NextGIS 2018) and Maximum Entropy (MaxEnt) for Species Distribution Modeling version 3.4.1 (S. J. Phillips, Dudík, and Schapire. 2017). ArcGIS purpose to convert and adjust the data for the same extension and domain for MaxEnt modeling process. QGIS was installed by add MOLUSCE plugin to produce the prediction LULC map for future scenario analysis.

3.2.1. Cellular Automata and Artificial Neural Network for LULC changes

Simulation of LULC changes provide the baseline scenario to show future scenario and the pattern in future development. It can provide the anthropogenic impact, identify the land use problem such as the degradation and deforestation, and the prepare the land use planning (Li and Yeh 2002). Cellular Automata (CA) is used to modeling the LULC changes by applying the Artificial Neural Network (ANN). ANN-CA aim to determine the transition probability using multiple output neurons for simulating multiple LULC changes. The structure of ANN-CA provided by the figure 1.

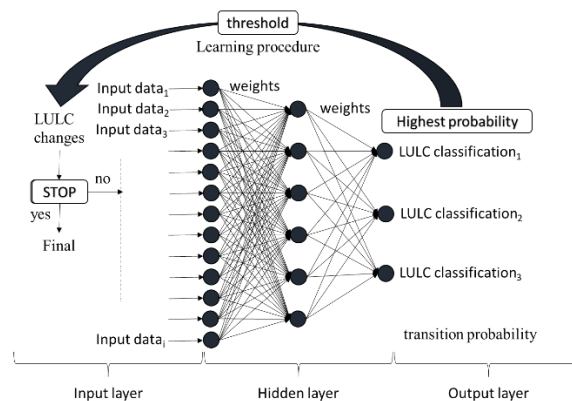


Figure 1. ANN-CA model for simulating the LULC modify from Li and Yeh (2002)

Neural Network structure consists of three layers namely input, hidden and output layers that showed in figure 5. The neurons that represented as the black circle and weight as the line between neurons. The neuron is the basic unit to process the signal and weight use to address the strengths of network between neurons. Each neuron is associated with classification of LULC. The weights use the training data to obtain the optimum weights based on learning procedure that called as back-propagation learning algorithm. The LULC cell changes take a place if the highest transition probability above the threshold value and LULC cell unchanged when the threshold value higher than the maximum transition probability. The threshold used to prevent the LULC changes keep stable in each iteration to obtain the fine patterns of simulation (Li and Yeh 2002).

The LULC changes was provided using the ANN-CA model that lying in MOLUSCE program. The procedure was followed to obtain the LULC prediction in the year 2050 and 2070. The procedure presented in figure 2.

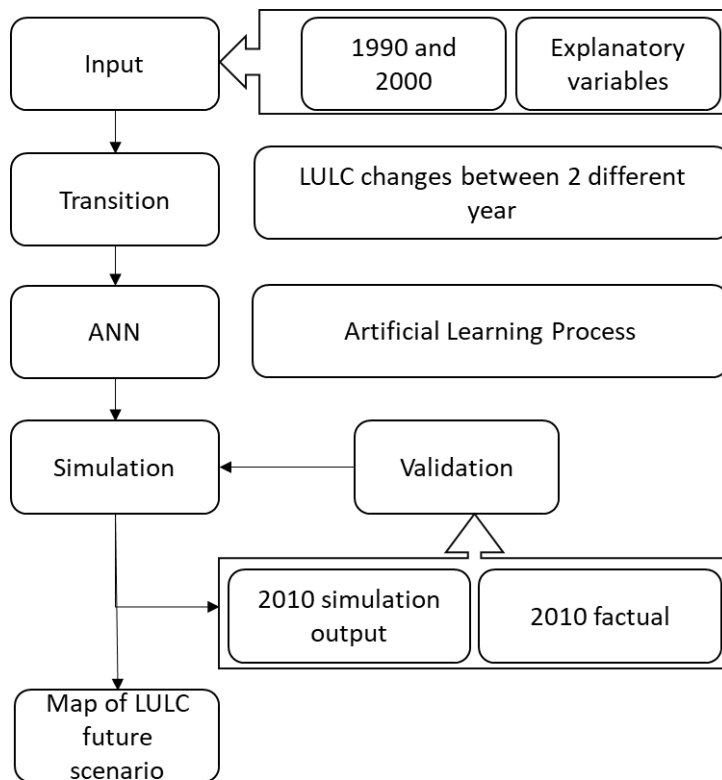


Figure 2. Procedure on land use changes analysis

The LULC changes was produced from the projection on LULC in the year 1990 and 2000. We calculate the changes from 1990 to 2000 and make a validation from the result of LULC at the year 2010 by comparing it with LULC in real condition in the same year. To analyze this procedure we use modules and simulation in QGIS program (NextGIS 2018). The result from the LULC changes was used to simulate the prediction of LULC in future scenario.

3.2.2. Maximum Entropy Approach

Maximum entropy uses the probability distribution to enhance the maximum entropy or area with the highest similarity. MaxEnt idea estimates a target probability distribution by finding the probability distribution of maximum entropy (the individual presence that is most spread-out), constrained by the data relating presence to the environment (S. J. Phillips, Dudík, and Schapire 2004). The program starts with a uniform distribution, and perform several iterations, each of which increases the probability of the sample locations for the species. The algorithm stops when the number of iterations has been performed or when the change in log loss in an iteration falls below a convergence threshold (S. Phillips 2008).

MaxEnt programs use presence-only data and collect the information related to the environment condition at the exact point where the location of sample exist (S. J. Phillips, Dudík, and Schapire 2004). Two input which is the sample point of *Styrax sumatrana* occurrence and the sets of environmental data for the layer for each thematic raster map. Each of environmental variable required to be in the same extension, resolution, and projection.

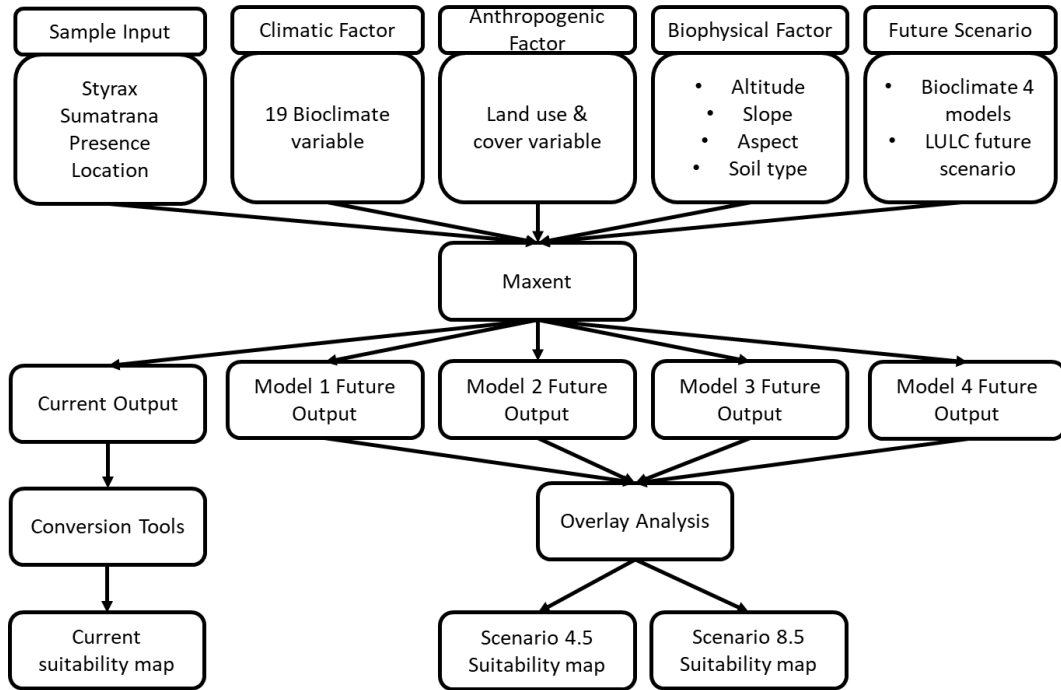


Figure 3. MaxEnt flowchart process

MaxEnt works base on the probability distribution of Baye's rule (S. J. Phillips and Dudík 2008)

$$P(y = 1|x) = \frac{P(x|y = 1)P(y=1)}{P(x)} \quad (1)$$

where: $P(y = 1|x)$ is the probability that the species is present at the site x (y ranges from 0-1)

$P(x|y = 1) = \pi(x)$ is the present observation or realized distribution at x area

$P(y = 1)$ is the probability of presence

$P(x) = \frac{1}{|X|}$ is the all-area probability from the X site

The new formula become

$$P(y = 1|x) = \pi(x)P(y = 1)|X|$$

However, the presence-only data is used in MaxEnt. Rather than estimating the Baye's estimation rule, MaxEnt use the Gibbs distribution from the sets of features f_1, \dots, f_n and weights $\lambda = \lambda_1, \dots, \lambda_n$. This distribution calculated the realized distribution ($\pi(x)$) from the Baye's rule. The formula defined by (S. J. Phillips and Dudík 2008)

$$q \lambda(x) = \frac{\exp(\sum_{j=1}^n \lambda_j f_j(x))}{Z \lambda} \quad (2)$$

where: $q \lambda(x)$ is MaxEnt distribution

$\exp(\sum_{j=1}^n \lambda_j f_j(x))$ is an exponential distribution parameterized by a vector of feature (f) weights (λ).

$Z \lambda$ is a normalization constant ensuring the $q \lambda(x)$ sum to one over the area.

Due to MaxEnt idea is to estimate the probability of presence by maximum entropy we include the formula that delivered from Information theory by Shanon (S. J. Phillips and Dudík 2008)

$$H = -\sum q \lambda(x) \ln(q \lambda(x))$$

where: H is maximum entropy

$q \lambda(x)$ is a MaxEnt distribution from (2) formula

MaxEnt use the probability as the output of species distribution in raster map. The range from 0 to 1 represented the probability by considered the percentage of contribution for each variable input. The probability is displayed as gain which is started at zero (the gain of the uniform distribution) and increases as the program increase the probabilities of the sample location (S. J. Phillips, Anderson, and Schapire. 2006; S. Phillips 2008).

MaxEnt use receiver operating characteristic (ROC) to compares model performance evaluation by threshold-independent evaluation. The model performance provides by the Area under the ROC curve (AUC) were ranged from 0-1%. This ROC plotting sensitivity and 1-specificity. The higher AUC mean the model perform better (S. J. Phillips,

Anderson, and Schapire. 2006).

3.2.3. Analysis procedures

The procedures start with the data collection from presence data and environmental datasets. Then, we analyze the Species distribution of the *Styrax sumatrana* from three function which is bioclimate that consists of present and future climate datasets; Bio physic consists of altitude, slope, aspect and soil type that not changes from present to future; and the last is anthropogenic that represented by the LULC which are consists of present LULC and future prediction of LULC. The Maximum Entropy Approach is used to predict the species distribution at current condition and predict the future condition to produce the future scenario that might occur as the result of Climate Change impact. The overall procedure presented in figure 4.

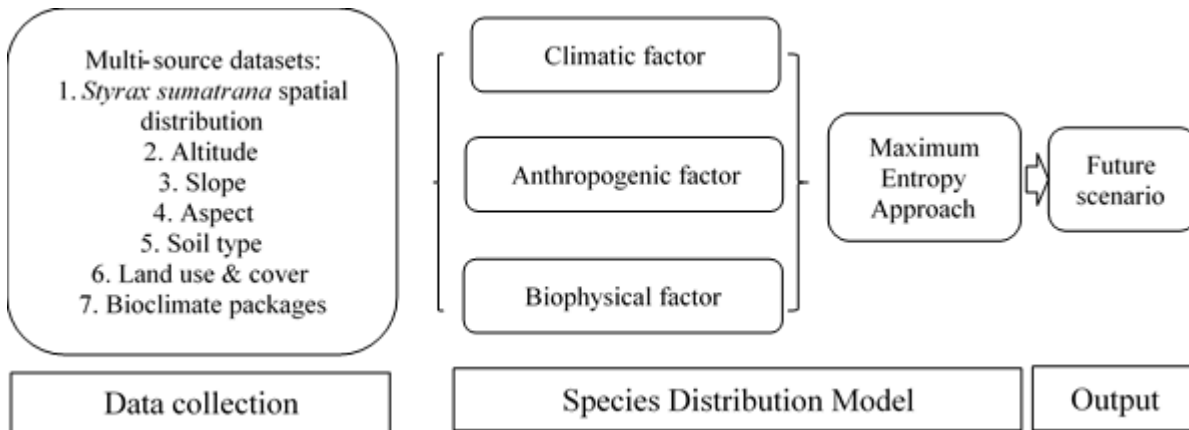


Figure 4. Procedure of the research

The MaxEnt analysis procedures start with the presence data. The presence *Styrax sumatrana* location will be placed into an administrative map of North Sumatra as the base map that will be used to standardize the extent of domain area for each of environmental layers in data sets. Next, we divide those data into three main variables namely Bioclimate, Bio physic, and Anthropogenic. Bio physic consists of altitude, aspect, slope, and soil. Those data considered as the same data for future prediction. Meanwhile, Bioclimate which is consists of 19 bioclimate data that representing precipitation and temperature condition for every monthly, seasonally and annually information have two future scenarios which are RCP4.5 where the temperature estimate increase around 1.4 to 1.8°C and RCP8.5 by estimation 2 to 3.7°C temperature increments globally. Moreover, the LULC changes in the future presented anthropogenic activities will be used to coincide with both climate changes future scenarios. The output will be interpreted by estimate the changes from current to the future scenario where the *Styrax sumatrana* potential distribution occurs.

3.2.4. Future scenarios

We use the climate and anthropogenic variables in the future scenario which are applied in MaxEnt modeling. The 19 Bioclimate represent the climate variable. The scenario was chosen from RCP4.5 and 8.5. The data collected from 4 models namely: CCSM4, CNRM-CM5, MIROC5, and MRI-CGCM3. The future scenario was presented by Hijmans (2005) by interpolated climate surfaces for global land areas at a spatial resolution of 30 arc second that produce a higher spatial resolution data. This data available in www.worldclimate.org (Hijmans, Cameron, and Parra 2005) website for version 1.4 that cover historical, present and future climate packages. Another future scenario was LULC that represented the anthropogenic factor.

We use the raster map of LULC from the year 1990, 2000, and 2010 as the input in the program. The program uses the Artificial Neural Network to analyze the changes and modeling the future scenario of LULC. The Cellular Automata model was used to run the simulation of the projection map. Finally, the validation was made for the LULC map in the year 2010 with the real map in the year 2010. Thus, we apply the simulation for the projection in the year 2050 and 2070 as the same year as climate changes scenario. LULC changes scenario in each year was installed in the same file with both scenarios on climate changes which are RCP 4.5 and 8.5. In this research, we did not divide the LULC scenario into a low and high scenario that represented by RCP 4.5 and 8.5 respectively

4. Results

4.1. LULC prediction

The LULC prediction was calculated using the ANN-CA model. The percentage of area changes was presented by a transformation matrix that used as the input for the neural network to learn the transition probability for every input to produce the LULC output layer. The LULC changes matrix produced by comparing the percentage of LULC area

between LULC in the year 1990 with the year 2000. ANN-CA model shows the prediction of LULC for the year 2010 by calculating the transition probability of every cell in the layer changes between two different LULC raster map by considered the altitude and distance from the road as the explanatory variables. The validation was implemented by comparing the factual LULC in the year 2010 with the prediction LULC in the same year. The simulation shows the percentages of correctness 87.82% with a kappa value of 0.83. The percentages of correctness show the percentage of predicted area that precisely same as the real area in the same year. The kappa value shows the degree of accuracy and reliability in a statistical classification. The value 0.83 show the high agreement between two LULC different maps in the same year (Landis and Koch 2016).

LULC prediction shows the land use changes of the suitable LULC classification for *Styrax sumatrana*. To underline the impact of LULC on *Styrax sumatrana* distribution in MaxEnt, the changes of land use classification need to consider. The percentages of changes presented in table 2.

Table 2. Percentage of land use land cover changes

Classification	Percentage (%) of land use changes				
	2070-2050	2070-2000	2050-2000	2010-2000	2000-1990
Crop	-0.0012	-1.2860	-1.2848	-0.9777	1.3730
Forest and Plantation	-0.0477	-1.7256	-1.6779	-1.5164	-1.9777
Garden and rice field	0.0073	0.3606	0.3532	0.6102	0.0485
Shrub	0.0220	0.1768	0.1547	0.0471	-1.2761

They are 12 classifications that used in the analysis where four classifications were chosen as the potential distribution area for *Styrax sumatrana*. MaxEnt provides the information for categorical data to underline the category that has presence record data information and the suitable probability of *Styrax sumatrana* in every category. The MaxEnt result for LULC variable show crop; forest and plantation; garden and rice field and shrub have the highest probability for *Styrax sumatrana* distribution. The changes of those areas shifted the potential distribution of *Styrax sumatrana* in the future scenario. Table 8 revealed the percentage of shrub and garden and rice field will higher around 0.1547% and 0.3532% between 2000 to 2050 and 0.0220 and 0.0073% between 2050 to 2070 respectively. However, the crop and forest and plantation area will decrease by 1.24848% and 1.6779% between 2000-2050 followed by 0.0012% and 0.0477% between 2050 to 2070 respectively. The changes trend followed the changes from 2000 to 2010.

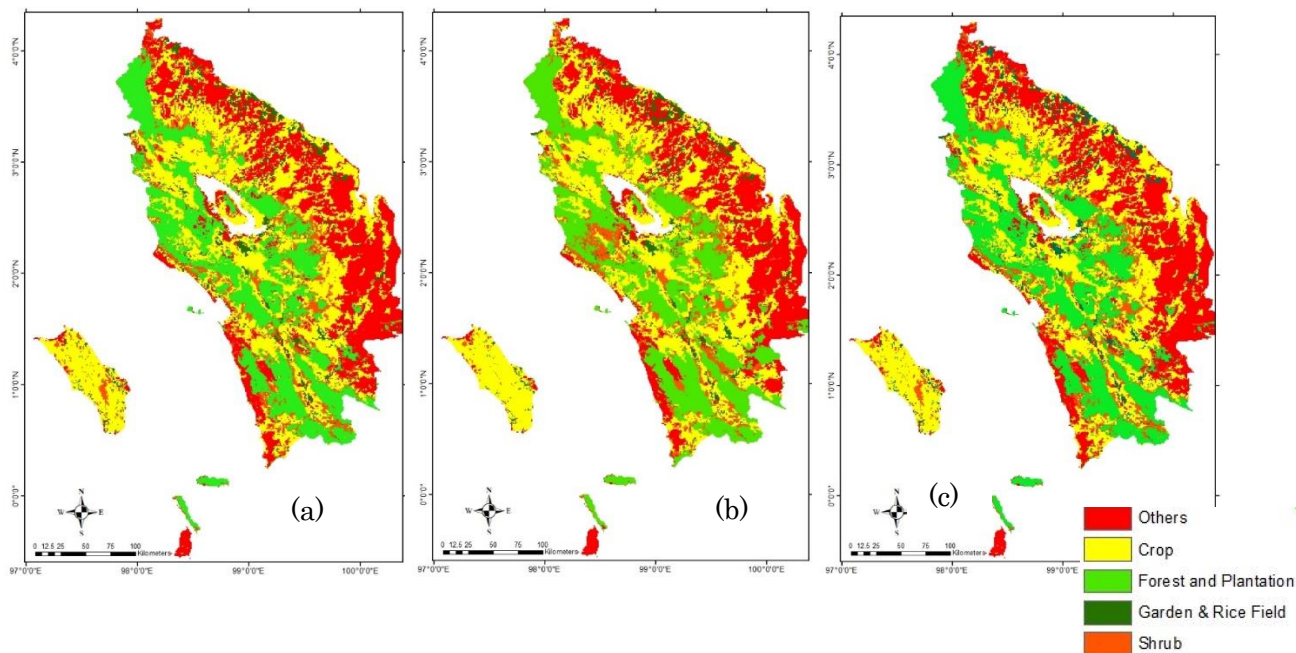


Figure 5. The LULC classification based on the suitable land use for *Styrax sumatrana* by maxent model (a) the LULC at the present year 2000, (b) the LULC prediction in the year 2050, (c) the LULC prediction in the year 2070

4.2. Species distribution of *Styrax sumatrana*

Based on the species occurrence they are 63 individual trees location that has been recorded. From this number, 34 presence records used for training. The number decrease because of the 1 km² resolution that used at raster map. However, the omission on the training sample close enough with the predicted omission that shows the training sample represented the area well.

Maximum entropy program output gives the result of Area Under Curve (AUC) for validated the performance of the model. The result showed the AUC number is 0.949. The highest value in AUC describes the best model by considered all variable that used in the model and the lower than 0.5 show the model not even good rather than random prediction.

The probability potential area for *Styrax sumatrana* distributed in the region based on the variable that includes in the model. The probability values ranging from 0 to 1 where the higher values show the highest probability for the species to distribution in the site. The color in figure 8 represent the potential distribution for *Styrax sumatrana* and the white plot show the occurrence tree that being use as a sample.

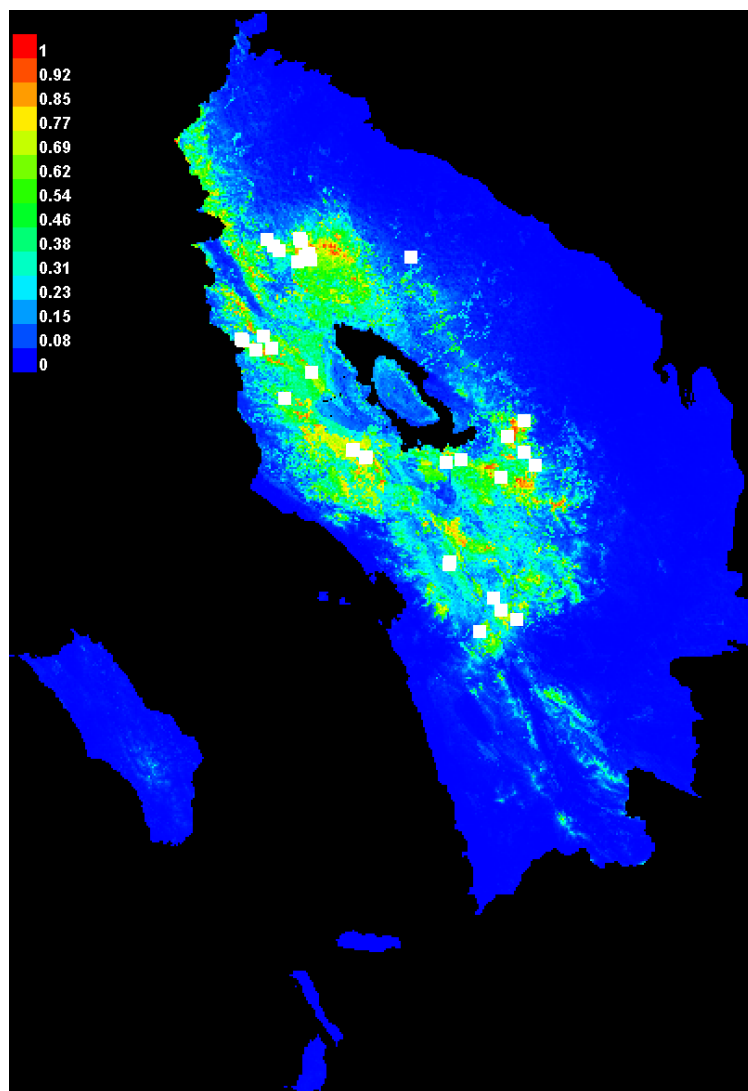


Figure 6. The presence suitability of *Styrax sumatrana* using MaxEnt program

The result in the Maximum Entropy model shows the probability of area that suitable distribution for *Styrax sumatrana* in North Sumatra region spreading around LTCA. The warm color (yellow to red) cover the area in small percentages. The suitable area represented by the probability values that show besides the colors that ranged from 0.4 to 1.

The other results provide the percent contribution of each variable that being use as environmental input in the model. High contribution shows the value of the variable in decided the potential distribution of each grid in the area. The percent contribution of the variable in the MaxEnt model provided in table 3.

Table 3. percent contribution for every variable in the MaxEnt model

Variable	Description	Percent contribution
bio 11_styrax	Mean temperature of coldest quarter	28.5
alt_styrax	Elevation	26.3
lulc_styrax	Land use and land cover	15.4
soiltype_styrax	type of soil based on FAO classification	7.4
bio2_styrax	Annual mean diurnal range temperature	5
bio19_styrax	Precipitation of coldest quarter	3.1
aspect_styrax	The degree of aspect related compass	2.8
bio3_styrax	Iso-thermality	2.7
bio17_styrax	Precipitation of driest quarter	2.3
bio16_styrax	Precipitation of wettest quarter	2.1
slope_styrax	The degree of slope	1.5
bio18_styrax	Precipitation of warmest quarter	0.7
bio15_styrax	Precipitation seasonality	0.5
bio5_styrax	The Maximum temperature of warmest month	0.4
bio7_styrax	Annual temperature range	0.4
bio4_styrax	Temperature seasonality	0.3
bio13_styrax	precipitation of wettest month	0.2
bio8_styrax	Mean temperature of wettest quarter	0.1
bio6_styrax	The Minimum temperature of the coldest month	0
bio10_styrax	Mean temperature of warmest quarter	0
bio14_styrax	Precipitation of driest month	0
bio9_styrax	mean temperature of the driest quarter	0
bio12_styrax	Annual precipitation	0
bio1_styrax	Annual mean temperature	0

High percent contribution for the model was noticed by bio 11 (the mean temperature of the coldest quarter). This variable has 28.5% contribution to predicting the potential area for *Styrax sumatrana* distribution area in North Sumatra region. While 26.3% by elevation and 15.4% by LULC. The other 2 variables that have more than 5% contribution are soil type and annual mean diurnal range temperature by 7.4% and 5% respectively. In this research, we considered the variable that represents the Bioclimate (temperature and precipitation), Anthropogenic (LULC) and Bio physic (Altitude and Soil type) that have high percent contribution to be discussed. Even though, the others variable still have the impact to estimate the potential distribution area for *Styrax sumatrana*. The changes in the future affect the model and total area that suitable for this species to survive and distributed.

4.3. Climate changes impact on *Styrax symatrana*

The climate change impact was measured by the future prediction of *Styrax sumatrana* distribution in two different times which is 2050 and 2070. As the base distribution model of *Styrax sumatrana*, the result at present year was produced by implementing the climate package for present time and LULC raster map at the same time. The result of species distribution modeling presented in figure 7.

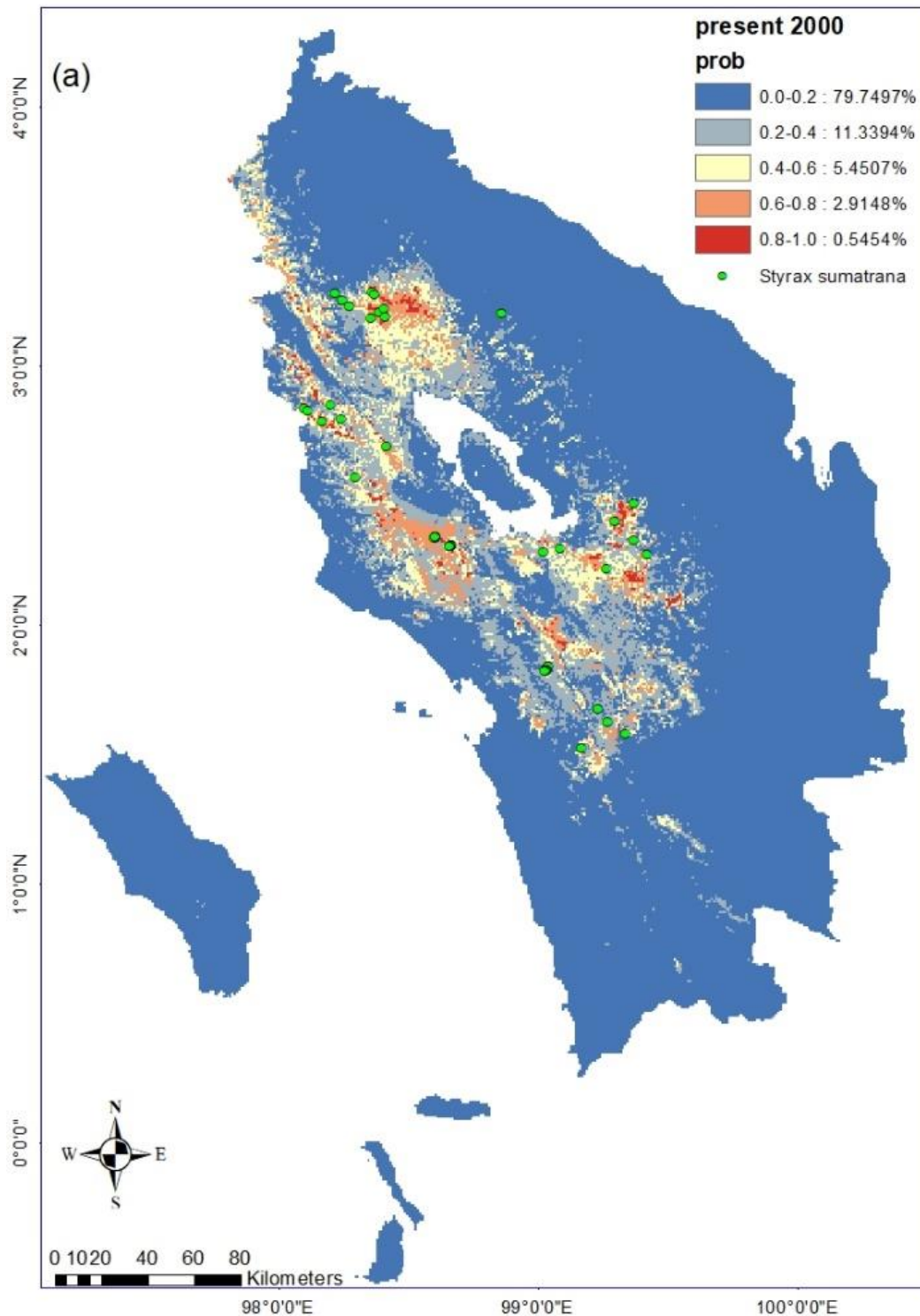


Figure 7. Potential distribution model of *Styrox sumatrana* at present year (2000) (a). The probability of presence as predicted by the MaxEnt model (0-1) is shown with the percentage of area for each suitable classification. The green points show the occurrence of trees in site

The figure 7 showed the total area that highly suitable for *Styrox sumatrana* is 0.5454% of the total area with the probability between 0.8 to 1. The area becomes wider by the decreased probability for *Styrox sumatrana* to distributed. The future prediction shows the differences in the suitable area between four models as the input in climatic factor. The MaxEnt output provides 8 results of the future probability distribution for each prediction year. However, the differences between models have the same direction of the probability of distribution area for *Styrox sumatrana*. The comparison of suitability area changes for each scenario provided in figure 8.

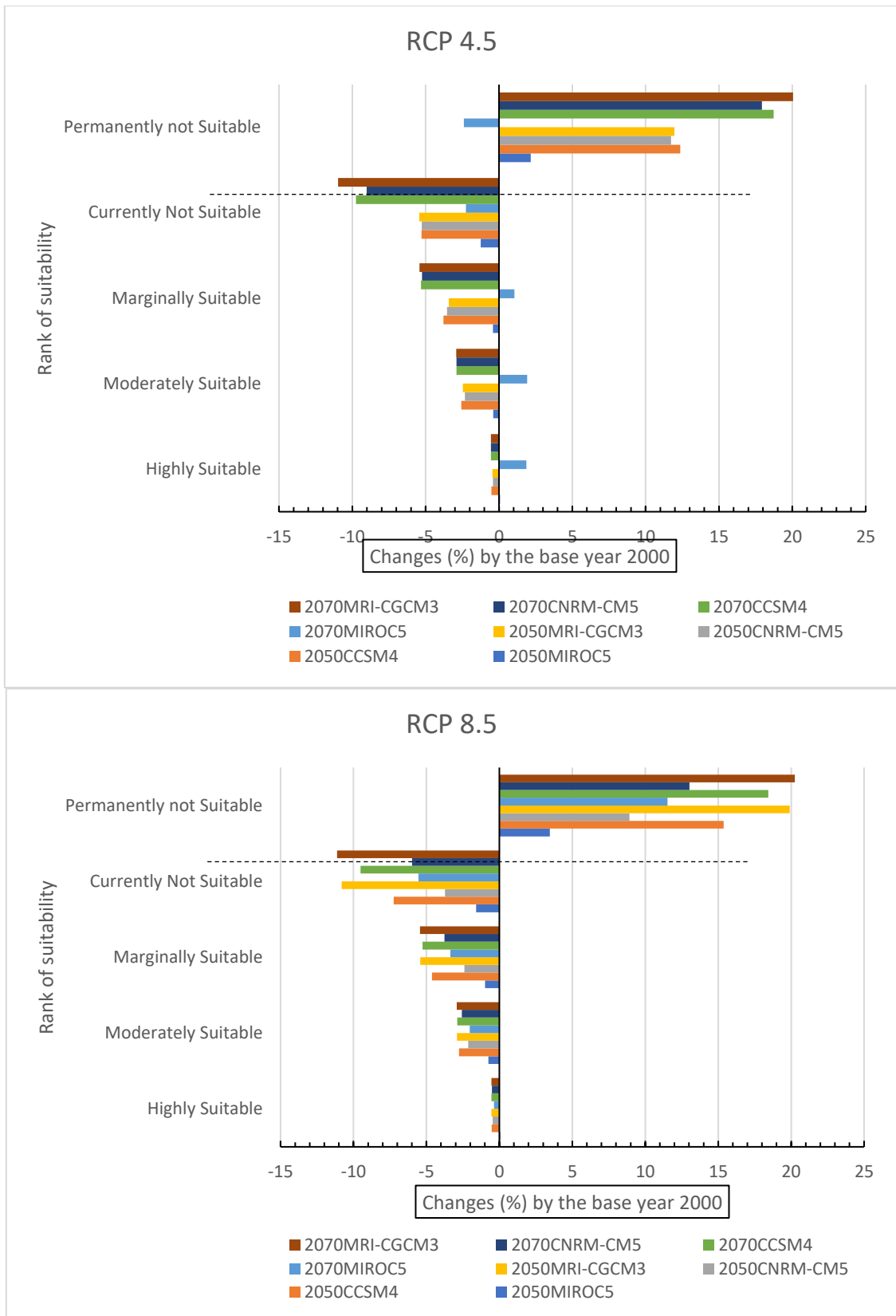


Figure 8. The comparison between 4 models of the climatic factor by the different year for RCP scenario 4.5 (a) and RCP scenario 8.5 (b).

The result from 4 models per each scenario was overlaying by giving the same weight for each model to produce the average suitable area for *Styrax sumatrana* distribution model. The result was applying in the projection map for two scenarios which is 4.5 and 8.5 which is presented in figure 9.

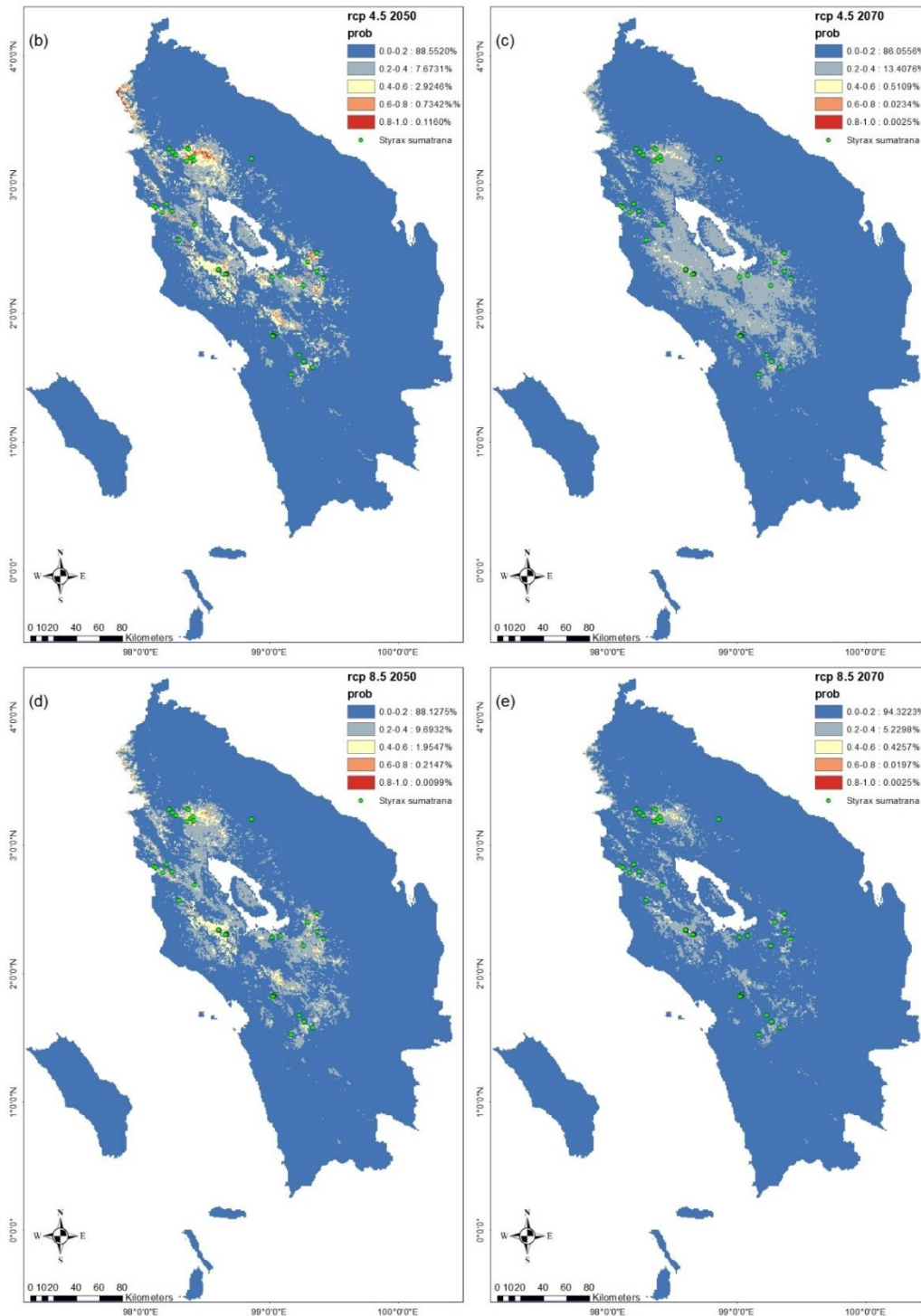


Figure 9. The number presented the percentage of suitable area for *Styrax sumatrana* distribution by equal distribution of probability 20 % which is represented by color. Blue (light and dark) shown the area that not suitable or probability < 40 % and the others as the suitable area. The projection map by 4.5 scenarios in 2050 (b) and in 2070 (c); by 8.5 scenarios in 2050 (d) and in 2070 (e)

The climate change impact for *Styrax sumatrana* has been calculated using MaxEnt program by added two scenarios for 2050 and 2070 years. The result was showed in table 4.

Table 4. Percentage (%) of suitable area for *Styrax sumatrana* distribution per year

Climate Change Scenario	Percentage (%) of suitable area for <i>Styrax sumatrana</i> distribution per year		
	2000	2050	2070
RCP4.5	8.91	3.87 (2.05-8.19)	3.54 (0.03-13.76)
RCP8.5	8.91	3.04 (0.03-7.27)	1.36 (0-3.15)

The percentage that presented in the table is the total suitable area from three probability class highly suitable, moderately suitable and marginally suitable that probabilities are ranged from 0.4 to 1. During the number of models that were used in projection, the average percentage of the area was used in each year by showing the range from low to high area that suitable for *Styrax sumatrana*. The first scenario shows the potential distribution in 2050 is 3.87% followed with 3.54% in 2070. The result in the second scenario drops from 3.04% in 2050 to only 1.36% in 2070. The range in RCP8.5 prevails the extinction of *Styrax sumatrana* in 2070 with 0% of the potential distribution in the North Sumatra region.

5. Discussion and Limitation

5.1. Maximum Entropy result

Maximum entropy provides the result of potential distribution for *Styrax sumatrana* in certain areas that sufficient by environment requirement. *Styrax sumatrana* is the species that rely on the dry soil which mean it cannot survive in the inundated area. The high porosity on soil is important for this species to survive (Jayusman 2014). The result shows that mean temperature of the coldest quarter and precipitation of coldest quarter have a great contribution to the model. This means that the temperature and precipitation in the coldest quarter is the variable that creates the limitation for the species to survive. The MaxEnt result present that the high probability for *Styrax sumatrana* distribution located in the area with the temperature below 22°C and precipitation between 390-400 mm/day in the coldest quarter.

The temperature increase in the future scenario shows the extinction for most of the current location in the North Sumatra region. The high temperature over the species sufficient threshold can lead to the extinction and drought for the species (Sohel et al. 2017). Most of the area that suitable in current condition was distributed on the altitude more than 600 to 2,000meter asl. However, the future scenario shows that most of the tree in lower altitude will be extinct and survive in the mountainous area.

The future scenario shows that the increase in temperature in 2050 and 2070. This condition shifting the suitable area for *Styrax sumatrana* from the area around LTCA to the northern of LTCA (showed in figure 10). This area has the high altitude rather than other places. This shows that the temperature has a linear correlation with the increasing of elevation. This distribution area has a similar condition with the research that shows the pines tree in Southeast Asia will increase in highland and reduce in lowland area due to the increasing of mean annual temperature, seasonal temperature and annual precipitation (Zonneveld et al. 2009), the research by Rodrigues (2015) shows the reduction area for three species in Brazilian tropical dry forest and completely lost by 2080. In his research precipitation of wettest quarter and temperature seasonality have the high percent contribution for the suitability area probability.

The altitude of styrax distribution ranged from 600 to 2,000 m above sea level (Jayusman 2014). This altitude provides the best condition for the *Styrax sumatrana* to distributed as the result form MaxEnt probability distribution prediction area. This result supported by the same research for *Styrax sumatrana* that being implemented in North Sumatra region using the GIS analysis that gives the high value for elevation as the important variable for *Styrax sumatrana* to distribute in the area (Sunandar 2012). This variable followed by the LULC of the area. The jackknife analysis interpreted that LULC is the important variable that will decrease the probability of distribution when its omitted from the model. *Styrax sumatrana* is the species that mostly spread around human settlement as Styra garden (García-Fernández, Casado, and Ruiz Pérez 2003) besides in Forest and shrub area where the competition of nutrition is less (Jayusman 2014). The changes of the LULC give the direct impact on the distribution of *Styrax sumatrana* due to the decreasing of the forest and crop area where the species occurrence is highest besides the garden and rice field and shrub area.

5.2 Impacts of land use changes

The management of *Styrax sumatrana* has been developed for a decade in the indigenous forest management systems (García-Fernández, Casado, and Ruiz Pérez 2003). This management represents the harmony of the economic, ecological and social objective in forest management. However, the changes of LULC create the disturbances in this management from the economic,

ecologic and in the social aspect.

One of the indigenous forest management in North Sumatra is Benzoin garden or known as the *Styrax sumatrana* garden. This species is important for the forest community that depends on the benzoin from the *Styrax sumatrana* yield. The research shows that the total area of *Styrax sumatrana* has a positive correlation with the production of *Styrax sumatrana* benzoin (Purba, Budiani, and Mardhiansyah 2017). This condition shows that the reduction of area for the *Styrax sumatrana* to distributed will decrease the income for the forest community as also known as the benzoin farmers. In economic value, *Styrax sumatrana* benzoin gives the income for the benzoin farmers around 47.64% to 79.23% from the total income. This sample collected from 3 - 4ha area of benzoin garden which produces 98 - 554kg/ha benzoin per year(Purba, Budiani, and Mardhiansyah 2017; Jayusman 2014). For the ecological aspect, the reducing of suitable area correlated with the land use change of the forest and crop area. The research shows this area give the high percentage of the *Styrax sumatrana* to regrowth from the coppice system which is used to regenerate the trees without cutting the trees(García-Fernández, Casado, and Ruiz Pérez 2003). MaxEnt result shows the high probability of this species to distribute are in the crop, forest, open area and garden and rice field. Meanwhile, the scenario from MOLUSCE model shows the deforestation increase by the changes to plantation (5%) and open area (2%). Even the other suitable area such as garden and rice field and open area increase, the value is below the deforestation and conversion from crop to other land use. These land use changes give the impact to the future projection of *Styrax sumatrana* distribution that will decrease. In social aspect, the land use change mostly occurs as the intervention of plantation company that occupied the forest, crop and garden area from the benzoin farmer and other forest community(Ambarita and Sitorus 2015). The benzoin or styrax garden is an important area that contributes to forest and green area protection. The yield from the *Styrax sumatrana* as the non-timber product is essential in rehabilitation and reforestation program. However, the changes in LULC and the impact of climate change in the future will be the challenge for the forest management authority. In one hand the rehabilitation with the valuable tree species (*Styrax sumatrana*) is beneficial, on the other hand, the suitable area will decrease in the future. When the authority changes the species, most of the farmers will be shifting from the benzoin farmer to other farmers such as coffee, vegetable, or migration to the urban area. Furthermore, the forest sustainability will decrease and change into the plantation, or residential area. While many farmers loss of a job and income.

The MaxEnt result shows the suitable area for *Styrax sumatrana* at the present time is 8.91% of the total area of North Sumatra which is 71,068.68 km². However, the forest area in LULC classification will reduce. The scenario shows that in 2050 and 2070 this area will decrease by 2.9% and 3.01 % respectively. Moreover, the suitable area in the RCP scenario will decrease 3.87% in 2050 and 3.54% in 2070 by RCP 4.5 and 3.04% in 2050 and 1.36% in 2070 by 8.5 scenario.

Finally, the land use change will give the impact on economic, ecologic and social aspect for the benzoin farmers, *Styrax sumatrana* distribution and forest management system. The *Styrax sumatrana* distribution in the future will decrease as the impact of climate change that supported by the land use changes.

5.3 Limitations

This research uses the Maximum entropy model to assess the impact of climate change on the *Styrax sumatrana* distribution and the MOLUSCE program to predict potential changes of LULC for the years of 2050 and 2070. However, several limitations were raised during the research as follows:

- The input data used in this research still have limitations. The number of sample and diversity is low, which give the drawback to analysis the data using MaxEnt model. The input data for LULC collected from the secondary data which is needed to produce the more suitable prediction.
- The number of station and climate data need to increase for better evaluation and validation. The future climate data used in this research is limited to four models from CMIP5 and two scenarios such as RCP4.5 and RCP8.5.
- The resolution that was used is around 1km² is rather rough for LULC analysis. The detail of LULC area can be a merge between one classification with another classification.

6. Things to be done further

The result still has limitations that need to be solved in the future. Regarding to the objectives of this research, further improved research need to be done.

- The higher resolution (around 30 meters) can be used to produce more detail classification of LULC.
- Providing the primary data for LULC from satellite image to produce better LULC map
- Increasing the sample number and location to minimize the bias and increase the data to analyze. The comparison with data in low altitude can be used to improve the analysis.
- Upgrade the number of climate model and station for improve the validation.
- Extent the research area to broaden the probability for species distribution area

References

- Affandi, Oding, and Alfonsus H. Harianja. 2008. "Sistem Tenurial Dan Pengelolaan Lahan Secara Kolaboratif." ITTO PROJECT PD 394/06 REV.1 (F). ITTO Project, CFNCRD and Pusat Penelitian dan Pengembangan Hutan dan Konservasi Alam.
- Ambarita, Elisabeth Christina, and Hendry Sitorus. 2015. "Modal Sosial Komunitas Petani Kemenyan Dalam Pelestarian Hutan Kemenyan Di Desa Pandumaan, Kecamatan Pollung, Kabupaten Humbang Hasundutan." *PERSPEKTIF SOSIOLOGI* 3 (1): 42–57.
- Anas, Aswandi, and Cut Rizlani Kholibrina. 2017. "Estimation Models for Incense Resin Productivity (Styrax Sumatrana J.J. SM) in North Sumatra." *Jurnal Penelitian Kehutanan Sumatrana Jurnal* 1 (1): 10–21.
- . 2018. "Growth and Yield Model for Non-Timber Forest Product of Kemenyan (Styrax Sumatrana J . J . Sm) in Tapanuli , North Sumatra Growth and Yield Model for Non-Timber Forest Product of Kemenyan (Styrax Sumatrana J . J . Sm) in Tapanuli , North Sumatra." In *IOP Conference Series: Earth and Environmental Science* 122 012036. IOP Publishing. <https://doi.org/10.1088/1755-1315/122/1/012036>.
- Benítez-Badillo, Griselda, Maite Lascurain-Rangel, José Luis Álvarez-Palacios, Jorge Antonio Gómez-Díaz, Sergio Avendaño-Reyes, Raymundo Dávalos-Sotelo, and Juan Carlos López-Acosta. 2018. "Influence of Land-Use Changes (1993 and 2013) in the Distribution of Wild Edible Fruits From Veracruz (Mexico)." *Tropical Conservation Science* 11: 194008291875866. <https://doi.org/10.1177/1940082918758662>.
- Booth, Trevor H., Tom Jovanovic, and Chris E. Harwood. 2014. "A Generic Method for Climate Change Impact Analysis of Tree Species Planting Domains." *New Forests* 45: 507–522.
- Dait, Jennifer Madonna G. 2015. "Effect of Climate Change on Philippine Agriculture." *International Journal of Science and Research (IJSR)* 4 (9): 1922–24.
- Dale, Virginia H. 2001. "Climate Change and Forest Disturbances." *BioScience* 51 (9): 723–34.
- Dove-Thompson, Darlene, Cheryl Lewis, Paul A. Gray, Cindy Chu, and Warren I. Dunlop. 2011. "A Summary of the Effects of Climate Change on Ontario's Aquatic Ecosystems." CRR-11. Ontario: Ontario Ministry of Natural Resources.
- García-Fernández, Carmen, Miguel A. Casado, and Manuel Ruiz Pérez. 2003. "Benzoin Gardens in North Sumatra, Indonesia: Effects of Management on Tree Diversity." *Conservation Biology* 17 (3): 829–36. <https://doi.org/10.1046/j.1523-1739.2003.01487.x>.
- Hartini, Sri, and Dwi Murti Puspitaningtyas. 2005. *Flora Sumatera Utara Eksotik Dan Berpotensi*. Bogor: Pusat Konservasi Tumbuhan Kebun Raya Bogor, LIPI.
- Hijmans, Robert J., Susan E. Cameron, Juan L. Parra, Peter G. Jones, and Andy Jarvis. 2005. "Very High Resolution Interpolated Climate Surfaces for Global Land Areas." *International Journal of Climatology* 25 (15): 1965–78. <https://doi.org/10.1002/joc.1276>.
- Hijmans, Robert J., Susan Cameron, and Juan Parra. 2005. "Worldclim." Very High Resolution Interpolated Climate Surfaces for Global Land Areas. 2005. <http://worldclim.com/version1>.
- Jayusman. 2014. *Mengenal Pohon Kemenyan (Styrax Spp .)*. Edited by Mohammad Na'iem, Mahfudz, and Sigit Prabawa. Jakarta, Indonesia: IPB Press.
- Kholibrina, Cut Rizlani, Aswandi Anas, and A Susilowati. 2018. "Flowering and Fruiting Phenology of Kemenyan Toba (Styrax Sumatrana J . J . Sm .) in AekNauli." In *IOP Conference Series: Earth and Environmental Science* 122 (2018) 012061.
- Landis, J Richard, and Gary G Koch. 2016. "The Measurement of Observer Agreement for Categorical Data Published by : International Biometric Society Stable URL : <Http://Www.Jstor.Org/Stable/2529310>" 33 (1): 159–74.
- Li, Xia, and Anthony Gar-On Yeh. 2002. "Neural-Network-Based Cellular Automata for Simulating Multiple Land Use Changes Using GIS." *International Journal of Geographical Information Science* 16 (4): 323–43. <https://doi.org/10.1080/13658810210137004>.
- Measey, Mariah. 2010. "Indonesia: A Vulnerable Country in the Face of Climate Change." *Global Majority E-Journal* 1 (1): 31–45.

- NextGIS. 2018. "MOLUSCE (Modules for Land Use Change Simulations)." <http://hub.qgis.org/projects/molusce>.
- Nimasow, Gibji, Oyi Dai Nimasow, Jawan Singh Rawat, Gendan Tsering, and Takom Litin. 2016. "Remote Sensing and GIS-Based Suitability Modeling of Medicinal Plant (*Taxus Baccata* Linn.) in Tawang District, Arunachal Pradesh, India." *Current Science* 110 (2): 219–27. <https://doi.org/10.18520/cs/v110/i2/219-227>.
- O'Donnell, Michael S., and Drew A Ignizio. 2012. "Bioclimatic Predictors for Supporting Ecological Applications in the Conterminous United States." *U.S Geological Survey Data Series* 691, 10.
- Phillips, Steven. 2008. "A Brief Tutorial on Maxent." *AT&T Research*, 1–38. <https://doi.org/10.4016/33172.01>.
- Phillips, Steven J., and Miroslav Dudík. 2008. "Modeling of Species Distribution with Maxent: New Extensions and a Comprehensive Evaluation." *Ecography* 31 (December 2007): 161–75. <https://doi.org/10.1111/j.2007.0906-7590.05203.x>.
- Phillips, Steven J., Miroslav Dudík, and Robert E. Schapire. 2017. "[Internet] Maxent Software for Modeling Species Niches and Distributions (Version 3.4.1)." http://biodiversityinformatics.amnh.org/open_source/maxent/.
- Phillips, Steven J, Robert P Anderson, and Robert E. Schapire. 2006. "Maximum Entropy Modeling of Species Geographic Distributions." *Ecological Modelling* 190: 231–59. <https://doi.org/10.1016/j.ecolmodel.2005.03.026>.
- Phillips, Steven J, M Dudík, and R E Schapire. 2004. "A Maximum Entropy Approach to Species Distribution Modeling." *Twentyfirst International Conference on Machine Learning ICML 04* 69: 83. <https://doi.org/10.1145/1015330.1015412>.
- Purba, Binton Harianto, Evi Sri Budiani, and M Mardhiansyah. 2017. "REVENUE CONTRIBUTION THE COMMUNITY FORESTS OF *Styrax* Spp. ON FARMERS HOUSEHOLD INCOME." *Jurnal Ilmu-Ilmu Kehutanan* 1 (2): 10–17. <https://ejournal.unri.ac.id/index.php/JIHK/article/view/4559>.
- Ray, Duncan, Dave Wainhouse, Joan Webber, and B Gardiner. 2008. "Impacts of Climate Change on Forests and Forestry in Scotland." EH25 9SY. *Forest Research Report*. Scotland: Forestry Commission Scotland. http://sccr.ac.uk/downloads/cci_ray.pdf.
- Rodrigues, P M S, J O Silva, P V Eisenlohr, and Cegr Schaefer. 2015. "Climate Change Effects on the Geographic Distribution of Specialist Tree Species of the Brazilian Tropical Dry Forests." *Brazilian Journal of Biology* 75 (3): 679–84. <https://doi.org/10.1590/1519-6984.20913>.
- Silalahi, Johansen, and Ahmad Dany Sunandar. 2017. *Kemenyan (Styrax Spp .) Getah Berharga Tano Batak*. Forestry Research of Aek Nauli.
- Sohel, Shawkat Islam, Sayma Akhter, Hadayet Ullah, Ekramul Haque, and Parvez Rana. 2017. "Predicting Impacts of Climate Change on Forest Tree Species of Bangladesh: Evidence from Threatened *Dysoxylum Binectariferum* (Roxb.) Hook.f. Ex Bedd. (Meliaceae)." *IForest* 10 (1): 154–60. <https://doi.org/10.3832/ifor1608-009>.
- Sunandar, Ahmad Dany. 2012. "Peta Kesesuaian Jenis Kemenyan (*Styrax* Spp .) Di Sumatera Utara (Utilization of Geographic Information System to Develop Land Suitability Map for *Styrax* Spp . in North Sumatera)." *Jurnal Penelitian Hutan Tanaman* 9: 63–73.
- Utomo, Budi, Afifuddin Dalimunthe, and Frans Hutagalung. 2015. "Public Perception on the Success of Reforestation in a Degraded Land" 5: 422–28. <https://doi.org/10.17265/2161-6264/2015.06.007>.
- Vlam, Mart, Patrick J. Baker, Sarayudh Bunyavejchewin, and Pieter A. Zuidema. 2014. "Temperature and Rainfall Strongly Drive Temporal Growth Variation in Asian Tropical Forest Trees." *Oecologia* 174: 1449–1461.
- Zonneveld, M van, J Josjela, B Vinceti, and A Jarvis. 2009. "Impact of Climate Change on the Distribution of Tropical Pines in Southeast Asia." *Unasylva* 60: 24–28.

Quantitative Assessment of Climate Change Impacts on Flood-Prone Areas in Davao Oriental, Philippines

Jonathan Salar Cabrera^{1,2}

¹Graduate School for International Development and Cooperation, Hiroshima University, 1-5-1 Kagamiyama, Higashi-Hiroshima 739-8529, Hiroshima, Japan.

²Institute of Computing and Engineering, Davao Oriental State College of Science and Technology, Guang-guang, Dahican, Mati City, Davao Oriental. E-mail: jonathan.cabrera@doscst.edu.ph

Abstract

Flooding is one of the major destructive natural disasters in Davao Oriental, Philippines, and results primarily from a high incidence of typhoons and heavy rainfalls. The main objective of this study was to identify flood-prone risk areas by mapping them based on the integration of multi-criteria data, including rainfall, slope, elevation, drainage density, soil type, distance to the main channel and population density. For this purpose, a GIS-based flood risk spatial assessment was conducted by using analytic hierarchy process (AHP), weights by rank (WR), and ratio weighting (RW) frameworks in the province of Davao Oriental. The multi-criteria analysis using the AHP, WR, and RW methods allowed the integration of several indicators under two criteria, hazard and vulnerability, for flood risk mapping. The comparison results shows that AHP is the most appropriate method among them to assess flood hazard. The multi-criteria analysis using the AHP method allowed the integration of several indicators under two criteria, hazard and vulnerability, for flood risk mapping. The resulting flood risk map shows that 94.03% of Davao Oriental is presently under the low and moderate flood risk categories, and those categories should slightly decrease to 93.46% in the future. The high and very high flood risk areas cover approximately 2% of the province at present and show no dramatic change in the future. Presently, 19 out of the 183 barangays (towns) are at high risks of floods, whereas in the coming years, only one barangay will be added to the very high risk of floods. These barangays under the high category of flood risk are primarily situated on riversides and coastal areas. Thus, immediate actions from decision-makers are needed to develop a community-based disaster risk plan under the future conditions.

Keywords: flood risk, ranking, rating, analytic hierarchy process, multi-criteria analysis, Davao Oriental, GIS

1. Introduction

1.1 Background

Flooding is considered one of the most serious and widespread natural hazards due to its devastating effects that endanger lives and cause property damage in the affected areas (Danumah et al., 2016; Elkhrachy, 2015; Forkuo, 2011; Gigović et al., 2017; Kazakis et al., 2015; Papaioannou et al., 2015). The changing climate behaviour of extreme rainfalls and typhoons are the primary contributors to this problem. Human activities such as urbanization and the growth of settlements and assets in flooding areas likewise contribute to the increasing impacts of floods (Danumah et al., 2016; Gigović et al., 2017).

Phenomena commonly contributed to flooding are the limited capacity of river channels, human settlements in low-lying areas and rapid growth of human settlements without upgrading the drainage infrastructures. The problems related to flooding have increased extensively, and there is a need for efficient modelling to help mitigate the worst effects of flood disasters (Otieno, 2004). Effective modelling will help in proper flood risk management planning and provides various insights into addressing the hazard and disaster problems. It is necessary to establish and implement a systematic approach to define areas that may have disastrous flood events.

Hazard mapping is a vital component of flood risk management. A flood hazard map shows the extent of water level in a flooded area. Another critical element in flood risk management is flood risk mapping, which shows the potential risk to the population, economy and environment due to flooding (Gigović et al., 2017).

In the Philippines, the occurrence of natural hazards and disasters is frequent due to the physical environment of the country, which faces the Pacific Ocean where catastrophic typhoons originate from. Furthermore, the Philippines is located in a part of the Pacific Ring of Fire. The Philippines is vulnerable to typhoons, floods, earthquakes, storm surges, and tsunamis (Gurenko and Lester, 2004). The primary causes of the disasters in this area are typhoons and flooding because of their frequent occurrence and their magnitude of impact to the society. Approximately 20

typhoons per year approach or make landfall, and this is the highest frequency of typhoon events in the entire world (Otieno, 2004).

On the other hand, Mindanao Island, as described, is known to be rather typhoon free regions with less flood and storm surge risk in the Philippines. However, disasters due to tropical storm Sendong (international name, Washi) in 2011 and Super Typhoon Pablo (international name, Bopha) in 2012 changed that. Mindanao is now considered to be in one of the typhoon paths. These two deadly storms killed more than 1,000 persons and led to approximately 100 missing persons because of heavy rains that triggered the rivers to overflow and that caused flash floods and landslides (National Disaster Risk Reduction and Management Council, 2012a, 2012b). Davao Oriental is located in the southeast of Mindanao Island, and disasters due to floods and storm surge in this region are anticipated to be more frequent under global warming. Therefore, Davao Oriental is considered for the study area.

Because of the prevailing occurrences of natural disasters that regularly hit the Philippines, the government created a law to reinforce preparation for possible calamities. The Republic Act 10121, also known as An Act Strengthening the Philippine Disaster Risk Reduction and Management (DRRM) System, was implemented, providing the national disaster risk reduction and management framework and institutionalizing the national disaster risk reduction and management plan (Republic of the Philippines, 2010). Despite the enactment of the DRRM law, the local government units were not ready to face natural calamities such as typhoons and heavy rainfalls that cause massive flooding. Thus, effective flood risk assessment and strategies should be established, especially at the barangay (local term for town) level since each barangay area has its own physical and social characteristics.

Even though flooding is a severe hazard in Davao Oriental due to the typhoon, heavy rainfalls and storms, insufficient attention has been paid to flood hazard assessment. Recent scientific work undertaken in the province of Davao Oriental by Lagmay et al. (2017) was concentrated on flood mapping in major river basins, which is a significant research gap identified by this study. They used a piecemeal approach because only river run-off and the inefficiency of the drainage network were considered to cause river overflow, and their study did not provide further insight into the entire province. Another study on the vulnerability assessment after Typhoon Pablo was conducted by Ross (2015) using light detection and ranging (LiDAR) as the primary tool. A high-resolution DEM was used to generate two-dimensional flood simulations of the floodplains using FLO2D. Ross (2015) determined that 12 – 28% of each of the eight municipalities are susceptible to flooding; mostly residential, business and community centers. Ross (2015) also revealed that a storm surge with a height of approximately 1 m reached 500 m inland from the coastline during Typhoon Pablo. Unfortunately, this study focused only on the east coast municipalities, and Typhoon Pablo affected the entire province.

All the flooding-related studies in Davao Oriental are beneficial to providing a spatial presentation of the distribution of the flooded areas. However, no studies have yet to undertake the evaluation and flood risk mapping of the entire province of Davao Oriental using multiple datasets. Thus, the objective of this study is to identify flood-prone risk areas and map them based on several factors that are relevant to the study area. For this purpose, a GIS-based process for the spatial assessment of flood hazard was conducted by using the concepts of the analytic hierarchy process (AHP), ratio weighting (RW), and weights by rank (WR) frameworks with the multi-criteria including rainfall, slope, elevation, drainage density, soil type, distance to the main channel and population density.

1.2 Literature Reviews

1.2.1 Flood risk assessment methodology

There are general three ways of flood susceptibility assessment using; i) hydrological models such as SWAT (Yu et al., 2017), HEC-RAS (Veleda et al., 2017), and FLORA-2D (Manfreda et al., 2015), ii) non-linear machine learning algorithms such as decision tree (Tehrany et al., 2013), artificial neural network (Kia et al., 2012), support vector machine (Hong et al., 2018b), and random forest (Wang et al., 2015), iii) quantitative approaches such as frequency ratio (Tehrany et al., 2017), logistic regression (Tehrany et al., 2017), weights-of-evidence (Tehrany et al., 2017), genetic algorithm (Hong et al., 2018a), differential evolution (Hong et al., 2018a), and analytic hierarchy process (Cabrera and Lee, 2018a; Danumah et al., 2016; Gigović et al., 2017).

The abovementioned methods successfully provided flood susceptibility assessment, but every method faced some limitations. In hydrological modelling, the preparation and calibration of parameters are time consuming (Hong et al., 2018a) and it needs high requirements of computer resources. While the quantitative modelling like statistical and data-driven methods increased the subjectivity as it requires an expert to select the flood conditioning factors. In the non-linear machine learning algorithms, it may lead to poor projections due to the large and inconsistent value ranges in the datasets (Bui et al., 2016; Hong et al., 2018a). In this study, the quantitative approach, AHP, was used for flood risk assessment. Furthermore, other quantitative approaches such as RW, and WR were also applied for flood risk assessment, and their results were compared with that from AHP. These approaches have the capability to include multiple datasets and can be used on limited computer resources. Also, using multiple data sources potentially allows for more reliable disaster risk reduction plan, especially in the context of flood management and mitigation.

For multi-data sources, the multi-criteria analysis approach has become widely used to solve complex phenomena and to assess flood risk (Danumah et al., 2016; Gigović et al., 2017; Wang et al., 2011; Yahaya, 2010).

AHP is a popular and widely used method developed by Saaty (1980) to solve a wide range of multi-criteria decision-making problems, combined with the use of a pairwise comparison matrix that calculates the weights of every criterion considered. The uniqueness of applying AHP in different studies helps in modelling situations of uncertainty without losing subjectivity and objectivity of any evaluation measure (Danumah et al., 2016). Recently, researchers have given considerable attention to using AHP in flood risk assessment. In those case studies, it has been shown that AHP can assess and map flood risk areas with reliable accuracy. However, the result is based on expert opinions and thus may be subjected to intellectual limitations due to uncertainty and subjectivity. In Danumah et al. (2016), AHP was used to integrate several elements under two criteria, hazard and vulnerability, for flood risk assessment and mapping. The slope, drainage density, type of soil, and isohyet were the elements used to generate their hazard map. The land use, population density, and drainage system were the elements used to create their vulnerability map. Danumah et al. (2016) evidenced the reliability and the powerful role of geoinformation techniques in natural disaster assessment that requires the contribution of multi-source data. In Elkhrachy (2015), a flash flood map was generated by using satellite images and the AHP was used to determine the relative impact or weight of flood-causative factors: the runoff, soil type, surface slope, surface roughness, drainage density, distance to the main channel and land use. Gigović et al. (2017) conducted a study of the hazard zone mapping of urban flood-prone areas using a GIS multi-criteria methodology by considering six factors relevant to urban flooding: the height, slope, distance to the sewage network, distance from the water surface, water table, and land use. Their results indicated that the scenario in which the methodology was used provides the highest level of compatibility with historical flooding data. The case studies of Danumah et al. (2016), Gigović et al. (2017), and Elkhrachy (2015) were highly accurate in determining flood risk assessments with different causative factors. However, the result is based on expert opinions and thus may be subjected to intellectual limitations due to uncertainty and subjectivity. Moreover, the criteria differ in each case study because of the availability of data and the characteristics of the study area.

1.2.2 Applications in global scale

A warmer climate would increase the risk of floods (IPCC, 2012). Floods events account for two-thirds of the global population affected by all naturally triggered disaster events (IPCC, 2012). However, only a few types of research (Alfieri et al., 2017; Hirabayashi et al., 2013, 2008; Milly et al., 2002) have projected changes in floods on a global scale. This is primarily because of the limitation of spatial coarse resolution in GCMs. Milly et al. (2002) investigated changes in flood extremes using monthly river discharge data for both gauge observations and GCM simulations. They found that the risk of great floods increased during the 20th century, mainly over the high northern latitudes, and that this increase may continue. Moreover, Milly et al. (2002) and Alfieri et al. (2017) study results indicate a clear positive correlation between atmospheric warming and future flood risk on a global scale. Changes in flood risk are unevenly distributed, with the most substantial increases in Asia, U.S., and Europe. Another study (Hirabayashi et al., 2013), a global-scale flood risk assessment using multiple change models concluded that an ensemble of projections under a new high-concentration scenario demonstrates a substantial increase in flood frequency in Southeast Asia. Furthermore, Hirabayashi et al. (2013) revealed that the global exposure to floods would increase depending on the degree of warming. As a conclusion, the study of (Milly et al., 2002), (Alfieri et al., 2017), and (Hirabayashi et al., 2013) reveals that the Philippines as part of the Southeast Asia is substantially flood-prone country. Thus, flooding in the Philippines is the result of extreme rainfall and typhoon occurrences (Cabrera and Lee, 2018a). The next sub-section will discuss the application of the flood-related studies focusing on the Philippines.

1.2.3 Applications in the Philippines

Over the past decades, recurrent flooding associated with typhoons, monsoons, and heavy rains, has proven to be a significant issue in the Philippines. Recent large-scale floods associated with typhoons Haiyan (Yolanda) in 2013, Bopha (Pablo) in 2012, Nesat (Pedring) and Washi (Sendong) in 2011 as well as Ketsana (Ondoy) and Parma (Pepeng) in 2010 have all led to massive flooding and thousands of casualties (Cadag et al., 2017; Gilbuena et al., 2013). With the continued population growth in hazard-prone areas, it is expected that damage to infrastructures, agriculture, and human losses would persist unless appropriate measures are immediately implemented by the government. Several studies conducted to determine the impacts of floods among the population in the poor urban area (Zoleta-Nantes, 2002), transportation (Yu et al., 2013), education (Cadag et al., 2017), and agriculture (Toda et al., 2017). The agriculture sector is profoundly affected because of the typhoon that brings extreme rainfall and flooding. Toda et al. (2017) conducted a LIDAR-based flood modeling approach for mapping rice cultivation. The study used a LiDAR-based digital elevation model (DEM), river discharge and rainfall data to generate flood inundation maps. By applying spatial analysis, rice cultivation zone maps were derived. This study is instrumental in avoiding damages in rice cultivation even during typhoon season. Thus, a resilient approach to fight against the flooding.

On the aspect of impacts of the flood in the poor urban area, Zoleta-Nantes (2002) conducted impacts of flood hazards among street children, the urban poor and residents of wealthy neighborhoods in Metro Manila,

Philippines. This study argued that being poor is not the only reason why this sector is more vulnerable to floods, the lack of participation in decision making intensify their present and future vulnerability, as well. Several policy recommendations on hazard management and disaster mitigation are identified in this study to reduce flood losses in Metro Manila. Recurrent flooding impacts on educational continuity in the Philippines was conducted by Cadag et al. (2017). This study provides an understanding of the impacts of both large and small-scale floods in the education sector of Metro Manila, Philippines. Findings suggest that impacts of small-scale floods to school communities (students, teacher, and staffs) mainly to the most marginalized students were considerable and their cumulative impacts may be comparable or more important than large-scale floods. However, they remain poorly documented and are not addressed by any disaster risk reduction policies in the country. Also, local capacities of school communities which are more apparent in times of small-scale floods are also neglected. The study then argues that meaningful policies and actions which aim to reduce disaster risk and thus address the global learning crisis in the education sector should fully consider small-scale disasters and floods.

According to Yu et al. (2013), natural disasters cause unexpected disruptions to the flow of goods and services in an economy. These disruptions may affect production in a single sector, but sector interdependence guarantees that this will trickle down to other sectors, leading to increased damages. This study seeks to provide an estimate of the impact of a disruption in the transportation sector in the largest island in the Philippines and its ripple effects. Aside from inoperability, economic loss is also assessed. Results show that the sectors that were strongly affected, both regarding inoperability and economic loss are mainly manufacturing, agriculture and private services.

Flood assessment varies according to its purpose as shown in the abovementioned researches. In this study, the potential impacts of climate change on flood hazards and population risks are investigated using the temperature and rainfall projections from the CMIP5 predictions of the IPCC under the RCP4.5 and RCP8.5 scenarios.

2. Objectives

- To investigate the rainfall projections for the region from the CMIP5 predictions of the IPCC under the RCP4.5 and RCP8.5 scenarios.
- To identify the potential impacts of climate change on flood hazards in the province of Davao Oriental based on the multi-criteria data analysis (MCDA) using Analytic Hierarchy Process (AHP), Ratio Weighting (RW), and Weights by Rank (WR) approaches.

3. Data and methodology

3.1 Data

3.1.1. Rainfall Records

The observed rainfall data were obtained from the Hinatuan and DOST-RXI Stations (Figure 1(D)). The Hinatuan Station has observed daily rainfall data from 1990 to 2015. The DOST-RXI Station has observed daily rainfall data from 2006 to 2015. These two stations are far from the boundary of Davao Oriental. The distances of the Hinatuan and DOST-RXI Stations from the nearest border of the province are 43.9 km and 33.4 km, respectively, as shown in Figure 1(D). Therefore, using the rainfall data from these two stations would give an unreliable result because of their geographic locations.

To address the geographic limitation of the weather stations, rainfall data were obtained from the National Climate Data Center (NCDC) and the Global Precipitation Climatology Centre (GPCC) (Table 1). The NCDC rainfall data are the global daily forms of precipitation with a spatial grid resolution of 0.5° latitude x 0.5° longitude. In contrast, the GPCC rainfall data are the global daily forms of precipitation on a regular grid with a spatial resolution of 1.0° latitude x 1.0° longitude. The rainfall data from sixty-three coordinates were extracted within the boundary of Davao Oriental (Figure 1(B)). Additionally, the nearest grid points were compared to the Hinatuan Station and DOST-RXI Station to evaluate the reliability of the data. Figure 2 reveals that the NCDC rainfall data show good agreement with the observed rainfalls at the two stations. The GPCC rainfall, however, depicts lower values at Hinatuan, while the rainfall at DOST-RXI shows good agreement with the observed and NCDC rainfalls. Then, the NCDC rainfall data were interpolated since most of the related studies of flood hazard mapping used an interpolation method to create the rainfall distribution map (Danumah et al., 2016; Kazakis et al., 2015; Wang et al., 2011; Zhang et al., 2015).

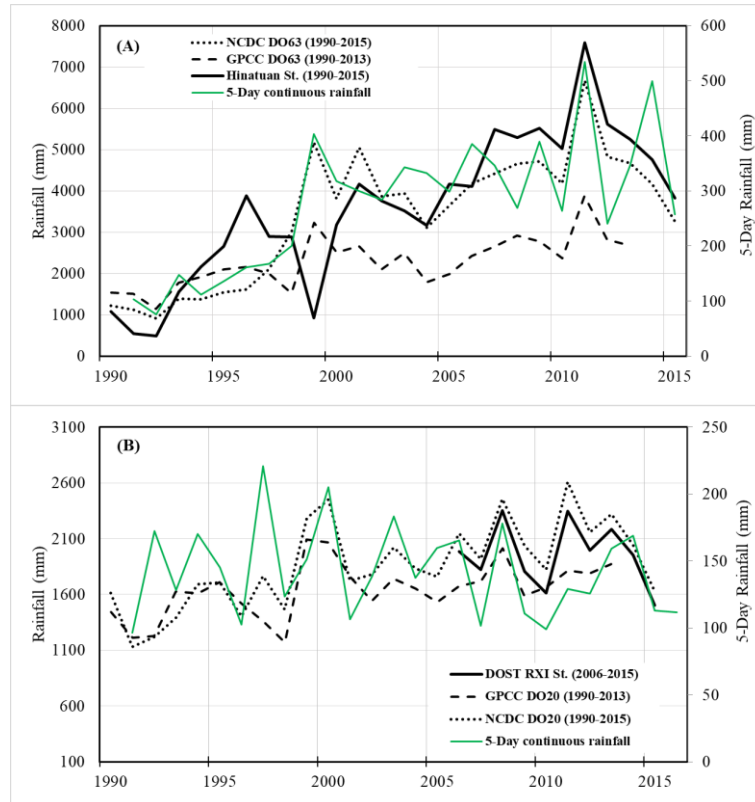


Figure 1. Comparisons of the observed annual rainfalls at the (A) Hinatuan and (B) DOST-RXI Stations with the NCDC and GPCP rainfall datasets. The locations of DO20 and DO63 are 7.083°N, 125.95°E, and 8.00°N, 126.33°E, respectively.

Table 1. Summary of the dataset used in this study; rainfall, climate change data, DEM, administrative map, soil type, population and socio-economic data.

Data	Location / Station	Description	Duration / Year	Source	Data Format
Rainfall records	DOST-RXI Station	Daily observed rainfall at an elevation of 17.29 metres	2006-2015	Philippine Atmospheric Geophysical and Astronomical Services Administration (PAGASA)	Spreadsheet file
	Hinatuan Station	Daily observed rainfall at an elevation of 3 metres	1973-2015	National Center for Environmental Information (www.ncdc.noaa.gov)	Text file
	NCDC dataset	Global daily precipitation with a spatial coverage of 0.5° lat. & 0.5° long.	1979-2016	National Climatic Data Center (ftp.cpc.ncep.noaa.gov/precip/CPC_UNI_PR)	NetCDF
	GPCP dataset	Global daily land surface precipitation with a spatial resolution of 1° lat. & 1° long.	1988-2013	Global Precipitation Climatology Centre (http://gpcc.dwd.de)	NetCDF
Rainfall and temperature projections	CMIP5 dataset	Multi-model daily rainfall and temperature	2006-2100	Climate Variability and Predictability Project (http://clivar.ouce.ox.ac.uk)	Text File

predictions				k/cmip5)	
DEM	Davao Oriental	ASTER GDEM V2 with a spatial resolution of 30 metres	2011	-Ministry of Economy, Trade, and Industry of Japan -United States National Aeronautics and Space Administration (NASA) (https://asterweb.jpl.nasa.gov/gdem.asp)	GeoTIFF
Administration map	Davao Oriental	Provincial, municipal and barangay boundaries.	2015	-Planning and Development Office of Davao Oriental. -Global Administrative Areas (https://gadm.org/index.html)	Shapefile
Soil Map	Davao Oriental	Soil types	2007	Philippine GIS Organization (www.philgis.org)	Shapefile
Population and Socio-economic data	Davao Oriental	Census of Population and Housing	2010 and 2015	Philippine Statistics Authority (http://psa.gov.ph/)	Book and spreadsheet file

3.1.2. Rainfall projections: CMIP5 dataset

Many studies on the climate change impacts on floods have used various climate change scenarios to evaluate the effects on floods. Mohammed et al. (2015), for instance, used the CMIP5 dataset for the RCP4.5 and RCP8.5 scenarios to simulate the climate change impacts on flow regimes within the Lake Champlain Basin. A study on predicting extreme floods by Wu et al. (2015) employed five GCMs for three emission scenarios (RCP2.6, RCP4.5, and RCP8.5) with 10 downscaling simulations for each emission scenario and included extreme flood predictions for two stages of future periods (2020–2050 and 2050–2080).

In this paper, the temperature and rainfall projections under climate change are utilized from the CMIP5 predictions of IPCC for the RCP4.5 and RCP8.5 scenarios. From several GCM models of the CMIP5 dataset, the thirty-nine GCM models, as shown in Table A1 (see Appendix A), are used to obtain the rainfall projections for the Davao Oriental region. Moreover, the future temperature for the Davao Oriental region was also obtained from the same CMIP5 GCMs for the rainfall projections.

3.1.3. Digital Elevation Model (DEM)

The Advanced Spaceborne Thermal Emission and Reflection Radiometer Global Digital Elevation Model (ASTER GDEM) is one of the most widely used DEM datasets. ASTER GDEM has been applied in many fields, such as soil erosion, topography, geomorphology, and hydrology (Chatterjee et al., 2014; Frey and Paul, 2012). ASTER GDEM is also widely used in developing flood hazard maps to extract drainage networks, flow accumulations and directions, basin boundaries, watershed boundaries, slopes and elevations (Fhong and Akbari, 2016; Huong and Nagasawa, 2014; Othman et al., 2011; Reddy et al., 2017).

The first version of ASTER GDEM, released in June 2009, was generated using stereo-pair images collected by the ASTER instrument on board the Terra satellite. The ASTER GDEM coverage spans from 83° north latitude to 83° south, encompassing 99% of the landmass of Earth (Tachikawa, 2011). The latest version of the ASTER GDEM V2 dataset was released in October 2011. The improved ASTER GDEM V2 dataset adds 260,000 additional stereo-pairs, improving coverage and reducing the occurrence of artefacts. The refined production algorithm provides improved spatial resolution, increased horizontal and vertical accuracy, and superior water body coverage and detection (Tachikawa, 2011). Therefore, the ASTER GDEM V2 dataset is of better quality than the first version and has a 30-m spatial resolution in the GeoTIFF image format with decimal degrees and WGS84 datum. The ASTER GDEM V2 dataset for the study site is shown in Figure. 1(D).

3.1.4. Administration Boundaries

The administrative boundaries of Davao Oriental include provincial, municipal and barangay boundaries. Davao Oriental is the easternmost province of the country. On the west side of Davao Oriental is the province of Compostela Valley, and the provinces of Surigao del Sur and Agusan del Sur are to the north. The Philippine Sea, part of the Pacific Ocean, is to the east of Davao Oriental. The administrative boundaries include ten municipal boundaries and 183 barangay boundaries. The ten municipal boundaries and their barangay boundaries are displayed in Figures 1(B). The administrative boundaries were provided as shapefiles from the global administrative areas and Philippine GIS organization, as indicated in Table 1. These shapefiles are in decimal degrees and have a WGS84 datum. The data were then projected to the UTM coordinate system zone 51N.

3.1.5. Population and Socio-economic Data

Based on the 2015 Census of Population and Housing (CPH) (Philippine Statistics Authority, 2015) as shown in Table 2, the province of Davao Oriental had a total population of 558,958 in 2015. The 2015 census includes 41,340 more persons than were counted in the 2010 CPH, which determined a total population of 517,618 persons. This increase in the population from 2010 to 2015 translates into an average annual population growth rate of 1.47%.

Mati City has the highest population of all municipalities, with 25.3% of the total provincial population. The municipality of Lupon is the second largest, with 11.8% of the total provincial population, followed by the municipalities of Baganga and Governor Generoso, with 10.1% and 9.9%, respectively. The rest of the municipalities contribute 43% of the total provincial population.

Table 2. Census of Population and Housing by municipality/city (Philippine Statistics Authority, 2015).

Municipality	District	Population				Annual growth rate (%)	Area (km ²)	Density (/km ²)	No. of Brgy.
		Ratio (%)	2010	2015					
Baganga	1 st	10.1	53,426	56,241	0.98	945.50	59	18	
Banaybanay	2 nd	7.4	39,121	41,117	0.95	408.52	100	14	
Boston	1 st	2.4	12,670	13,535	1.27	357.03	38	8	
Caraga	1 st	7.2	36,912	40,379	1.72	642.70	63	17	
Cateel	1 st	7.3	38,579	40,704	1.03	545.56	75	16	
Gov. Gen.	2 nd	9.9	50,372	55,109	1.73	365.75	150	20	
Lupon	2 nd	11.8	61,723	65,785	1.22	886.39	74	21	
Manay	1 st	7.6	40,577	42,690	0.97	418.36	100	17	
Mati City	2 nd	25.3	126,143	141,141	2.16	588.63	240	26	
San Isidro	2 nd	6.4	32,424	36,032	2.03	220.44	160	16	
Tarragona	1 st	4.7	25,671	26,225	0.41	300.76	87	10	
Total			517,618	558,958	1.47	5,679.64	98	183	

To evaluate the flood risk under climate change scenarios in the short-term (2020-2030), medium-term (2050-2060), and long-term (2090-2100), the population is also projected according to each period. Cabrera and Lee (2018b) stated that population settlements and the drastic increase in populations are among the factors that intensify the risk of floods. In this study, the Arithmetic Increase Method (AIM) was used to calculate the future population projections. Using the AIM, the average increase in population per decade is calculated from the past census reports (Ghangrekar and Kharagpur, 2015). This increase is added to the present population to determine the population of the next decade. Thus, it is assumed that the population is increasing at a constant rate, following the Eq. (1) as below:

$$P_n = P + (n \times C) \quad (1)$$

where P_n is the population after “ n ” decades, P is the present population, and C is the rate of change of the population with respect to time (i.e., the average increment of the census data).

3.1.6. Soil Type

The Davao Oriental soil cover is mainly loam and sandy clay loam, and a section of rough mountainous land has an unidentified soil type. The area of Davao Oriental is classified into four sets of input parameters based on USDA-NRCS (1986). The Camasan sandy clay loam and undifferentiated mountain soil are classified as sandy clay loam. The San Manuel silty clay loam and San Miguel clay loam are classified as clay loam. The Malalag loam is classified as loam, and the Bolinao clay is classified as clay.

3.2 Methodology

In this paper, the methodology is based on a GIS-based spatial assessment process for flood hazards and conducted by using MCDA and machine learning approaches. This approach used the spatial data management capabilities of GIS and the flexibility of MCDA to combine factual evidence with value-based information (Gigović et al., 2017). The factual evidence considered in this paper were slope, elevation, soil type, rainfall, drainage density and distance to the main channel, and defined as criteria. The value-based information approach, following Saaty (1980), uses an expert decision to identify which criteria are the most crucial in flood hazard map. Figure 3 presents the flowchart of the methodology applied in this paper.

The criteria considered in this paper were the slope, elevation, soil type, rainfall, drainage density and distance to the main channel. The value-based information approach, following Saaty [30], uses an expert decision to identify which criterion are the most crucial in the flood hazard map. Figure 3 presents the flowchart of the flood risk assessment using MCDA and machine learning approaches. The following are the steps in the MCDA approach.

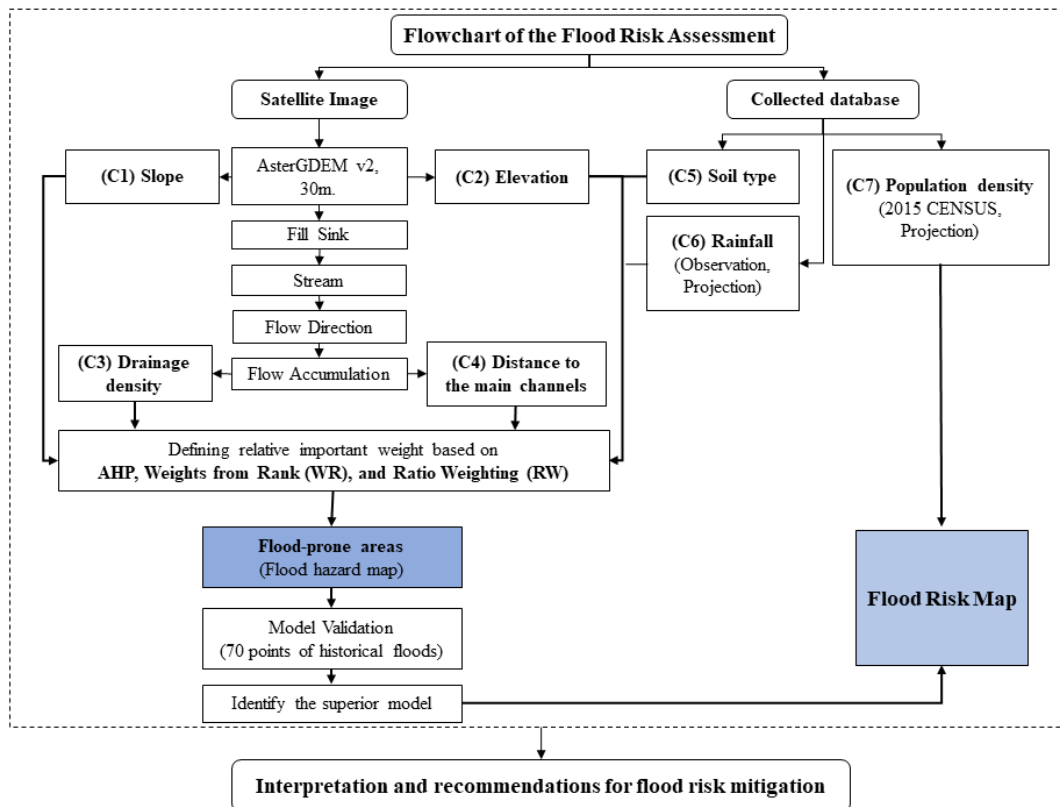


Figure 2. Flowchart of the flood risk assessment using multi-criteria data analysis (MCDA) approach.

3.2.1 Criteria Selection

An important step of this analysis is the criteria selection for evaluating the flood risks. The criteria considered are flood *hazard* and *vulnerability*. The barangay population density was used as the criteria in the vulnerability map. There are many criteria affecting flood hazard identification and modelling, and they vary from one study area to another. For instance, urban flood modelling is incredibly complex compared to rural flood modelling due to the interactions with manmade structures, such as buildings, roads, channels, tunnels and underground structures. This paper used a composite flood risk map index based on seven criteria. These criteria were selected based on various case studies (Baldassarre et al., 2009; Danumah et al., 2016; Elkhrachy, 2015; Kazakis et al., 2015; Yahaya, 2010) and are based on the available data in the study area.

3.2.1.1 Rainfall

At any location, the chance of flood increases as the amount of rain increases. A higher rainfall intensity can result in more runoff because the ground cannot quickly absorb the water. In this study, the 5-day continuous maximum rainfall in every year was determined for 1991-2016 as shown in Figure 2. Then, the average of the 5-day continuous maximum rainfall over the 25 years was used in the analysis for the current scenario. Also, the same concept is applied to the projected scenarios; that is short-term (2020-2030), medium-term (2050-2060), and long-term (2090-2100) in RCP4.5 and RCP 8.5. Due to the lack of weather stations in the study area, rainfall records from the NCDC were used, as described in sub-section 2.2.1 (see Table 1).

To investigate the climate change impact on flood hazards and risks, spatial areas covering an area of $2^\circ \times 2^\circ$, as depicted in Figure 1(D), are defined due to the coarse and inconsistent spatial horizontal resolutions among the CMIP5 GCMs, as summarized in Table A1. Area 1 covers Davao Oriental and its surrounding regions, and Areas 2-4 shift one degree each to the east in longitude from Areas 1-3, respectively. Then, the area-averaged rainfalls of each defined area from the thirty-nine GCMs for two scenarios, RCP8.5 and RCP4.5, in the short-term (2020-2030), medium-term (2050-2060), and long-term (2090-2100) are used for future flood hazards and risks. Then, spatial interpolations by using the Kriging method are carried out to address spatial rainfall patterns in the future projections of the Davao Oriental region with the following procedures:

(1) Convert the area-averaged daily rainfalls to point layers to be the same as the NCDC data points in Davao Oriental;

(2) The spatial rainfall patterns in the observed rainfalls are applied to the projected rainfalls, as follows:

$$RD_i = R_i - (\sum_{i=1}^N R_i)/N \quad (2)$$

$$RP_i = R_{avg} + RD_i \quad (3)$$

where N is the number of NCDC points in Davao Oriental, R_i is the observed rainfall at the NCDC points, and R_{avg} is the area-averaged projected rainfalls for Davao Oriental from the CMIP5 dataset. The observed spatial rainfall patterns, RD_i in Eq. (2), are determined as a rainfall difference at each point between the observed annual rainfalls and the observed area-averaged annual rainfall over Davao Oriental, and then, the projected spatial rainfall pattern, RP_i in Eq. (3), is calculated by adding the observed rainfall pattern, RD_i , to the area-averaged projected rainfall, R_{avg} , in Davao Oriental.

(3) Re-project the outcome of Eq. (3) to UTM51 to be the same as the other criteria.

3.2.1.2. Soil

Soil type (Ebaid et al., 2016; Nyarko, 2002) and hydrological soil classification (Apollonio et al., 2016) are the significant factors in determining the water holding and infiltration characteristics of an area and consequently affects flood susceptibility. Generally, runoff from intense rainfall is likely to be faster and greater in clay soils than in sand (The University Corporation for Atmospheric Research., 2010). Additionally, rain runoff from intense rainfall is likely to be faster and greater in loam than in sand.

3.2.1.3. Slope

Slope is one of the crucial elements in floods. The danger of floods increases as the slope increases. Slope is a reliable criterion of flood susceptibility (Bapalu, 2006). When the river slope increases, the flow velocity in the river will also increase (Elkhrachy, 2015).

3.2.1.4. Elevation

In contrast to the slope, the elevation of an area is a major factor in floods. Low elevation is a good criterion of areas with a high potential for flood accumulation. Water flows from higher to lower elevations; therefore, the slope influences the amount of surface runoff and infiltration (Kazakis et al., 2015). Flat areas at low elevations may flood more quickly than areas the higher elevations with steeper slopes.

3.2.1.5. Drainage density

Drainage density is the length of all of the channels within the basin divided by the area of the basin (Yahaya, 2010). A dense drainage network is a good criterion of flow accumulation pathways and of areas with a high potential for floods (Bapalu, 2006).

3.2.1.6. Distance to the main channel

The distance to the main channel significantly impacts flood mapping. Areas located close to the main channel and flow accumulation path are more likely to flood (Gigović et al., 2017).

Once the criteria were defined, the next step was to build the spatial database. Each criterion was converted into raster data with a 30 m x 30 m grid resolution. The ASTER GDEM data were registered and projected to the UTM coordinate system, zone 51N. The slope and elevation were obtained using the 3D Analyst algorithm based on a DEM. The drainage density and distance to the main channel were obtained using Arc Hydro, which is a set of data models that operate within ArcGIS to support geospatial and temporal data analyses. All data were integrated into the GIS environment using the AHP, RW, and WR methods. Likewise, in the maximum entropy modelling, all data entered as inputs together with the 70 points of survey historical events of flood. Finally, the weighted overlay was used to calculate the flood hazard map, which was then combined with the vulnerability map to create a flood risk map in the study area.

In the future flood hazard and risk assessment, the criteria such as slope, soil type, drainage density, elevation, and distance to the main channel are assumed to be the same as the current conditions, whereas the projections for population density and rainfall are considered in the assessment.

3.2.2 Pairwise Comparison

The first step in the AHP is to make a pairwise comparison of each criterion based on the scales by Saaty (1980). The results of the comparison were described in terms of integer values from 1 to 9, where a higher number means that the chosen criterion is considered more important than the other criterion used in the comparison. In this study, the pairwise comparison matrix is shown in Table 4.

Table 3. Saaty Scale of relative importance and its description.

Scale	Preference	Description
1	Equal importance	Two factors contribute equally to the objective
3	Moderate	Experience and judgement slightly favor one over the other
5	Strong	Experience and judgement strongly favor one over the other
7	Very strong	Experience and judgement very strongly favor one over the other
9	Extreme importance	The evidence favoring one over other is of the highest possible validity
2,4,6,8	Intermediate values	When compromise is needed

Table 4. Pairwise comparison matrix used in this study¹.

Criteria	R	SI	E	Dc	Dd	St
Rainfall (<i>R</i>)	1	2	3	4	5	6
Slope (<i>SI</i>)	1/2	1	2	3	4	5
Elevation (<i>E</i>)	1/3	1/2	1	2	3	4
Distance to main channel (<i>Dc</i>)	1/4	1/3	1/2	1	2	3
Drainage (<i>Dd</i>)	1/5	1/4	1/3	1/2	1	2
Soil type (<i>St</i>)	1/6	1/5	1/4	1/3	1/2	1
Sum	2.45	4.28	7.08	10.83	15.50	21.00

Table 5. Matrix normalization with criteria weights (priority vector) and consistency measure (*CM*).

Criteria	R	SI	E	Dc	Dd	St	Total	PV	CM
R	0.41	0.47	0.42	0.37	0.32	0.29	2.36	0.379	6.21
SI	0.20	0.23	0.28	0.28	0.26	0.24	1.55	0.249	6.21
E	0.14	0.12	0.14	0.18	0.19	0.19	0.99	0.160	6.15
Dc	0.10	0.08	0.07	0.09	0.09	0.14	0.62	0.102	6.07
Dd	0.08	0.06	0.05	0.05	0.05	0.10	0.40	0.065	6.03
St	0.07	0.05	0.04	0.04	0.03	0.05	0.26	0.043	6.06
Sum	1.00	1.00	1.00	1.00	1.00	1.00	-	1.000	-

Table 6. Random index matrix and its corresponding number of criteria compared.

No. of criteria	2	3	4	5	6	7	8	9	10
RI	0.00	0.58	0.90	1.12	1.24	1.32	1.41	1.45	1.49

3.2.3 Normalization

This step is the process of normalizing the matrix by adding the numbers in each column. Each entry in the column is then divided by the column sum to yield its normalized score, as described in Eq. (4). The sum of each

¹ This table is based on the average ranking of the four decision-maker (DM). The DMs who evaluated the criteria; City Engineering Officer, City Planning Officer, Provincial Director – Environment and Natural Resources Office, and Director – Integrated Coastal Resource and Management Program.

column should be 1. Lastly, the priority vector (*PV*) is computed by dividing the sum of the normalized column of the matrix by the number of criteria used (*n*), as shown in Eq. (5). Table 5 shows the normalized matrix in this study.

$$X_{ij} = \frac{C_{ij}}{\sum_{i=1}^n C_{ij}} \quad (4)$$

$$PV_{ij} = \sum_{j=1}^n \frac{X_{ij}}{n} \quad (5)$$

where C_{ij} is the value of a criterion in the pairwise comparison matrix, X_{ij} is the normalized score, and PV_{ij} is the priority vector of a criterion.

3.2.4 Consistency Analysis

There are three steps to determine the *CR*. First, the consistency measure (*CM*) is calculated multiplying the pairwise matrix by the *PV*, and then, the result is divided by the weighted sum vector with the criterion weights. Second, the consistency index (*CI*) is calculated, as described in Eq. (6). Lastly, the *CR* is computed, as described in Eq. (7).

$$CI = \frac{(\lambda_{max} - n)}{(n - 1)} \quad (6)$$

$$CR = \frac{CI}{RI} \quad (7)$$

where λ_{max} is the sum of the *CM* divided by the number of criteria (*n*) and set to 6.123. The results of the random index (*RI*) are given in Table 6.

The results of the pairwise comparison matrix for this work are presented in Table 4. In Table 5, the column *PV* contains the relative importance weights for each criterion. From the input values in the pairwise comparison and the weights calculation, the *CR* was found to be 0.02. The *CR* result indicates a reasonable level of coherency in the pairwise comparison.

The hazard index (*HI*) was used to consider the rate of probability and was calculated based on Eq. (8) as follows:

$$HI = St \times 0.04 + Sl \times 0.25 + Dd \times 0.07 + Dc \times 0.10 + E \times 0.16 + R \times 0.38 \quad (8)$$

where *St*, *Sl*, *Dd*, *Dc*, *E*, and *R* represent the soil type, slope, drainage, distance to main channel, elevation, and rainfall, respectively.

Finally, the hazard index was computed using a weighted overlay analysis. The values of *HI* were classified into five categories such as very low (*VL*), low (*L*), moderate (*M*), high (*H*) and very high (*VH*).

3.3. Ratio Weighting

In this method, the decision-makers compare two criteria at a time and ask for the preference (importance) ratio between them. It uses the pairwise comparisons to establish the relative importance among criteria. It is likely that the pairwise comparisons will be inconsistent. Therefore, these approaches require more information to compensate for the inconsistencies of human judgement. Efficient techniques to retrieve weights from pairwise comparison data include eigenvector prioritization method by Saaty (1980). Saaty (1980) presented the simplified prioritization method as follows:

Step 1. Input Coding. A decision-maker (*DM*) assesses importance (weight) ratios between criteria using pairwise comparisons. In this study, four *DMs* are asked to rank the criteria. Table 7 shows the *DMs* judgements among these criteria.

Step 2. Computing. Compute the geometric mean of each row of the comparison matrix, and then normalize the resulting numbers. The geometric mean and the numerical weights are calculated using *Eqs. (9)*, and *(10)*. Table 7 shows the geometric mean and weights of the *DMs* judgements.

$$GM_i = \left(\prod_{i=1}^n x_i \right)^{\frac{1}{n}} \quad (9)$$

$$W_i = \frac{(GM_i)}{\sum_{i=1}^n (GM_i)} \quad (10)$$

where GM_i is the geometric mean for *i* criterion, *n* is the number of criteria, and W_i is the normalized weight for *i* criterion. The hazard index (*HI*) based on the average weights (see Table 7) of the four *DMs* was used to consider the rate of probability as shown on Eq. (11).

$$HI = St * 0.04 + Sl * 0.31 + Dd * 0.06 + Dc * 0.09 + E * 0.17 + R * 0.33 \quad (11)$$

3.4. Weights by Rank

In this method, the importance of weight is arranging through a rank order. In that way, every criterion is ranked as per decision-makers (*DM*) preference. One (1) is the most important, and two (2) comes next, and so on. Once ranking is established for a set of criteria, the numerical weights are calculated using *Eq. (12)*.

$$W_i = (n - r_j + 1) / \sum_{i=1}^n ((n - r_k + 1)) \quad (12)$$

where W_i is the normalized weight for j criterion, n the number of criteria under consideration ($k = 1, 2, \dots, n$), and r_j is the rank position of the criterion. Each criterion is weighted $(n - r_j + 1)$ and then normalized by the sum of all weights $\sum(n - r_j + 1)$. Therefore, the ranking method estimated weight should be considered as an approximation. The results are given in Table 7. The average weight (AR) values are the aggregated results from the 4 decision-makers in the study area. The column weight (W) at Table 7 is the hazard index shown in the Eq. (13).

$$HI = St \times 0.07 + Sl \times 0.25 + Dd \times 0.11 + Dc \times 0.11 + E \times 0.20 + R \times 0.26 \quad (13)$$

Finally, the hazard index of the three models (AHP, Weights by Rank, and Ratio Weighting) was computed using a weighted overlay analysis. The results of weighted overlay analysis were classified using equal interval into 4 levels such as very low, low, moderate, and high.

Table 7. Decision maker (DM)'s matrix for WR and RW methods. Average ranking (AR) and weights (W) for WR method, and geometric mean (GM), normalized weights (NW), average normalized weights (ANW) for RW method are the average of the 4 DMs. The W and ANW are the relative importance weights used in the hazard index (HI) calculations in Eqs. (11) and (13), respectively².

Criteria	R	Sl	E	Dc	Dd	St	RW			WR	
							GM	NW	ANW	AR	W
R	1	2	3	4	5	6	2.99	0.38	0.33	1.5	0.26
Sl	1/2	1	2	3	4	5	1.98	0.25	0.31	1.75	0.25
E	1/3	1/2	1	2	3	4	1.26	0.16	0.17	2.75	0.20
Dc	1/4	1/3	1/2	1	2	3	0.79	0.11	0.09	4.75	0.11
Dd	1/5	1.4	1/3	1/2	1	2	0.51	0.06	0.06	4.75	0.11
St	1/6	1.5	1/4	1/3	1/2	1	0.33	0.04	0.04	5.5	0.07
Sum	-	-	-	-	-	-	7.86	1	1.00	-	1.00

3.5. Evaluation of Rainfall and Temperature projections

The area-averaged (Area 1 in Figure 1(D)) daily temperatures from the thirty-nine GCMs in Figure 4 show a significant increase of approximately 3°C and 1°C from 2016 to 2100 under the RCP8.5 and RCP4.5 scenarios, respectively. However, the area-averaged daily precipitation for Area 1 illustrate a slight increase in Figure 5. To further investigate the projected rainfall, the defined Area 1 was shifted one degree east and defined as Area 2 to 4 to determine a change in precipitation. As the defined area moves east to the open sea, the projected rainfall presents a slight increase in the mean value and the linear trend. Area 4 shows comparable increases in the mean value and the linear trend compared to those of Area 1 as the defined area gets farther from the shoreline. With respect to the difference in the projected rainfall between the two scenarios, RCP4.5 and RCP8.5, the difference is almost insignificant because the increment of the projected rainfall in the RCP8.5 scenario is very low. This behavior of the projected rainfall in the long term is remarkably different from the temperature projection, which might be partially due to incomplete microphysics parameterizations and coarse horizontal resolutions of the GCMs.

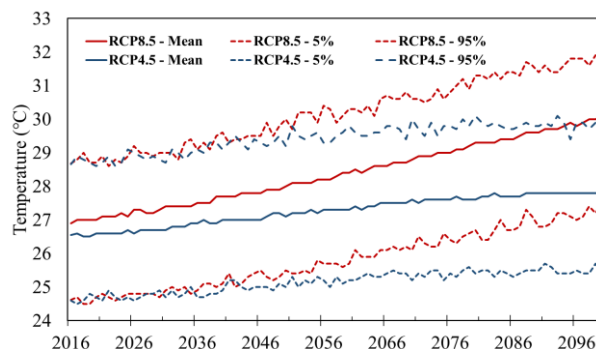


Figure 3. Area-averaged temperature projections for Area 1 (see Figure 1 (D)) from the thirty-nine GCMs for the period of 2016-2100.

²This table is based on the average ranking of the four decision-maker (DM). The DMs who evaluated the criteria; City Engineering Officer, City Planning Officer, Provincial Director – Environment and Natural Resources Office, and Director – Integrated Coastal Resource and Management Program.

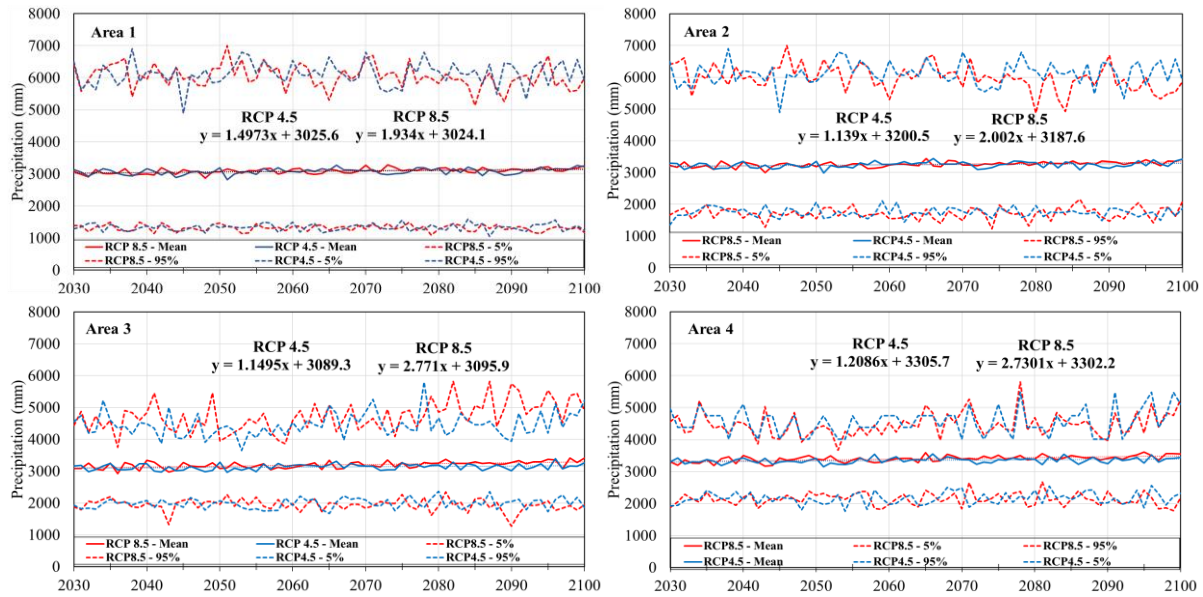


Figure 4. Area-averaged (Area 1, 2, 3, and 4) rainfall projections from the thirty-nine GCMs for the period of 2030-2100.

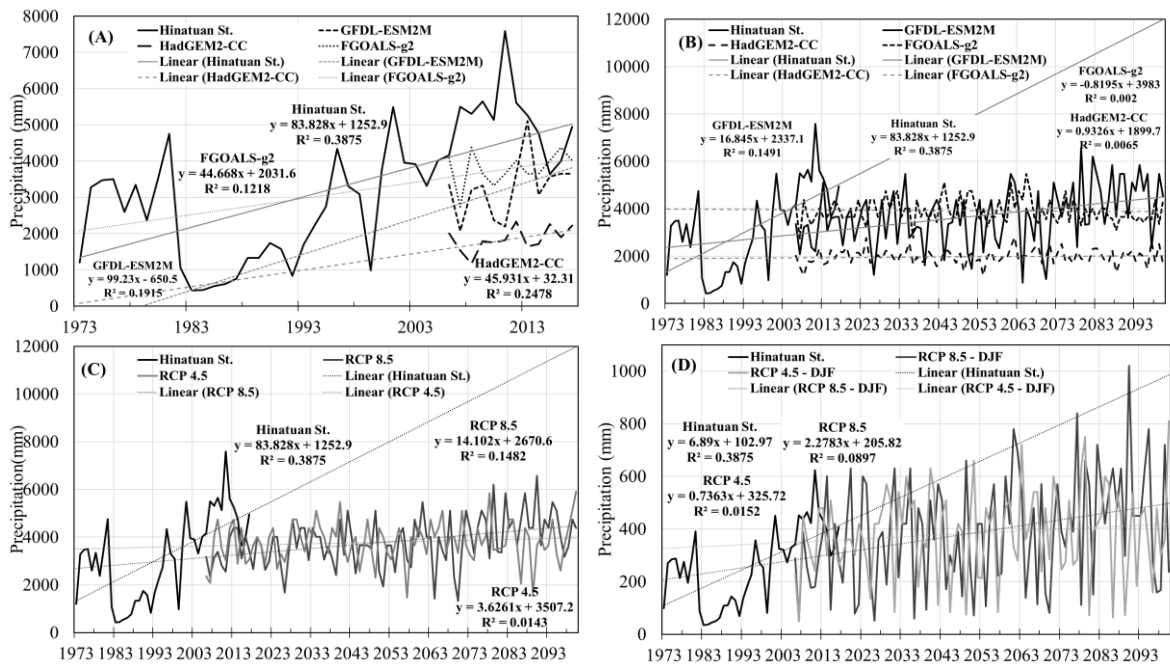


Figure 5. Projected rainfalls GCMs – CMIP5 39 model’s comparison, (A) Models with increasing trends in the period of 2006-2015, (B) Period extended from 2006-2100 for the models with increasing trends where GFDL-ESM2M model has the highest trend compare to other models, (C) GFDL-ESM2M model trends under RCP 4.5 and RCP 8.5, and (D) the DJF seasonal rainfalls the GFDL-ESM2M under RCP4.5 and RCP8.5.

Further, the rainfall projections of the thirty-nine GCMs of Area 4 were compared to the observed rainfall at Hinatuan Station for the 10-year overlapping period from 2006 to 2016 to identify which GCM result is appropriate to use in the flood assessment. Among the thirty-nine GCMs considered, three GCMs, such as the HadGEM2-CC, GFDL-ESM2M, and FGOALS-g2 models, illustrate a good agreement with the observed rainfall at Hinatuan in terms of increasing the linear trends, as in Figure 6(A), while the other GCMs showed almost no increasing trends, as implied in Figure 5. Figure 6(B) presents the rainfall projections and linear trends of the three GCMs over the extended period to 2100. The values of the GFDL-ESM2M model depict the outstanding increasing trend over the extended period, whereas the trends of the other two models are not significant in this long period. Figure 6(C) illustrates the area-averaged (Area 4) projected rainfalls of GFDL-ESM2M for two scenarios, RCP4.5 and RCP8.5. The difference between the two scenarios is not practically significant, but the linear trend of the RCP8.5 result shows

more increasing trends than RCP8.5. Since the study site can be divided into different climate zones with respect to the precipitation patterns as described, the seasonal rainfall variations were also investigated. In the evaluation of seasonal rainfall using the GFDL-ESM2M result, the DJF season has a high increase in precipitation compared to the other seasons (Figure 6(D)). Based on the above evaluation of the rainfall projections of the GCMs, the GFDL-ESM2M model rainfall projection for Area 4 was used for the rainfall criterion in the future flood hazard and risk assessment.

3.6. Validation

For validation of the resulting flood-prone areas by the AHP, WR, and RW methods, a GPS-based field survey to local people was carried out along the east coast of Davao Oriental to investigate ground true flooded points by historical flooding events. From the field survey, coordinates of 70 ground true points are collected and used for performance evaluation (see Figure 1D for their locations).

The performance evaluation is done using the accuracy assessment of the flood classification. One of the commonly used methods is to apply a confusion matrix or error matrix. This method can be used to compute several assessment elements such as overall accuracy (*ACC*), true positive rate (*TPR*), true negative rate (*TNR*), false positive rate (*FPR*), and false negative rate (*FNR*) using the Eqs. (14) ~ (18), respectively (Feng et al., 382 2015; Singh and Singh, 2017).

$$ACC = \frac{TP+TN}{P+N} = \frac{TP+TN}{TP+TN+FP+FN} \quad (14)$$

$$TPR = \frac{TP}{TP+FN} \quad (15)$$

$$TNR = \frac{TN}{TN+FP} \quad (16)$$

$$FPR = \frac{FP}{FP+FN} = 1 - TNR \quad (17)$$

$$FNR = \frac{FN}{FN+TP} = 1 - TPR \quad (18)$$

where *P*, *N*, *TP*, *TN*, *FP*, and *FN* are condition positive, condition negative, true positive, true negative, false positive, and false negative, respectively. In the accuracy assessment of the flood susceptibility map, a confusion matrix was calculated based on the field survey of ground points for historical flooding events. However, the field survey was not carried out in the Davao Gulf municipalities and thus the points do not cover all barangays in the study area. To solve this limitation, the elevations of 70 points are extracted from DEM. The elevations of 70 points are in the range between 10 m and 20 m above mean sea level. Then, the points are spatially interpolated, and the areas below 20 m elevation where all points are located are used to determine the flood and non-flood areas in Davao Oriental. The result is shown in Figure 1C. Finally, the accuracy assessment was performed using the confusion matrix. On the other hand, to assess the accuracy of the maxent model, area under ROC (AUC) curve is used.

4. Results

4.1. Flood Vulnerability Map

Vulnerability expresses the level of inability to resist a hazard or to respond when a disaster has occurred. For example, people who live in low-lying areas are more vulnerable to floods than people who live at higher elevations. Moreover, vulnerability is the most crucial component of flood risk because vulnerability determines if exposure to a hazard constitutes a threat. Flood vulnerability mapping is the process of determining the degree of susceptibility and exposure of a given place to flood (Danumah et al., 2016). The susceptibility and exposure issues include several factors, such as the age and health of the population, the socio-economic activities, the quality of buildings and their location with respect to floods. Pellicani et al. (2018) quantified the risk by using the vulnerability factors like land use, structures, and infrastructures with respect to the flood-prone areas. In this study, the only criterion used for the assessment of vulnerability to floods is the population density. The vulnerability map obtained from the barangay (town) population density, as shown in Figure 7, is divided into five classifications from *very low* to *very high* regarding the flood hazard. Four scenarios (2015, 2035, 2065, and 2105) of the vulnerability map based on population projections using the *AIM* were developed to complement the hazard projections.

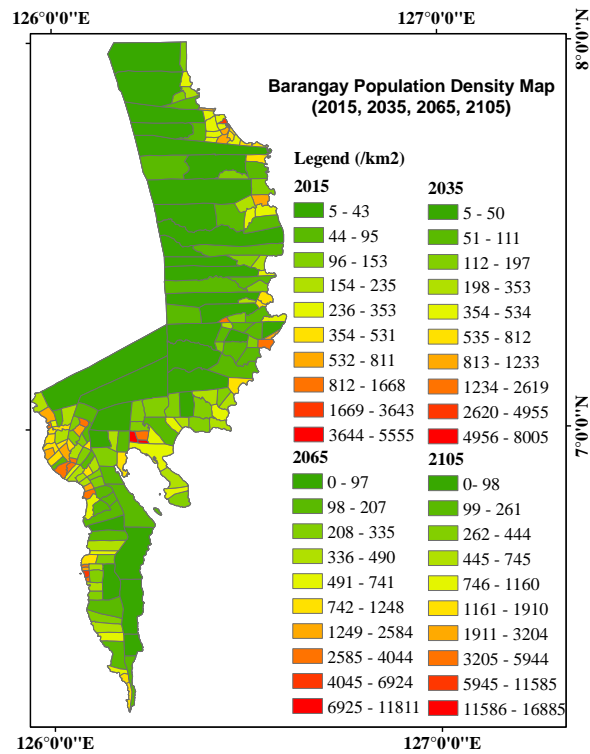


Figure 6. Barangay population density for 2015, 2035, 2065 and 2105 in Davao Oriental. Population projections is made using the arithmetic increment method and used for vulnerability assessment.

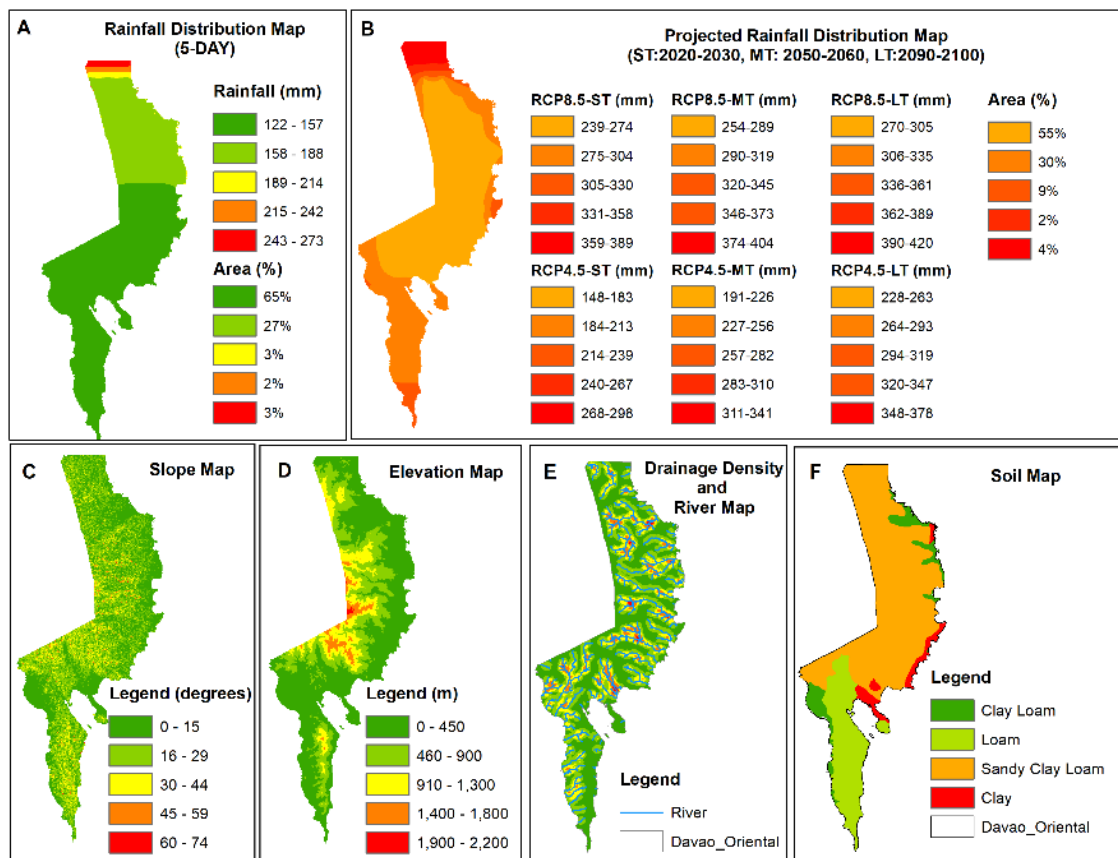


Figure 7. Criteria for flood hazard map: (A) historical rainfall distribution from the NCDC dataset, (B) projected rainfall pattern for short-, mid- and long-term future under RCP 4.5 and RCP8.5 scenarios, (C) slope map, (D) elevation map, (E) drainage density and distance to the main channel, and (F) soil map.

4.2. Flood Hazard Map

The multisource flood hazard mapping, where greater emphasis was placed on rainfall, is shown in Figure 8. Figure 8A and B are the different rainfall distributions under different scenarios. The rainfall distributions are difficult to compare from the current to the projected scenarios because no threshold is specified. However, note that the very low classification of rainfall in the projected scenarios (Figure 8B) belongs to the high classification in the current scenario. This means that the rainfall pattern increases in the coming years. Additionally, it is evident that Davao Oriental will experience heavy rainfall in the coming years, especially under the RCP8.5 (see Figure 8B).

Figure 9 shows that the hazard map is a combination of maps: rainfall (Figures 8A and 8B), slope and elevation (Figures 8C and 8D), drainage density and distance to the main channel (Figure 8E), and soil (Figure 8F). Each map has different weights that, in this paper, the rainfall is emphasized more. The rainfall map (Figure 8A and 8B) shows that each east coast municipality has a higher incidence of rainfall compared to that of the Davao Gulf municipalities. The slope and elevation maps (Figure 8C and 8D) indicate that most of the areas in Davao Oriental are at low elevations, less than 217 m and have slopes up to 16 degrees. All maps are classified based on equal interval classification.

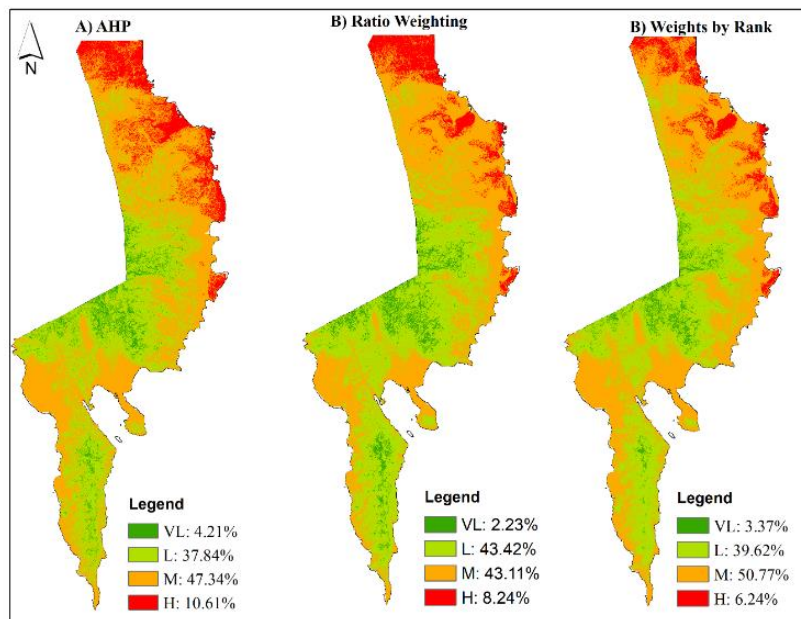


Figure 8. Results of flood hazard maps from AHP, RW, and RW models to identify the superior result using 5-day continuous maximum rainfall: (A) AHP model, (B) RW model, and (C) WR model.

The resulting flood hazard maps by the AHP, WR, and RW methods are illustrated in Figure 9. Table 9 shows the confusion matrix of the three models. The data in Table 9 is the number of pixels from the models (i.e., predicted) in high classification, and the observed data from the flood and non-flood area that shown in Figure 1C. In the overall assessment, AHP has superior results in ACC, TNR, and TPR as shown in Figure 10A. Moreover, Figure 10B shows the accuracy of the positive prediction (TPR) compare to the wrong prediction (FPR). The upper part of the redline in the Figure 10B means the model is accurate, otherwise not accurate. Therefore, AHP shows higher accuracy compared to the other two methods. In overall, the analysis reveals that AHP is much accurate and reliable for flood risk analysis in this study.

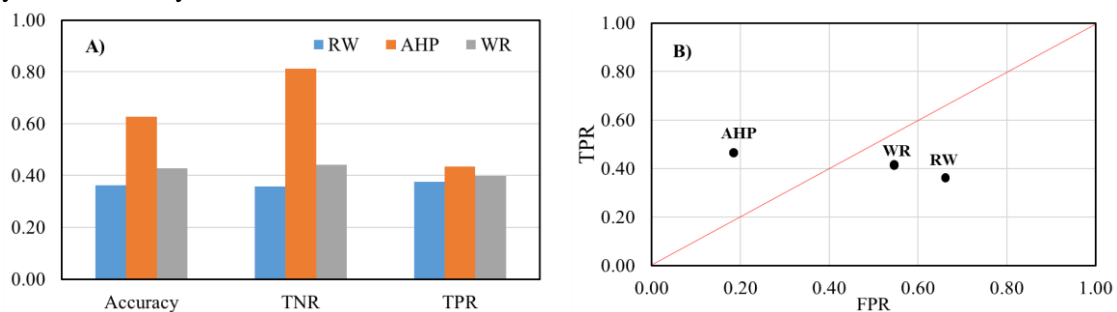


Figure 9. Results of accuracy assessment: A) Comparison of the accuracy assessment for the 3 methods using ACC, TNR, and TPR. B) Model evaluation using (TPR) and (FPR). Redline show the line of discrimination or random guess. Above the redline is the better, otherwise is worst prediction.

Table 8. Confusion matrix to calculate the accuracy (ACC), true positive rate (TPR), true negative rate (TNR), and false positive rate (FPR) for performance evaluation of three methods, AHP, WR, and RW.

Observed	Predicted		Sum
	Flood	Non-Flood	
Flood	True Positive, (TP)	False Negative, (FN)	P
Non-Flood	False Negative, (FP)	True Negative, (TN)	N
AHP			
Flood	228388	298332	526720
Non-Flood	102416	445224	547640
RW			
Flood	197607	329113	526720
Non-Flood	856542	447503	1334045
WR			
Flood	209746	316974	526720
Non-Flood	592507	467179	1059686

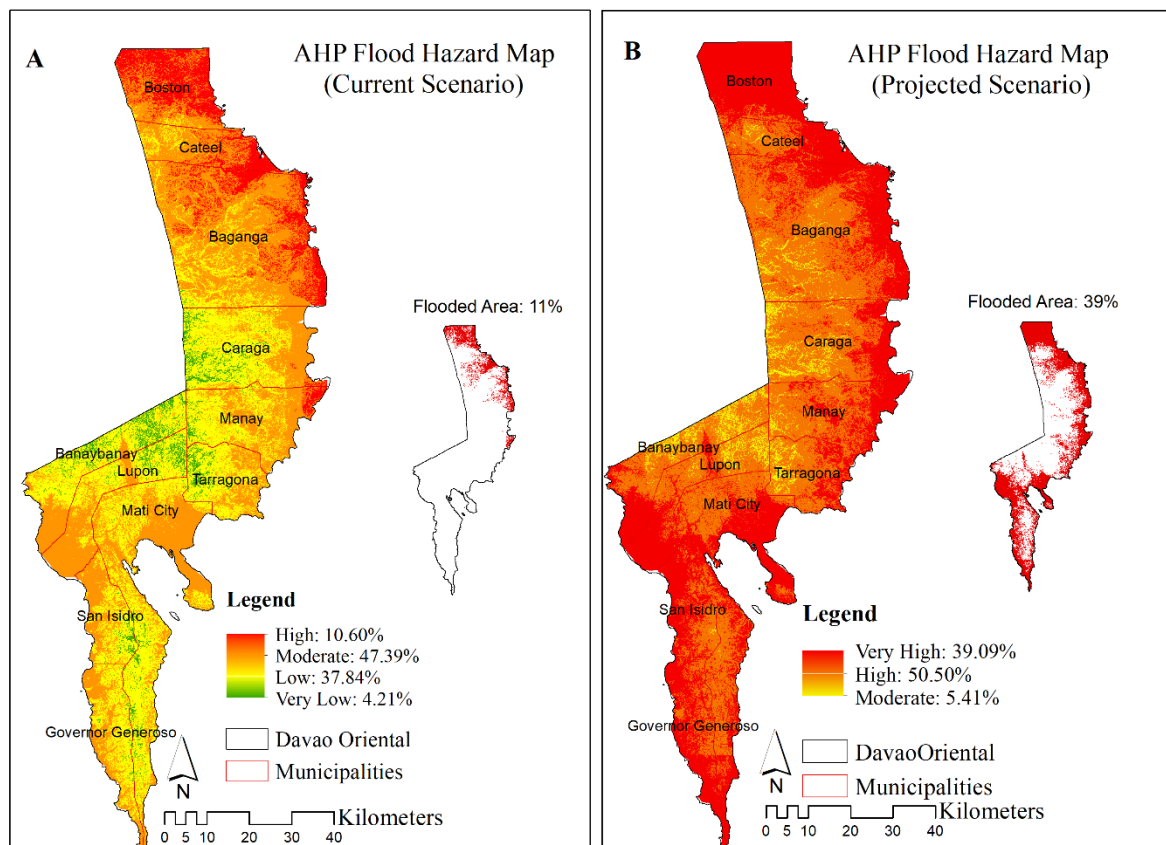


Figure 10. Multi-source flood hazard maps classified into *very low*, *low*, *medium*, *high*, and *very high* categories. (A) Current scenario, and (B) Projected scenarios (2030, 2060, and 2100).

The resulting flood hazard map in Figure 11 indicates five classifications of risk, *VL*, *L*, *M*, *H*, and *VH*. Figure 11A is the current situation of the flood hazard map, and Figure 11B is the projected scenario of the flood hazard map in Davao Oriental. The changes in the area distribution in the flood hazard map from the current situation to the projected scenarios are noticeable. Moreover, the intensity of rainfall will change and intensify in every future decade.

In the municipal level of flood hazard assessment (Figure 11), the majority of Boston municipality belongs to category *H* in the current to *VH* in the projected scenarios. All the east coast municipalities changes from *M* and *H* in to *H* and *VH* categories.

On the other hand, in the Davao Gulf municipalities of Davao Oriental, many changes will be occurring in the future, especially in the coastal areas. Most of the areas change into *H*, and some parts change into *VH* from the *M* and *H* categories in the current scenario.

Overall, Davao Oriental will experience severe flooding and rainfall in the future (Figure 11). The *VL* and *L* classes will no longer exist in the future scenario. The *M* classification decrease to 5.41%. Unfortunately, the high classification will drastically increase into 50.50%. Moreover, the *VH* is approximately 39% in the future, and this area are with high elevations, high slopes, and low drainage densities. This situation shows that majority of the province of Davao Oriental is classified as *H* to *VH* in the flood hazard in the future.

The hazard map shows that approximately 22% (current) and 90% (projected) of the area have *H* and *VH* hazard risks and that rainfall (42%) and slope (23%) are the most significant causative factors of flood occurrences. Unfortunately, the basis of the evaluation is the spatial distribution of the flood hazard map, where the classification of flood hazards into *VL*, *L*, *M*, *V*, and *VH* has no threshold values. Thus, it is difficult to directly compare the two hazard maps in the current and the projected scenarios. However, by referring to the absolute values of rainfall in Figs. 8A and 8B, note that the *very low* (*VL*) category in the projected scenarios (Figure 8B) belongs to the *very high* (*VH*) classification in the current scenario. A gradual increase in rainfall from 2020 to 2100 implying that Davao Oriental will experience heavy rainfall in the future.

4.3. Flood Risk Map

The flood risk map was generated by a weighted overlay of the hazard and vulnerability maps with equal weights under different scenarios. The current, short-term, medium-term and long-term hazard maps were overlaid in 2015, 2035, 2065, and 2105 vulnerability maps, respectively, using the population density projection. The risk map in this study is a combination of the AHP hazard map (Figure 10) and vulnerability map (Figure 7).

The resulting flood risk map in Figure 12 was classified into four categories. In the current scenario, the *VL*, *L* and *M* classes cover 3.74%, 68.68%, and 25.35% of the total area, respectively. In the flood-prone area 30% (168,034 persons) of the population are at a high of flooding at the current situation and it increases into 32% (178,866 persons) in the future. The categories of *H* is estimated to be 2.23% of the total area, respectively; these areas are barangays with high population densities and are mostly in riverside and coastal areas.

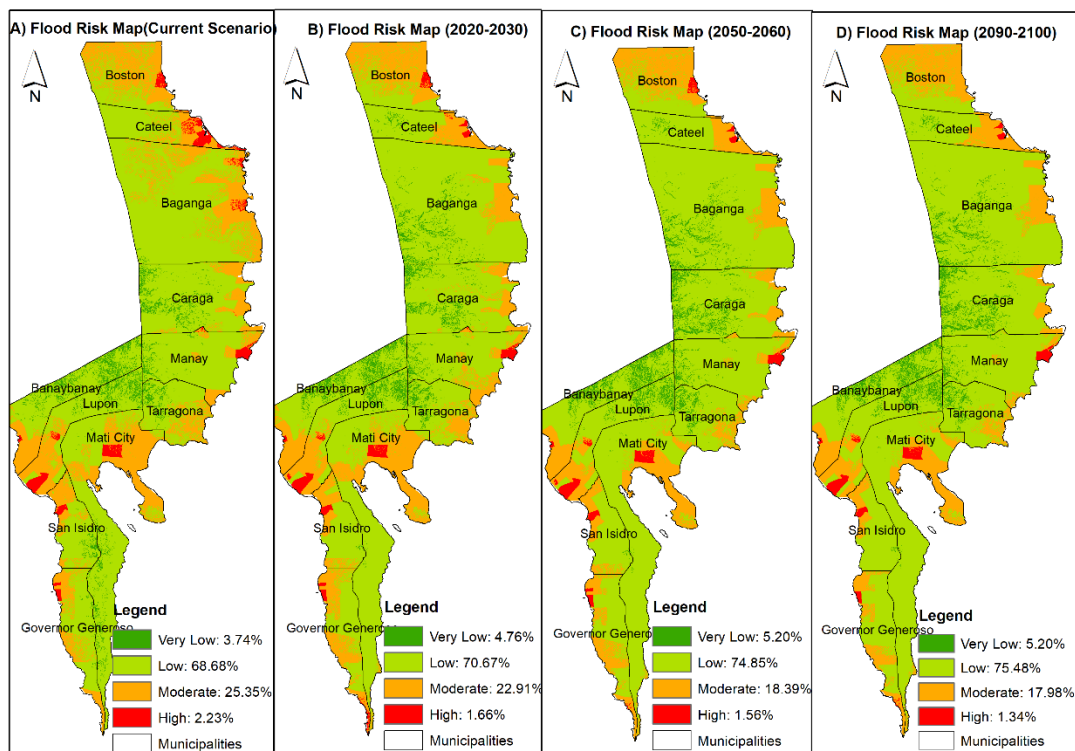


Figure 112. Flood risk maps: (A) current scenario, (B) short term period (2020-2030), (C) medium (2050-2060) period, and (D) long term (2090-2100) periods. The flood risk maps under RCP 4.5 and RCP 8.5 scenarios are identical.

In the short-term period, VL and L classifications are increasing. While, M and H are decreasing. Additionally, the VL classification increases from 3.74% to 4.76%, and 5.20% in the short-term and medium/long-term. Moreover, the L classification increases from 68.68% to 70.67% in the short-term, 74.85% in the medium-term, and 75.48% in the long-term period. Additionally, the M classification decreases from 25.35% to 22.91% in the short-term and eventually decreases to 18.39% and 17.98% in the medium-term and long-term period respectively. The H classification is decreasing from the short-term to the long-term period. It is notable that Davao Oriental can be classified as low to medium regarding the risk of the flood (Figures 12).

In most cases, the flood risk of the east coast municipalities (Boston, Baganga, Caraga, Manay, and Tarragona) decreases (Figure 12 and Table 9). In contrast, the flood risk of Davao Gulf municipalities (Lupon, Governor Generoso, and Mati) increases due to the increase in population in these areas (Figure 12 and Table 10). These areas are mainly urban, there is a fishing industry, and they are the areas to which most of the people in Davao Oriental migrate.

Table 11 shows the lists of the barangays that have H risks of flooding. A total of twenty-one, nineteen, and eighteen barangays belongs to the H risk of flood in the current, short-term/medium-term, and long-term period, respectively. Additionally, Mati and Lupon has the highest number of barangays that will experience the H risk of floods in all periods. These barangays need mitigation plans to cope with floods in the coming years. The results illustrate that Davao Oriental belongs to the *low* and *medium* risk of floods in the spatial area distribution.

Table 9. Flood risk classification in each municipality (%).

Municipality	Current Scenario				Short-Term (2020-2030)			
	VL	L	M	H	VL	L	M	H
Boston	-	38.75	58.92	2.33	-	38.13	59.68	2.19
Cateel	-	64.97	23.92	11.1	2.08	63.71	31.78	2.43
Baganga	0.12	75.48	23.48	0.91	4.35	88.18	7.47	-
Caraga	6.80	79.26	13.91	0.03	7.89	80.10	12.01	-
Manay	2.67	82.85	11.35	3.13	3.19	77.45	16.41	2.94
Tarragona	5.80	71.57	71.57	22.6	7.19	73.69	19.12	-
Mati	2.68	66.64	28.51	2.17	0.14	68.71	28.99	2.16
Lupon	9.04	58.58	26.46	5.91	10.65	58.13	25.19	6.03
Banaybanay	15.4	65.67	18.51	0.39	18.09	61.77	19.76	0.39
San Isidro	3.89	65.19	28.24	2.67	0.41	67.35	29.40	2.84
Governor Generoso	0.91	65.38	31.56	2.15	-	54.51	41.61	3.88
Municipality	Medium-Term (2050-2060)				Long-Term (2090-2100)			
	VL	L	M	H	VL	L	M	H
Boston	-	40.12	57.69	2.19	-	40.12	59.87	-
Cateel	2.08	71.33	24.50	2.09	2.08	63.82	32.00	2.09
Baganga	4.36	88.66	6.98	-	4.36	88.66	6.99	-
Caraga	11.76	79.28	8.96	-	11.76	79.98	8.26	-
Manay	3.20	86.23	7.69	2.87	3.21	88.51	5.41	2.87
Tarragona	7.2	78.61	14.18	-	7.21	78.61	14.18	-
Mati	0.16	77.94	19.74	2.16	0.16	77.94	19.74	2.16
Lupon	10.89	63.19	20.04	5.88	10.70	65.07	18.52	5.70
Banaybanay	18.17	65.44	15.99	0.39	18.17	65.44	15.99	0.39
San Isidro	0.41	71.53	25.22	2.84	0.43	78.61	18.12	2.83
Governor Generoso	-	61.00	36.44	2.56	-	66.73	31.35	1.92

Table 10. Summary of the number of barangays with high risk.

Municipality	Number of Barangays			
	Current Scenario	Short-Term	Medium - Term	Long-Term
Boston	1	1	1	0

Cateel	2	2	2	2
Baganga	2	0	0	0
Caraga	1	0	0	0
Manay	2	2	2	2
Mati	3	4	4	5
Lupon	3	5	5	5
Banaybanay	1	1	1	1
San Isidro	1	1	1	1
Gov. Generoso	3	3	4	4
Total	19	19	20	20

5. Discussion and Limitation

5.1. Temperature and rainfall projections

This study investigated the temperature and rainfall projections to assess the impacts of climate change on flood risks in Davao Oriental. Area-averaged temperature and rainfall projections for the future were utilized from the thirty-nine CMIP5 GCMs of the IPCC. The future temperatures from the CMIP5 predictions depict that Davao Oriental would experience approximately 1°C and 3°C increases under the RCP4.5 and RCP8.5 scenarios, respectively. However, the thirty-nine area-averaged rainfall projections slightly increase in the coming years, which might be partially due to the coarse horizontal resolutions of GCMs and incomplete parameterizations of microphysics in GCMs. Among the thirty-nine GCM models available from CMIP5, the GFDL-ESM2M model showed a good agreement in terms of increasing trends to the observed rainfall dataset at local stations. Thus, in this study, the GFDL-ESM2M model rainfall data were used for the rainfall criteria in the projection of the flood hazard and flood risk assessments.

The results of the rainfall from the GFDL-ESM2M model exhibit that it will increase to 36% on average in the two scenarios (RCP4.5 and RCP8.5), in comparison with the current average rainfall in the next century. The increase in temperature and rainfall will significantly influence the floods in the future. As a result, the flood risk will be more intensive regarding its occurrences and scale and could be more extreme in the future.

5.2. Weighted overlay analysis

The crucial part of the MCDA is the weighted overlay. The weighted overlay combines all criteria to make the hazard, vulnerability, and risk maps that standardize the values from all criteria. Each criterion has its absolute value, such as the rainfall dataset in millimeters and the slope in degrees. A reclassification will classify the absolute values of the *VL*, *L*, *M*, *H*, and *VH* into 1, 2, 3, 4, and 5, respectively, in all criteria. This approach will result in a percentage area distribution of every criterion. Thus, the results will give importance to the percentage area distribution according to classification rather than the classification of the absolute value. Hence, the changes in rainfall from the current into the short term, medium term, and long term will not be shown in this analysis.

Another vital part of the weighted overlay analysis is the standardization of the grid resolution across all criteria. All criteria were changed into a raster dataset with a grid resolution of 30×30 meters. In the flood risk map, the vulnerability map was transformed into a raster dataset. The rasterization of the population density will change the population density according to the area of the barangay into the population density according to the grid resolution. This process turns the interpretation of the risk from barangay level into the raster level, where the risk is according to a 30×30 meter grid resolution. Additionally, most of the barangays in Davao Oriental are in rural areas that have a low population density. The rasterization process will significantly increase the low population number regarding the grid resolution. Additionally, in the projected scenarios (2035, 2065, and 2105) of the population density, some barangays will decrease their population in the future. These events will give high shares of the area distribution in the *low* category of population density in the future. Thus, the overlaying hazard map and vulnerability map to assess flood risk will illustrate that Davao Oriental belongs to the *L* to *M* flood risk classification because the flood risk map is generated by a weighted overlay of the hazard and vulnerability maps with equal weights. However, for the preparedness of the worst-case scenario in the disaster management and mitigation plan, giving a higher weighting value for the vulnerability map to assess flood risk is highly recommended.

5.3. Multi-criteria decision analysis (MCDA)

Integrating multiple data sources in the multi-criteria analysis presents a real advantage, and the results show that the AHP, WR, and RW approaches allowed a better understanding of all the criteria's contributions in the flood assessment because a weight was given to each criterion. However, data from different sources with different

resolutions were factors of bias during the processing and analysis. On the other hand, the addition of weights reduced the bias and uncertainty in the result.

The *CR* is the crucial element generating the hazard index (*HI*) for the MCDA using the AHP method. However, the AHP method shows some limitations due to the subjectivity in choosing the value of the criterion weighting from the arbitrary judgements of experts (Cabrera and Lee, 2018b; Danumah et al., 2016). According to Saaty (1980), this subjectivity problem was reduced by the *CR* test. The *CR* threshold must be less than 0.10 or 10% to make a coherent judgement. The lower the *CR*, the better, and if *CR* is zero (0), it means the hazard index is perfect. Unfortunately, the range of the *CR* between 0 and 9.9% is a rough estimation. The *HI* is coherent if the *CR* is 9.9% or the *CR* is 0%, but the weights of the criteria vary in every *CR* generation. Cabrera and Lee (2018b, 2018a) presented the sensitivity of *HI* to varying *CR* values based on experiments in which the change in *CR* did not significantly affect the result of the flood hazard map. The overall average change according to the classification is 0.02%, and the changes are acceptable. The lowest criteria ratio is more appropriate to use, according to Saaty (1980), so that the lower *CR* makes the judgement more coherent. Therefore, the *CR* with 0.02 is used for to obtain the flood risk in this study.

6. Things to be done further

To further enhance the result of this study, the author recommended the following:

1. Immediate installation of the weather measurement instruments in at least one station per municipality will give us precise weather forecasting especially during extreme events like drought, heavy rainfalls, storms, and typhoon.
2. Since the national government has no specific flood-risk mitigation plan, the municipal government in coordination with the office of the disaster risk reduction and management council (DRRMC) can design a flood-risk education program in every barangay. The flood-risk education program is an education campaign on how to act before, during, and after the event of flooding.
3. Adding more factors such as socio-economic variables (gender, income, educational attainment, housing) into the vulnerability map and applying the MCDA methods can provide higher resolution in future vulnerability assessments. Additionally, the results may improve by adding land use/land cover (LULC) through image analysis methods that use high-resolution images (Landsat 8+).
4. This study cannot solve the depth of the flooding. Thus, the hydrological modelling in 2D or 3D can be a complement to address this limitation. It is proven that hydrological modelling is an effective way to simulate flooding.
5. To eliminate the subjectivity of the analysis, continue to apply the MaxEnt modelling and increase the sample of the historical events of flooding. It is recommended to generate random points as stated in the paper of Samanta et al. (2018) and survey to the location of the random points to determine the flood and non-flood points. Also, in the survey, additional data can be included such as damage cost of flooding, and socio-economic criteria.
6. To further increase the quality of the paper, applying another machine learning models like artificial neural network, decision tree, Bayesian network, maximum entropy, random forest, logistic regression, support vector machine, etc., and compare the accuracy of the results is highly recommended.

References

- Alfieri, L., Bisselink, B., Dottori, F., Naumann, G., de Roo, A., Salamon, P., Wyser, K., Feyen, L., 2017. Global projections of river flood risk in a warmer world. *Earth's Futur.* <https://doi.org/10.1002/2016EF000485>
- Apollonio, C., Balacco, G., Novelli, A., Tarantino, E., Piccinni, A., 2016. Land Use Change Impact on Flooding Areas: The Case Study of Cervaro Basin (Italy). *Sustainability* 8, 996. <https://doi.org/10.3390/su8100996>
- Baldassarre, G. Di, Castellarin, A., Montanari, A., Brath, A., 2009. Probability-weighted hazard maps for comparing different flood risk management strategies: a case study, in: *Natural Hazards*. pp. 479–496. <https://doi.org/10.1007/s11069-009-9355-6>
- Bapalu, G., 2006. GIS in flood hazard mapping: a case study of Kosi river basin, India, in: *Natural Hazard Management*. pp. 1–6. <https://doi.org/10.13140/RG.2.1.1492.2720>
- Bui, D.T., Pradhan, B., Nampak, H., Bui, Q.-T., Tran, Q.-A., Nguyen, Q.-P., 2016. Hybrid artificial intelligence approach based on neural fuzzy inference model and metaheuristic optimization for flood susceptibility modeling in a high-frequency tropical cyclone area using GIS. *J. Hydrol.* 540, 317–330. <https://doi.org/10.1016/j.jhydrol.2016.06.027>
- Cabrera, J.S., Lee, H.S., 2018a. Impacts of Climate Change on Flood-Prone Areas in Davao Oriental, Philippines. *Water* 10, 893. <https://doi.org/10.3390/W10070893>
- Cabrera, J.S., Lee, H.S., 2018b. Flood-prone Area Assessment using GIS-based Multi-Criteria Analysis: A Case Study in Davao Oriental, Philippines. *J. Hydro-environment Res.* In-review.
- Chatterjee, S., Krishna, A.P., Sharma, A.P., 2014. Geospatial assessment of soil erosion vulnerability at watershed level in some sections of the Upper Subarnarekha river basin, Jharkhand, India. *Environ. Earth Sci.* 71, 357–374.

- <https://doi.org/10.1007/s12665-013-2439-3>
- Danumah, J.H., Odai, S.N., Saley, B.M., Szarzynski, J., Thiel, M., Kwaku, A., Kouame, F.K., Akpa, L.Y., 2016. Flood risk assessment and mapping in Abidjan district using multi-criteria analysis (AHP) model and geoinformation techniques, (cote d'ivoire). *Geoenvironmental Disasters* 3, 12. <https://doi.org/10.1186/s40677-016-0044-y>
- Ebaid, H.M., Farag, H.A., Falaky, A.A. El, 2016. Using GIS and remote sensing approaches to delineate potential areas for runoff management applications in Egypt. *Int. J. Environ. Sci. Eng.* 7, 85–93.
- Elkhrachy, I., 2015. Flash flood hazard mapping using satellite images and GIS tools: A case study of Najran City, Kingdom of Saudi Arabia (KSA). *Egypt. J. Remote Sens. Sp. Sci.* 18, 261–278. <https://doi.org/10.1016/j.ejrs.2015.06.007>
- Fhong, N.Z., Akbari, A., 2016. ASTER-GDEM derived flood inundation map using 1D-2D flood modeller pro in Kuantan river basin. pp. 1–2.
- Forkuo, E.K., 2011. Flood hazard mapping using aster image data with GIS. *Int. J. Geomatics Geosci.* 1, 932–950. <https://doi.org/ISSN 0976-4380>
- Frey, H., Paul, F., 2012. On the suitability of the SRTM DEM and ASTER GDEM for the compilation of: Topographic parameters in glacier inventories. *Int. J. Appl. Earth Obs. Geoinf.* 18, 480–490. <https://doi.org/10.1016/j.jag.2011.09.020>
- Ghangrekar, M.M., Kharagpur, I., 2015. Population Forecasting [WWW Document]. URL http://scetcivil.weebly.com/uploads/5/3/9/5/5395830/m5_15-population_forecasting.pdf (accessed 12.4.17).
- Gigović, L., Pamučar, D., Bajić, Z., Drobnjak, S., 2017. Application of GIS-interval rough AHP methodology for flood hazard mapping in Urban areas. *Water (Switzerland)* 9, 1–26. <https://doi.org/10.3390/w9060360>
- Gurenko, E., Lester, R., 2004. Rapid onset natural disasters: the role of financing in effective risk management. *World Bank Policy Res. Pap.* 3278, 34. <https://doi.org/https://doi.org/10.1596/1813-9450-3278>
- Hirabayashi, Y., Kanae, S., Emori, S., Oki, T., Kimoto, M., 2008. Global projections of changing risks of floods and droughts in a changing climate. *Hydrol. Sci. J.* 53, 754–772. <https://doi.org/10.1623/hysj.53.4.754>
- Hirabayashi, Y., Mahendran, R., Koirala, S., Konoshima, L., Yamazaki, D., Watanabe, S., Kim, H., Kanae, S., 2013. Global flood risk under climate change. *Nat. Clim. Chang.* 3, 816–821. <https://doi.org/10.1038/nclimate1911>
- Hong, H., Panahi, M., Shirzadi, A., Ma, T., Liu, J., Zhu, A.-X., Chen, W., Kougiyas, I., Kazakis, N., 2018a. Flood susceptibility assessment in Hengfeng area coupling adaptive neuro-fuzzy inference system with genetic algorithm and differential evolution. *Sci. Total Environ.* 621, 1124–1141. <https://doi.org/10.1016/j.scitotenv.2017.10.114>
- Hong, H., Tsangaratos, P., Ilija, I., Liu, J., Zhu, A.-X., Chen, W., 2018b. Application of fuzzy weight of evidence and data mining techniques in construction of flood susceptibility map of Poyang County, China. *Sci. Total Environ.* 625, 575–588. <https://doi.org/10.1016/j.scitotenv.2017.12.256>
- Huong, D.T.V., Nagasawa, R., 2014. Potential flood hazard assessment by integration of ALOS PALSAR and ASTER GDEM: a case study for the Hoa Chau commune, Hoa Vang district, in central Vietnam. *J. Appl. Remote Sens.* 8. <https://doi.org/DOI: 10.1117/1.JRS.8.083626>
- IPCC, 2012. Special report of the intergovernmental panel on climate change managing the risks of extreme events and disasters to advance climate change.
- Kazakis, N., Kougiyas, I., Patsialis, T., 2015. Assessment of flood hazard areas at a regional scale using an index-based approach and analytical hierarchy process: Application in Rhodope–Evros region, Greece. *Sci. Total Environ.* 538, 555–563. <https://doi.org/10.1016/j.scitotenv.2015.08.055>
- Kia, M.B., Pirasteh, S., Pradhan, B., Mahmud, A.R., Sulaiman, W.N.A., Moradi, A., 2012. An artificial neural network model for flood simulation using GIS: Johor River Basin, Malaysia. *Environ. Earth Sci.* 67, 251–264. <https://doi.org/10.1007/s12665-011-1504-z>
- Lagmay, A., Racoma, B., Aracan, K., Alconis-Ayco, J., Saddi, I., 2017. Disseminating near-real-time hazards information and flood maps in the Philippines through Web-GIS. *J. Environ. Sci.* <https://doi.org/10.1016/j.jes.2017.03.014>
- Manfreda, S., Samela, C., Gioia, A., Consoli, G.G., Iacobellis, V., Giuzio, L., Cantisani, A., Sole, A., 2015. Flood-prone areas assessment using linear binary classifiers based on flood maps obtained from 1D and 2D hydraulic models. *Nat. Hazards* 79, 735–754. <https://doi.org/10.1007/s11069-015-1869-5>
- Milly, P.C.D., Wetherald, R.T., Dunne, K.A., Delworth, T.L., 2002. Increasing risk of great floods in a changing climate. *Nature* 415, 514–517. <https://doi.org/10.1038/415514a>
- Mohammed, I.N., Bombliès, A., Wemple, B.C., 2015. The use of CMIP5 data to simulate climate change impacts on flow regime within the Lake Champlain Basin. *J. Hydrol. Reg. Stud.* 3, 160–186. <https://doi.org/10.1016/j.ejrh.2015.01.002>
- National Disaster Risk Reduction and Management Council, 2012a. Update re Effects of Typhoon “PABLO” (Bopha). <https://doi.org/10.1017/CBO9781107415324.004>
- National Disaster Risk Reduction and Management Council, 2012b. Final report on the effects and emergency management re Tropical Storm Washi.
- Nyarko, B.K., 2002. Application of a rational model in GIS for flood risk Assessment in Accra, Ghana. *J. Spat. Hydrol.* 2, 1–14.
- Othman, N., Jafri, M.Z.M., Lim, H.S., Tan, K.C., 2011. Using ASTER GDEM and SRTM digital elevation models to generate contour lines over rugged terrain of Makkah, in: 2011 IEEE International Conference on Space Science and Communication: “Towards Exploring the Equatorial Phenomena”, IconSpace 2011 - Proceedings. pp. 11–13.

- <https://doi.org/10.1109/IConSpace.2011.6015842>
- Otieno, J., 2004. Scenario study for flood hazard assessment in the lower Bicol floodplain Philippine using a 2D flood model : based on the 1988 flood event caused by typhoon Yonning : a case study for the flood hazard assessment, WP 4500 SLARIM and ITC research project.
- Papaioannou, G., Vasiliades, L., Loukas, A., 2015. Multi-criteria analysis framework for potential flood prone areas mapping. *Water Resour. Manag.* 29, 399–418. <https://doi.org/10.1007/s11269-014-0817-6>
- Pellicani, R., Parisi, A., Iemmolo, G., Apollonio, C., 2018. Economic Risk Evaluation in Urban Flooding and Instability-Prone Areas: The Case Study of San Giovanni Rotondo (Southern Italy). *Geosciences* 8, 112. <https://doi.org/10.3390/geosciences8040112>
- Philippine Statistics Authority, 2015. Philippine Statistics Authority. Davao Oriental.
- Reddy, G.P.O., Kumar, N., Sahu, N., Singh, S.K., 2017. Evaluation of automatic drainage extraction thresholds using ASTER GDEM and Cartosat-1 DEM: A case study from basaltic terrain of Central India. *Egypt. J. Remote Sens. Sp. Sci.* <https://doi.org/10.1016/j.ejrs.2017.04.001>
- Republic of the Philippines, 2010. REPUBLIC ACT 101211: An act strengthening the Philippine disaster risk reduction and management system, providing for the national disaster risk reduction and management framework and institutionalizing the national disaster risk reduction and management 1–34.
- Saaty, T.L., 1980. *The Analytic Hierarchy Process: Planning, Priority settingm Resource allocation.* Mc Graw-Hill, New York.
- Samanta, S., Kumar, D., Babita, P., 2018. Flood susceptibility analysis through remote sensing , GIS and frequency ratio model. *Appl. Water Sci.* 8, 1–14. <https://doi.org/10.1007/s13201-018-0710-1>
- Tachikawa, 2011. ASTER Global Digital Elevation Model Version 2 – Summary of Validation Results. *Japan Sp. Syst.* 7. <https://doi.org/https://doi.org/10.1017/CBO9781107415324.004>
- Tehrany, M.S., Pradhan, B., Jebur, M.N., 2013. Spatial prediction of flood susceptible areas using rule based decision tree (DT) and a novel ensemble bivariate and multivariate statistical models in GIS. *J. Hydrol.* 504, 69–79. <https://doi.org/10.1016/j.jhydrol.2013.09.034>
- Tehrany, M.S., Shabani, F., Jebur, M.N., Hong, H., Chen, W., Xie, X., 2017. GIS-based spatial prediction of flood prone areas using standalone frequency ratio, logistic regression, weight of evidence and their ensemble techniques. *Geomatics, Nat. Hazards Risk* 8, 1538–1561. <https://doi.org/10.1080/19475705.2017.1362038>
- The University Corporation for Atmospheric Research., 2010. Flash flood early warning system reference guide (p. 204).
- USDA-NRCS, 1986. *Urban Hydrology for Small Watersheds [WWW Document].* URL https://www.nrcs.usda.gov/Internet/FSE_DOCUMENTS/stelprdb1044171.pdf (accessed 6.30.18).
- Veleda, S., Martínez-Graña, A., Santos-Francés, F., Sánchez-SanRoman, J., Criado, M., 2017. Analysis of the Hazard, Vulnerability, and Exposure to the Risk of Flooding (Alba de Yeltes, Salamanca, Spain). *Appl. Sci.* 7, 157. <https://doi.org/10.3390/app7020157>
- Wang, Y., Li, Z., Tang, Z., Zeng, G., 2011. A GIS-based spatial multi-criteria approach for flood risk assessment in the Dongting Lake Region, Hunan, Central China. *Water Resour. Manag.* 25, 3465–3484. <https://doi.org/10.1007/s11269-011-9866-2>
- Wang, Z., Lai, C., Chen, X., Yang, B., Zhao, S., Bai, X., 2015. Flood hazard risk assessment model based on random forest. *J. Hydrol.* 527, 1130–1141. <https://doi.org/10.1016/j.jhydrol.2015.06.008>
- Wu, C.H., Huang, G.R., Yu, H.J., 2015. Prediction of extreme floods based on CMIP5 climate models: A case study in the Beijiang River basin, South China. *Hydrol. Earth Syst. Sci.* 19, 1385–1399. <https://doi.org/10.5194/hess-19-1385-2015>
- Yahaya, S., 2010. Multicriteria analysis for flood vulnerable areas in hadejia-jama'are river basin, Nigeria. *Eur. J. Sci. Res.* 42, 71–83.
- Yu, D., Xie, P., Dong, X., Hu, X., Liu, J., Li, Y., Peng, T., Ma, H., Wang, K., Xu, S., 2017. Improvement of the SWAT model for event-based flood forecasting on a sub-daily time scale. *Hydrol. Earth Syst. Sci.* <https://doi.org/10.5194/hess-2017-180>
- Zhang, K., Manning, T., Wu, S., Rohm, W., Silcock, D., Choy, S., 2015. Capturing the signature of severe weather events in Australia using GPS measurements. *IEEE J. Sel. Top. Appl. Earth Obs. Remote Sens.* 8, 1839–1847. <https://doi.org/10.1109/JSTARS.2015.2406313>

ArcSWAT Modeling: Study on Sustainable Management for Water and Energy Environment in Mindanao

Ismail Adal Guiamel¹

¹CHESS Lab, Graduate School of International Development and Cooperation, Hiroshima University.

iguamel@gmail.com

Abstract

The Philippines is naturally plenty of water resources and vast land for agriculture. Despite all these natural resources the country is facing several problems on optimal utilization of its potential resource. The water resource and energy management are very challenging. Thus, the electricity demand is increasing, and its shortage becomes one of the biggest problems in the country. The southern part of the country, the Mindanao region is rich in water resources and agriculture products. Hence, assessment of hydropower resources and site suitability analyses will be conducted in this region. Consequently, the authors of this study are currently conducting an ArcSWAT (Soil and Water Assessment Tool) modeling to assess and estimate the theoretical hydropower potential and determine the potentials sites. Thus, the authors applied the geospatial techniques and input datasets to simulate the model. This model will generate the discharge values of rivers and stream to be utilized in computing and analyzing the potential hydropower. The input datasets are combinations of the administrative boundaries, soil dataset, land use, Synthetic Aperture Radar - Digital Elevation Model (SAR-DEM) raster, and weather datasets from global observed data. Then, terrain analysis algorithm and discharge calculation from the water head and modeling values will be used to achieve the objective of this study. Thus, the results will be verified from the actual observed discharged of identified rivers of each watershed areas. From these values, the hydropower potential sites and classifications will be determined and presented in the mapping as an overall result. Therefore, the results of this study can be a reference to select a suitable area for setting up several classifications of hydropower plants in Mindanao Region. Furthermore, the modeling results can also be utilized as a basis for the future development of the water and energy in the region.

Keywords: Renewable Energy, Water resources, Soil and Water Assessment Tool (SWAT), Hydropower, and River Basin.

I. Introduction

The Philippines is situated in Southeast Asia in the western rim of the Pacific Ocean with 7,107 Islands, total land area 300,000 square sq.km, and coastline of around 36,289. Islands were group into three major part such as Luzon, Visayas and Mindanao with the land areas of 141,000 sq.km, 57,000 sq.km, and 102,000 sq.km respectively. It has 17 regions, 80 provinces, 138 cities, 1,496 municipalities and 42,025 barangays (*village-level administrative units*). Moreover, the Philippines has the total population of 100,981,437 with the density 330/sq.km [1]. In addition, there are four climate types as defined in a spatial distribution of monthly rainfall [2].

Philippines power sector is divided into three major components such as power transmission, power generation, and power distribution were the National Power and Private operators are coexisting for the operations and management of energy resources and allocations. Hence, in Luzon and Visayas regions the electricity transactions were observed through the wholesale power trading market while in Mindanao region is by means of a bilateral basis of a contract between power generation companies and electricity distribution companies or consumers [3]. As shown in figure 2, there are 38 electric companies working in Mindanao region.

According to the Department of Energy (DOE) the country's economy has been driven by the huge contribution of the power sectors. In fact, the total energy installed capacity of the country was increased from the level of 16,226.9 MW in 2011 to 17,025.0 megawatts (MW) in 2012, its around 6 percent. Regardless of the development efforts of the power sector to improve the services and sustaining the electricity supplies to the consumers but still, there is a big challenge on increasing electricity demand with an annual average rate of 4.3 percent. Accordingly, to meet the domestic power demand, the power sector needs to add at least 13,166.7 MW.

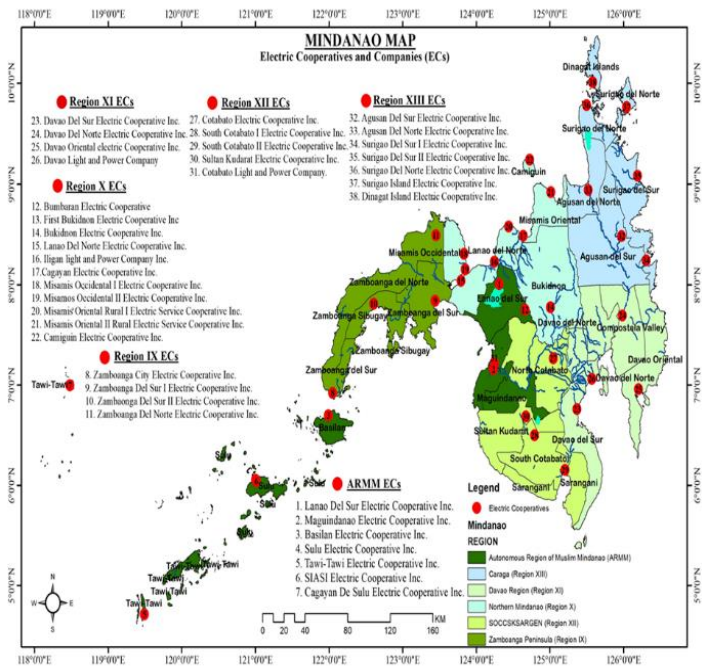


Figure 1: Location of the Philippines in the world, the regional administrative boundaries of Mindanao

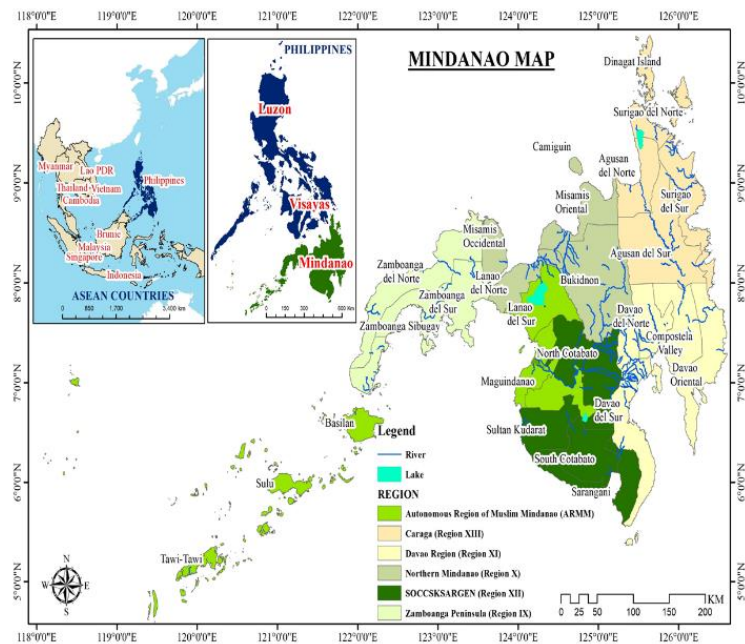


Figure 2: Map of Electricity Cooperation and Companies per regional administration in Mindanao.

According to the Philippine Energy Plan of 2012 – 2030, the 1,766.7 MW needed capacity will be provided by committed power sector while remaining 11,400MW will be available for the private sector investment. However, in islands grid's, the increasing demand is remained a major challenge and not enough assurance to add more capacity. On the other hand, Mindanao has 2,087 MW total rated power output in all generated facilities in 2017 as shown in figure 3, and total dependable power output is 2,685 MW. Generation capacity consists of coal 1070 MW, oil based 828 MW, geothermal 108, hydropower 1,061 MW, solar 59 MW and biomass 36 MW. From these power capacity, 1,264 MW is the total renewable energy generated. Furthermore, the transmission system in Mindanao is consist of “On-grid” and “Off-grid” and operated at the voltage class of 138kV and 69kV as shown in figure 4[4]. Moreover, the hydropower resources contributed a 9.9 percent share to the total indigenous energy supply of the country and production played a significant increase of 21.7 percent, from 1.9 MTOE in 2010 to 2.4 MTOE due to the additional 91.0 MW capacity in 2011 [5].

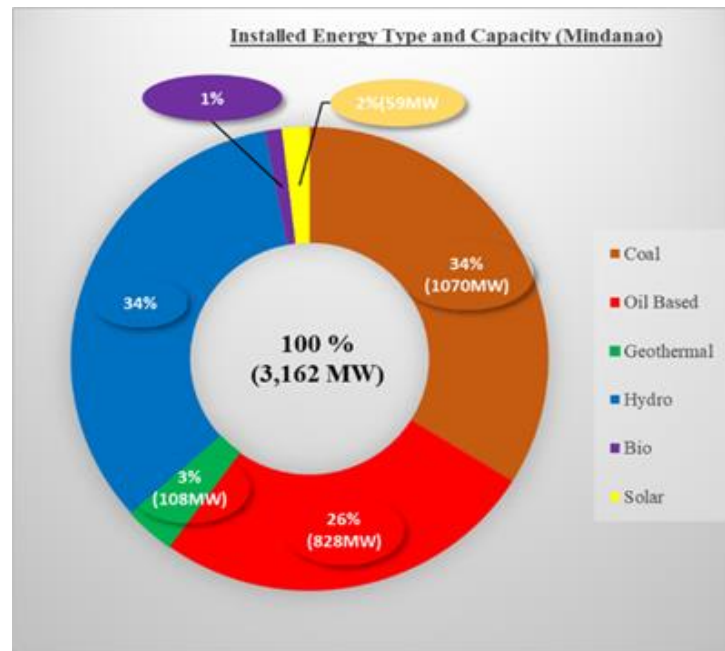


Figure 3: Mindanao Installed power capacity in 2017. Presented also the energy types.

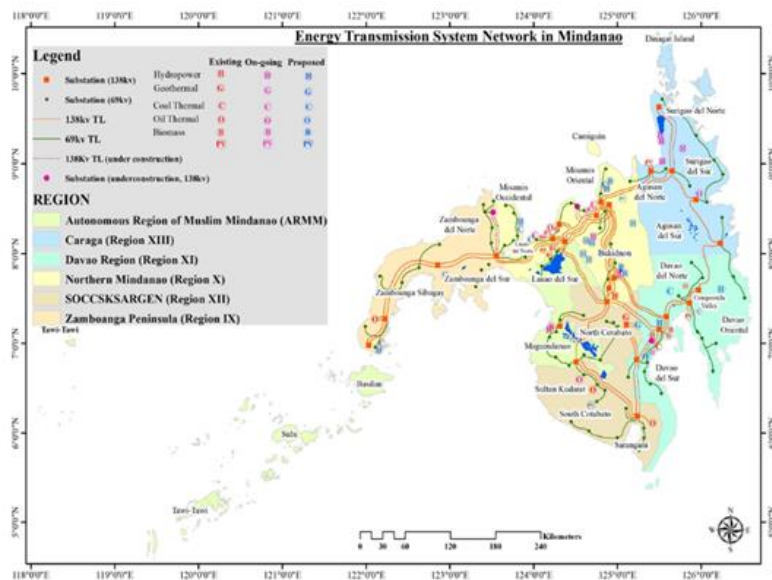


Figure 4: Map of the transmission plan, existing, On-going construction, and Proposed development. It also shows the location of Hydropower and other energy sources.

This study basically focusses in the Mindanao major basins as shown in figure 5. The Mindanao River Basin (MRB) is the second largest river basin in the Philippines with a total area of 21,503 square kilometers as shown in figure 6. It covers seven provinces such as Maguindanao, Lanao del Sur, Bukidnon, Sultan Kudarat, Davao del Norte, North Cotabato, and South Cotabato. MRB has 72 municipalities and 1,731 barangays [6]. Moreover, one of the large hydropower, Pulangi 4 Hydro-power Dam is in Bukidnon and one source of geothermal power located between north Cotabato and Davao del Norte shown in figure 4. In deeper, there are numbers of major rivers within the basin as shown in figure 5, other major rivers are including the Ala River, traversing the Ala Valley in the South; the Ambal-Simuay River System originating from Lanao del Sur, and; the Tamontaka Rivers in the Lower side of Mindanao river basin near between Cotabato city and Datu Odin Sinsuat Municipalities. In addition, this study also considered the environmental management policies under the Presidential Decree number 1152: Environment Code (1977) Under the title II-III, Water quality management and Land Use Management respectively (PD 1152). Also in 2008, the Renewable Energy Act had been passed to strengthen the government policy to accelerate the exploration of resources for Renewable Energy [8].

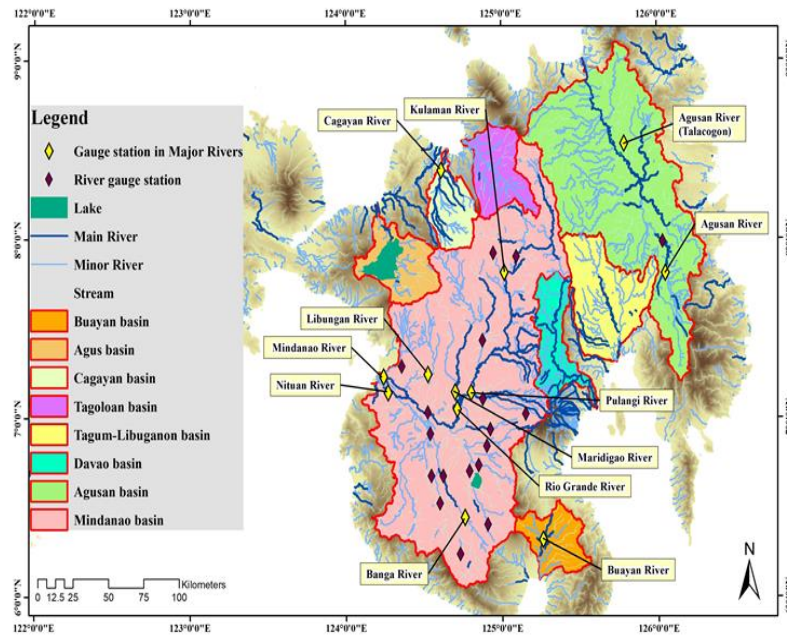


Figure 5: Map of the major river basin in Mindanao region; Includes also the major rivers in the basin, a location of the

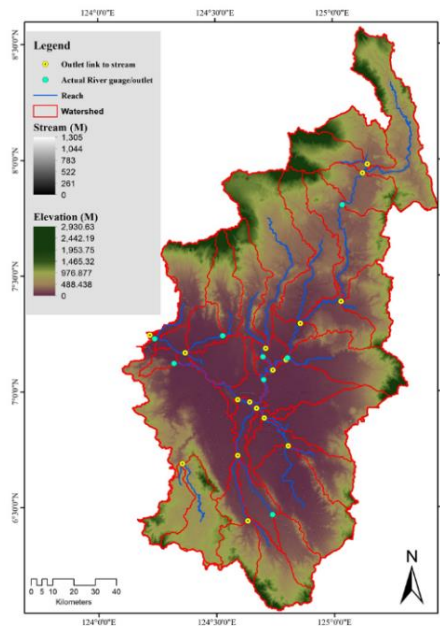


Figure 6: Map of Mindanao basin, watershed generated from arcSWAT

II. Objectives

1. To improve the electricity in Mindanao.
 - Calculated/Estimated theoretical Potential hydropower (Renewable energy source in the Region/Province/Municipalities)
2. To optimize the use of hydroelectricity (power facilities) in Mindanao.
 - Distinguish the power capacity from pico, micro, and large-scale hydropower.
3. To assess the environmental effects of the water resource development for energy.
 - Observe sustainable development works in water environment management through hydropower.

III. Data and Methodology

III.1 Data

The data used in this research was obtained and downloaded from various government agencies and global climate datasets, the following are the list of datasets.

- Digital Elevation Model (DEM) derived from a RADARSAT Synthetic Aperture (SAR), 10m resolution was obtained from Department of Science and Technology and University of the Philippines Project (<https://lipad.dream.upd.edu.ph>)
- Administrative Boundaries of the Philippines, shapefile downloaded from PhilGis (<http://philgis.org/>)
- Land use data set of will be requested from the National Mapping and Resource Information Authority (NAMRIA, <http://www.namria.gov.ph/>).
- The soil dataset was obtained from the Bureau of Soil and Water Management (<http://www.bswm.da.gov.ph/>)
- Climate data sets such as temperature, precipitation, and wind were downloaded from the global data of the National Climate Data Center (<https://www.ncdc.noaa.gov/>)
- Climate data sets such as solar radiation and humidity were obtained from Global Weather Data for SWAT (<https://globalweather.tamu.edu/>)
- The observed dataset for river discharge was obtained in the Department of Public Works and Highways, Bureau of Standards (<http://www.dpwh.gov.ph/dpwh/org-chart/bureau/BRS>)
- The dataset for development plans was retrieved from various development agencies of the Philippine government.

The datasets should be processed in ArcGIS prior to the actual ArcSWAT modeling, it must be projected with the Universal Transverse Mercator (UTM) Zone 51 projection and World Geodetic System (WGS) 1984 as the horizontal datum. Refer the figure III-1 for the flowchart of ArcSWAT modeling.

III.2 Methodology

The flowchart shows the modeling procedures and steps, by using the inputs and following the processing flow, by then you can able to generate the outputs for the computation and algorithm processes.

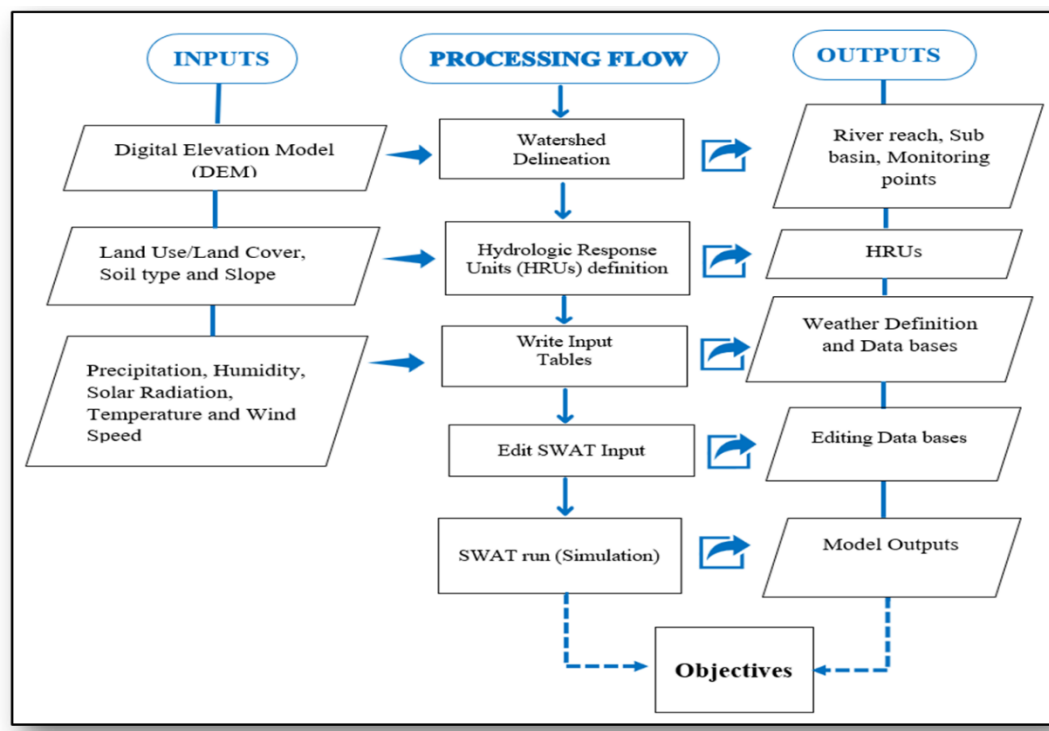


Figure 7: Flowchart of the ArcSWAT modeling.

The basic procedure for modeling is clearly explained in the ArcSWAT manual (Winchell, Srinivasan, Di Luzio, & Arnold, 2013). For this, there is a new release practical guide that explained interfaces and changes of the version of ArcSWAT [9]. Moreover, the SWAT modeling can be possibly done thru the open source GIS users, QGIS is a similar function to ArcGIS [10]. Thus, QSWAT modeling is useful also for similar research methods. Subsequently, SWAT modeling is useful for long-term, and continuous simulation watershed model and designed to predict the impact of water management [11]. It was developed to simulate the water cycle, and corresponding fluxes of energy to assess the impact of management practices [12]. Furthermore, “The SWAT model has proven to be an effective tool for assessing water resource and nonpoint-source pollution problems for a wide range of scales and

environmental conditions across the globe” [13]. And capable also to calibrate sensitive parameters of streamflow [14].

Power Calculation

Basically, the power generated will be calculated by the given formula $P = \rho \times g \times Q \times h \times \eta$; where P is the theoretical power in watts, ρ is the density of water (1000kg/m³), g is acceleration due to gravity (9.81 m/s²), Q is the volumetric flow rate in cubic meters per second, h is the head in meters, and η is the generator efficiency. To compute for theoretical hydropower potential for each river segments the above formula will be used and the head algorithm was spatially combined in ArcGIS to the discharged values from the hydrologic model [15].

Discharge calculation is very important to compare the results from the actual river discharged. Thus, this discharge formulas below will be used to calculate the theoretical river discharge

Velocity area method for streamflow or discharges [16].

$$Q = V_1 A_1 + V_2 A_2 + V_3 A_3 + \dots V_n A_n \text{ ----- Equation 1.}$$

where: Q is discharged in m³/s, V is velocity in m/s and A is the area of streamflow.

Using discharge Myer formula to estimate flows of watersheds surface values if the rivers are similar [17].

$$\left(\frac{S_1}{S_2}\right)^\alpha = \frac{Q_1}{Q_2} \text{ ----- Equation 2.}$$

where: Q₁ is a discharge of watershed 1, Q₂ is the discharge of watershed 2, S is surface/length of the rivers/streams and α is regional coefficient that usually varies between 0.5 and 1 depending on the watershed's shape and the slopes.

In addition, to improve the quality of the modeling method and result then it is necessary to observe the efficient computation and includes the regression calculations to describe the relationship between the input and output parameters [18].

IV. Results

As of now, the modeling activities is not yet completed. Only initial modeling results in Buayan basin. It is just for familiarizing the several technical terms, process flow, commands, inputs, and possible outputs. The simulation results in Buayan Basin serves as a guide to avoid more errors in running the next models. Moreover, the initial results of simulation would give an overall idea of the methodology and inputs that need to be collected in the nearest weather station, river gauges and other environmental datasets such chemical being utilized in agriculture cultivations.

V. Discussion and Limitation

This study is limited to the assessment of the hydropower potentials, its sites, and theoretical power generation. The study may not able to cover the detail land use proposals for the development of the water resource in the region. This study is also not considering the water potable resource analysis since the data to be collected might be limited in a developing county and the challenge for understanding some chemical term to be used for inputs and calibration of the model output. Although SWAT can also model the water potability, and its potential sites [19].

VI. Things to be done further

The following are the things to be done in order to achieve the objective of this study:

- Data Collection especially the weather datasets/climate data from meteorological stations in the study areas.
- Data collection for actual river discharge of the simulated river basins, for verification modeling results.
- Running the models in arcSWAT with complete and correct datasets
- Improve learning on arcSWAT modeling through tutorial and reading related literature.
- Improve understanding of the terms, technical term for the inputs, and results
- If possible to join a workshop with the arcSWAT community to further improve the technical know-how and interpretations of the results.
- Review of basic principles of hydraulic engineering and electrical engineering terms.
- Reading more high-quality journal related to the research tools and modeling.

References

- [1] Philippine Statistic Authority, “The Philippines in figures: 2015,” 2015.
- [2] J. Cabrera and H. S. Lee, “Impacts of Climate Change on Flood-Prone Areas in Davao Oriental, Philippines,” *Water* 2018, Vol. 10, Page 893, vol. 10, no. 7, p. 893, 2018.

- [3] Bangsamoro Development Agency, “Comprehensive Capacity Development Project for the Bangsamoro Development Plan for the Bangsamoro Final Report Sector Report 3 : Environment Comprehensive Capacity Development Project for the Bangsamoro Development Plan for the Bangsamoro Final Report Sec,” 2016.
- [4] National Grid Cooperation of the Philippines, “Transmission Development Plan 2014 -2015.”
- [5] L. G. Ayson *et al.*, “Philippine Energy Plan 2012-2030,” *Dep. Energy* , vol. 223, no. 410, 2010.
- [6] U. of the P. College of Forestry and Natural Resources, “Development of Climate-Responsive Integrated River Basin Master Plan,” 2015.
- [7] O. of the President, *PRESIDENTIAL DECREE No. 1152*, no. 1152. pp. 1–13.
- [8] House of Representatives, *RA-9513-renewable_energy_act.pdf* .
- [9] M. Winchell, R. Srinivasan, M. Di Luzio, and J. Arnold, “SWAT Help,” *Texas Agrilife Res. United States Dep. Agric. Agric. Reseach Serv.*, 2013.
- [10] Y. T. Dile, P. Daggupati, C. George, R. Srinivasan, and J. Arnold, “Introducing a new open source GIS user interface for the SWAT model,” *Environ. Model. Softw.*, vol. 85, pp. 129–138, 2016.
- [11] M. Jha, “Hydrologic simulations of the Maquoketa river watershed Using SWAT,” no. June, 2009.
- [12] H. Rathjens and N. Oppelt, “SWAT model calibration of a grid-based setup,” *Adv. Geosci.*, vol. 32, pp. 55–61, 2012.
- [13] P. P. W. Gassman, M. M. R. Reyes, C. C. H. Green, and J. J. G. Arnold, “The Soil and Water Assessment Tool : historical development, applications, and future research directions,” *Trans. ASAE*, vol. 50, no. 4, pp. 1211–1250, 2007.
- [14] L. A. Anaba, N. Banadda, N. Kiggundu, J. Wanyama, B. Engel, and D. Moriasi, “Application of SWAT to Assess the Effects of Land Use Change in the Murchison Bay Catchment in Uganda,” *Comput. Water, Energy, Environ. Eng.*, vol. 06, no. 01, pp. 24–40, 2017.
- [15] J. Jason, S. Garcia, A. Marie, L. De La Serna, M. A. Fesalbon, and J. R. Silapan, “Estimation of Hydropower Potential Energy Using Gis and Swat Hydrologic Model in Western Visayas,” pp. 1–8.
- [16] W. Lowrie, *Fundamentals of Geophysics, second edition*. 2007.
- [17] C. Marie, “Hydrological study for a mini-hydropower plant in the Pyrenees,” *Dep. Civ. Environ. Eng.*, vol. Master’s t, no. 9, p. 33, 2007.
- [18] H. Q. Bang, N. H. Quan, and V. Le Phu, “Impacts of Climate Change on Catchment Flows and Assessing Its Impacts on Hydropower in Vietnam ’ s Central Highland Region,” *Glob. Perspect. Geogr.*, vol. 1, no. 1, pp. 1–8, 2013.
- [19] G. Cuceloglu, K. C. Abbaspour, and I. Ozturk, “Assessing the water-resources potential of Istanbul by using a soil and water assessment tool (SWAT) hydrological model,” *Water (Switzerland)*, vol. 9, no. 10, 2017.

Method for calculating snow losses on solar photovoltaic system production in Yamagata prefecture, Japan

Nicholas Denegre^{1,2}

¹ University of Graz

² CHESS Lab, Graduate School for International Development and Cooperation, Hiroshima University

Abstract (Summary of Research Proposal)

This research proposed presents a project in Yamagata prefecture (north of Japan) to develop a large solar PV plant in one of the snowiest regions in Japan. The target of this project is to develop a model which predicts the snow losses on energy production at different tilts and analyze what is the best orientation to avoid losses during snow season. Test's facility has been built adjacent to the project's land, the layout of the facility is made of 4 different racking systems at 20, 25, 30 and variable tilt one. The study is based on the calculation of the theoretical modules' electrical data, short-circuit current and maximum power, and the comparison against the short-circuit current measured from the modules during the experiment.

1. Introduction

In Yamagata prefecture (north of Japan), there is a project to develop a large solar PV plant. The Project's location is one of the snowiest locations in Japan and requires that the amount of expected production be calculated. The model will be largely dependent on different tilts, orientations, equipment types and other design components. The target of this procedure is calculating the snow losses on PV modules in a project in Kitamura, Yamagata, Japan.

2. Objectives

- The final goal is studying the snow losses at different tilts and analyze what is the best orientation to avoid losses during snow season.
- There is a concern from the Local authority (Oishida Municipality first) that the PV module Racking system will not be able to withstand the snow load existent in Kitamura Location. This project will assist in finding a solution which will give the Japanese authorities the right comfort.

3. Data and methodology

3.1 Data

Test's facility has been built adjacent to the project's land, the layout of the facility is made of 4 different racking systems at 20, 25, 30 and variable tilt one.

To run this experiment the following equipment has been installed:

- 3 cameras (Geovision ADR1300) on site that can remotely be accessed one by one, the images from the cameras are not recorded neither stored.
- 4 snow sensors (Sommer USH-8) to measure the snow cover,

- 1u installed on the ground
- 1u installed on the table at 25°
- 1u installed on the table at 30°
- 1u installed on the table at 20°
- 16 PT1000 adhesive sensors (Meteocontrol) to measure the modules' back sheet temperature.
- 1 PT1000 sensors (Brand and model ??) to measure the ambient temperature.
- 5 pyranometers (KippZonen SMP11):
 - 1 pyranometer to measure the Global Horizontal Irradiation
 - 1 pyranometer tilted at 25° to measure the Global Tilted Irradiation.
 - 1 pyranometer tilted at racking variable tilt to measure the Global Tilted Irradiation for the variable racking.
 - 1 pyranometer tilted at 30° to measure the Global Tilted Irradiation.
 - 1 pyranometer tilted at 20° to measure the Global Tilted Irradiation.

1) Experiment 1: Racking at 25° Table 1

Racking at 25°, 5x4 modules in landscape, only the last 5 modules on the right column of the racking will be tested.

2) Experiment 2: Variable tilt racking Table 2

Racking set up at 60°, 3 rows of 6 modules landscape, only the last 3 modules on the right column of the racking will be tested.

3) Experiment 3: Racking at 30° Table 3

Racking at 30°, 4x2 modules in landscape, only the last 4 modules on the right column of the racking will be tested.

4) Experiment 4: Racking at 20° Table 4

Racking at 20°, 4x2 modules in landscape, only the last 4 modules on the right column of the racking will be tested.

Data will be stored every 5 min as a minimum by the monitoring system. Data analysis will be performed by using the formulas described in the methodology section of this document every 5 and a summary will be done afterwards.

3.2 Methodology

The study is based on the calculation of the theoretical modules' electrical data, short-circuit current and maximum power, and the comparison against the short-circuit current measured from the modules during the experiment.

Isc and Power is mainly dependent on the irradiation and temperature of the cell, so it is possible to approx. the Isc calculation by the following formula:

$$I_{SC} = I_{SC}(STC) \times \left[\frac{GTI}{1000} + \alpha(T_{cell} - 25) \right] \quad (1)$$

where,

I_{SC} = Short circuit current at experiment conditions, (A)

$I_{SC}(STC)$ = Short circuit current at Standard Conditions (1000W/m² and 25 Tcell), (A)

GTI= Global Tilted Irradiation, Irradiation at the module plane. (W/m²)

α = Temperature coefficient of Isc (%/°C)

Tcell= Cell temperature (°C)

$$P_{mpp} = P_{mpp}(STC) \times \frac{GTI}{1000} \times [1 + \gamma(T_{cell} - 25)] \quad (2)$$

where,

P_{mpp} = Power at maximum power point at experiment conditions, (W)

$P_{mpp}(STC)$ = Power at maximum power point at Standard Conditions (1000W/m² and 25°C cell temp), (W)

GTI= Global Tilted Irradiation, Irradiation at the module plane. (W/m²)

γ = Temperature coefficient of Power (%/°C)

Tcell= Cell temperature (°C)

The snow losses are calculated as follow:

$$\% \text{ Losses} = \left[1 - \frac{I_{SC}(\text{measured})}{I_{SC}} \right] \times 100 \quad (3)$$

$$\text{Power}_{Loss} = P_{mpp} \times \% \text{ Losses} \quad (4)$$

4. Results

The following table shows an example of analysis of the snow losses during 7 days in December for the variable tilt racking at 60 degrees.

Table 1. Analysis example of snow losses in December

Date	Sum of Snowfall (cm)	Sum of GTI (W/h)	Sum of % Snow Losses	Sum of Snow losses (W)	Sum of Power module clean (W)
21/12/2017	-9.00	3429.38	70.97	5076.83	14332.49
22/12/2017	-4.00	887.82	30.86	548.99	3891.93
23/12/2017	-12.00	948.08	44.89	693.52	4160.72
24/12/2017	-4.00	881.62	28.53	585.52	3885.96
25/12/2017	3.00	716.86	49.08	697.25	3194.23
26/12/2017	51.00	290.93	81.00	1274.15	1324.66
27/12/2017	12.00	758.22	34.44	573.80	3485.37
Grand Total	37.00	7912.90	339.76	9450.06	34275.38

5. Discussion and Limitation

Depending on the type and amount of snow (powder, crud, sleet) it is possible that snow sliding off the panels will

not occur. The reason is that a layer of ice (thickness variable from few mm up to 20 mm (observed on site) is formed on top of the Module which create a stable contact for all the snow that fall on top of it.



Figure 12. Image of from snow cameras of test facility.

6. Things to be done further

Some limitations include:

- Install a fix tilt table on slope land $>10^\circ$ and evaluate if the terrain slope would improve the sliding of the snow.
- Install Coating Liquid end of Feb, begin of March when snow accumulation will be reduced to test the effectiveness
- Install the relative humidity sensor to establish a correlation between the snow sliding – tilt – humidity (worth

References

Marion, B.; Schaefer, R.; Caine, H.; Sanchez, G. (2013). "Measured and modeled photovoltaic system energy losses from snow for Colorado and Wisconsin locations." *Solar Energy* 97; pp. 112-121.

Rob W. Andrews, Andrew Pollard, Joshua M. Pearce, The effects of snowfall on solar photovoltaic performance, *Solar Energy*, Volume 92, June 2013, Pages 84-97, ISSN 0038-092X, 10.1016/j.solener.2013.02.014.

Townsend, T.; Powers, L., "Photovoltaics and snow: An update from two winters of measurements in the SIERRA," *Photovoltaic Specialists Conference (PVSC), 2011 37th IEEE*, vol., no., pp.003231,003236, 19-24 June 2011

Semester research activity summary

Alex Bunodiere¹

¹CHESS Lab, Graduate School for International Development and Cooperation, Hiroshima University

Currently I am not exactly sure about what my research will be about, at the beginning of the semester I planned to study the feasibility of floating offshore wind turbines in Japan, however after attending a conference called GRE2018, I realized that if I wanted to do a project that would make a real difference, I had to look at renewable energy policy, as it's the policy that drives renewable energy development, not the technology. However, in this semester my focus has been more with my subjects than my masters and I haven't much in the way of literature reviews. I acknowledge that I need to focus a lot more on my research and especially doing more literature reviews.

I believe that I have made some progress during this semester as I did do some research regarding the REIPPP (renewable energy independent power producer program) based in South Africa and the FIT (Feed in tariff) in Japan, as I wanted to compare the differences between them. This led to the idea of developing a new set of renewable energy policies for Japan, based on the success of the REIPPP, which has successfully reduced the price of renewable in South Africa by more than 350% in just over 7 years, while the renewable energy market in Japan has stagnated as the FIT tariff has been reduced. The FIT model is not sustainable in its current state because it requires full financial support from the government whereas the REIPPP model promotes more and more investment as the market becomes larger and larger. This is the main reasoning for choosing this topic as I believe that this is a true problem and I would like to try to make suggestions to fix it.

The main difference between the REIPPP and the FIT is that the REIPPP is an auction-based system, whereas the FIT is a tariff-based system. FIT tariff systems used to be the most used option however recently a growing number of countries have started to shift to an auction-based system due to its ability to drive cost down, thus increasing the renewable energy penetration in the area. The REIPPP is more than just an auction-based system, however, as it was specially designed to meet the needs of both the consumers of their electricity (The national Electricity provider) while also contributing to a better way of life for the local communities around the proposed renewable energy site. In fact, the economics of different proposals in the REIPPP only accounted for 70% of the total score of each bid, with the remaining 30% specifically focus on the social aspects. A newly designed action based system for Japan would have to take into account all of the specific problems that face renewable energy providers in Japan and the unique social issues.

My plan for this holiday is to focus solely on literature reviews, especially literature that deals with auction and FIT and how they affect the success/failure of renewable energy projects. My hope is that after this literature review I will have a clearer picture that will help me focus my work within the coming semester.

An Investigational Approach to the 1993 Tsunami Run-up Model on the Built-in Monai Beach used in GERRIS

Shiraj Md Morshed Bin¹

¹ Graduate School for International Development and Cooperation, Hiroshima University, 1-5-1 Kagamiyama, Higashi-Hiroshima 739-8592, Hiroshima, Japan.

Abstract

A tsunami run-up model is important to simulate the tsunami to compare with actual results. To consider inundation, we need to go through the tsunami run-up and its behavior. A laboratory experiment can be a benchmark to validate tsunami models. In Japan, Central Research Institute for Electric Power Industry (CRIEPI) creates a 1/400 scale laboratory experiment of the Monai runup which is one of the unexpected phenomena of the 1993 tsunami. This test has been taken as an example in GERRIS to simulate the Monai runup. Models are very sensitive about data, so we should investigate our data before use.

1. Introduction

Small scale tsunami run-up is much easier to understand comparing with the real-time tsunami run-up models. Understanding tsunami run-up is very important especially when we need to use new technical approaches for better simulation. After a successful study of using Adaptive Mesh Refinement (AMR) method in the open source flow solver GERRIS by (Lee, 2015), we are more interested to use the AMR method in GERRIS in case of tsunami run-up in order to consider inundation in different built-in coastal zones of Japan. The 1991 tsunami of Okushiri can be a good example to investigate. The Central Research Institute for Electric Power Industry (CRIEPI) conducted an 1/400 scale laboratory experiment using a large-scale tank which is of 205 m long, 6 m deep, 3.4 m wide that has been used as a benchmark test to validate the Monai runup of the 1993 Okushiri Tsunami in (Popinet, 2011). In the same article S Popinet has used Adaptive Quadtree Spatial Discretization for the solution of Saint-Venant Equation which has been added as Adaptive Quadtree Saint-Venant Solver in GERRIS to model 2004 Indian Ocean tsunami. That's why GERRIS is potential to reproduce tsunami run-up models with an opportunity of using AMR method in our future study.

2. Objectives

Our main objective is to do *tsunami run-up and inundation modeling using AMR on Onagawa Bay*. To achieve this goal two types of study is required to be conducted. Firstly, Literature reviews for understanding and making tsunami run-up and inundation model. Secondly, practicing useful technologies like GERRIS, Basilisk etc. for making the simulation.

3. Data and methodology

3.1 Data

In the benchmark problem prepared by CRIEPI, the following types of data have been provided:

I. Numerical simulation area

5.448m X 3.402m

Minimum depth: -0.125m (land)

Maximum depth: 0.13535m

Grid size 0.014m

Bathymetry data: *Benchmark_Bathymetry.txt* [with 393x244=95,892 data]

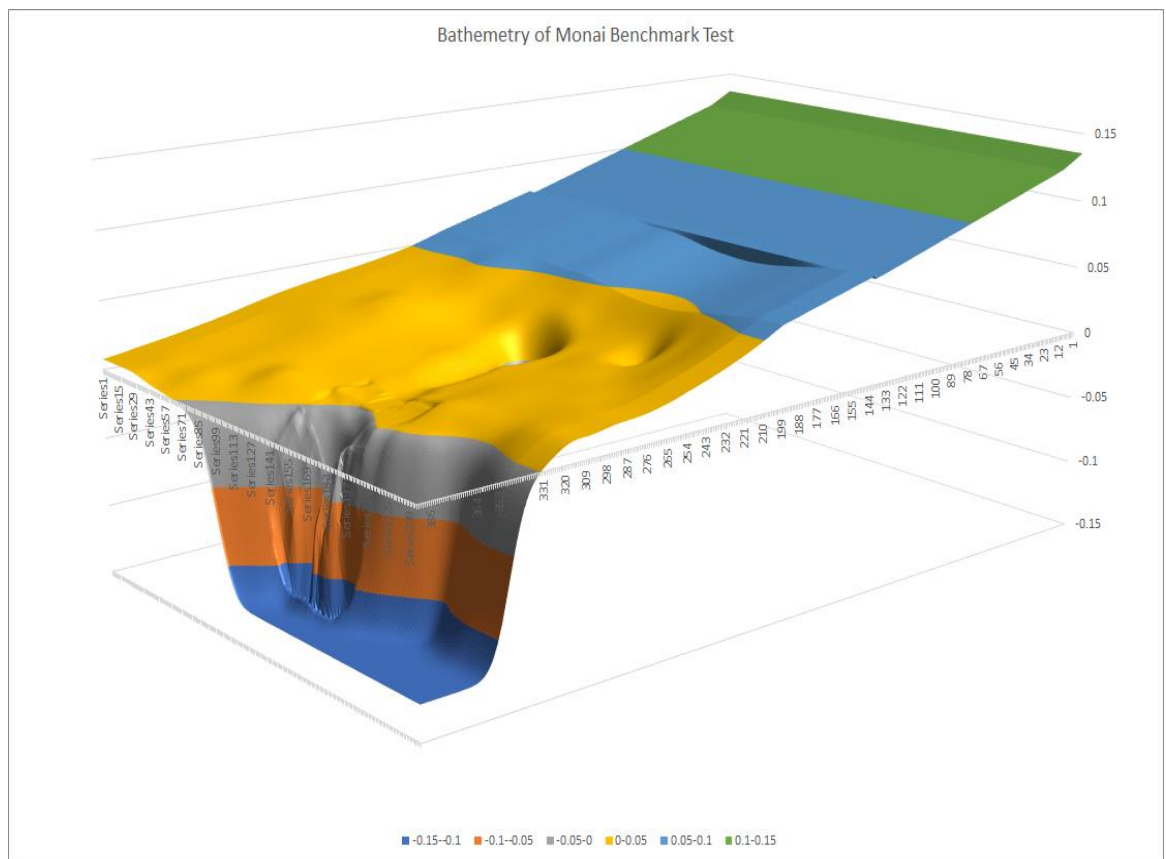


Fig 01: *Benchmark_Bathymetry.txt* has been converted into excel spreadsheet using MATLAB to obtain this figure showing the topography of the domain used in the simulation of GERRIS.

For the better understanding about the domain we use scatter plotting tool of MATLAB to see the difference.

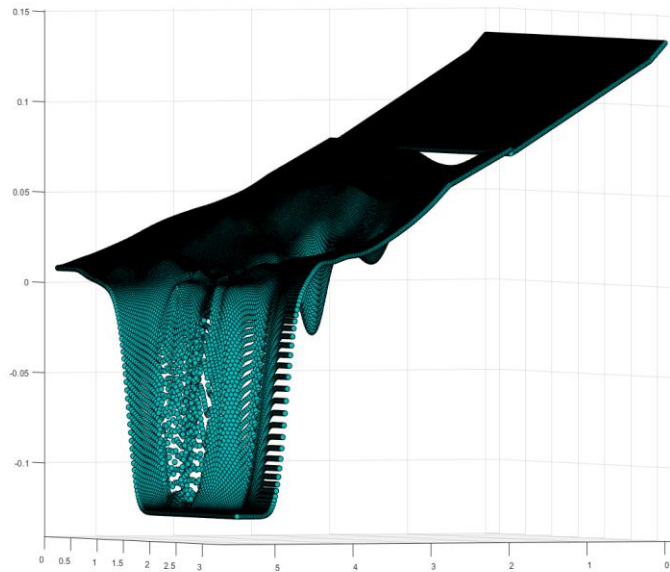


Fig 02: Using *scatter3* function of MATLAB the figure has been created that is more clear view of the inputted bathymetry data.

II. Boundary conditions

West: input wave

North: solid wall

East: solid wall

South: solid wall

III. Input wave data

Time domain: 0-22.5sec

Time step: 0.05sec

Input wave data: *input.txt*

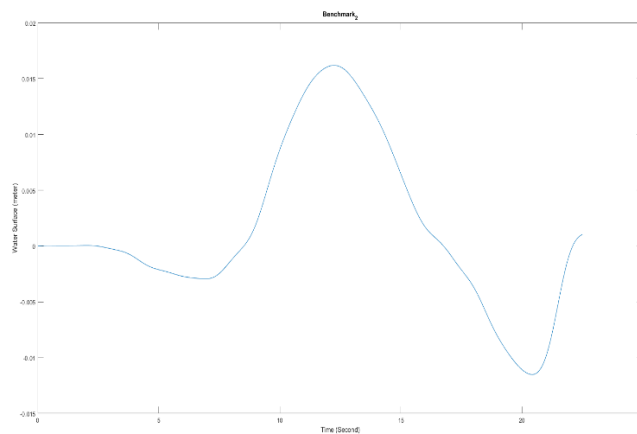
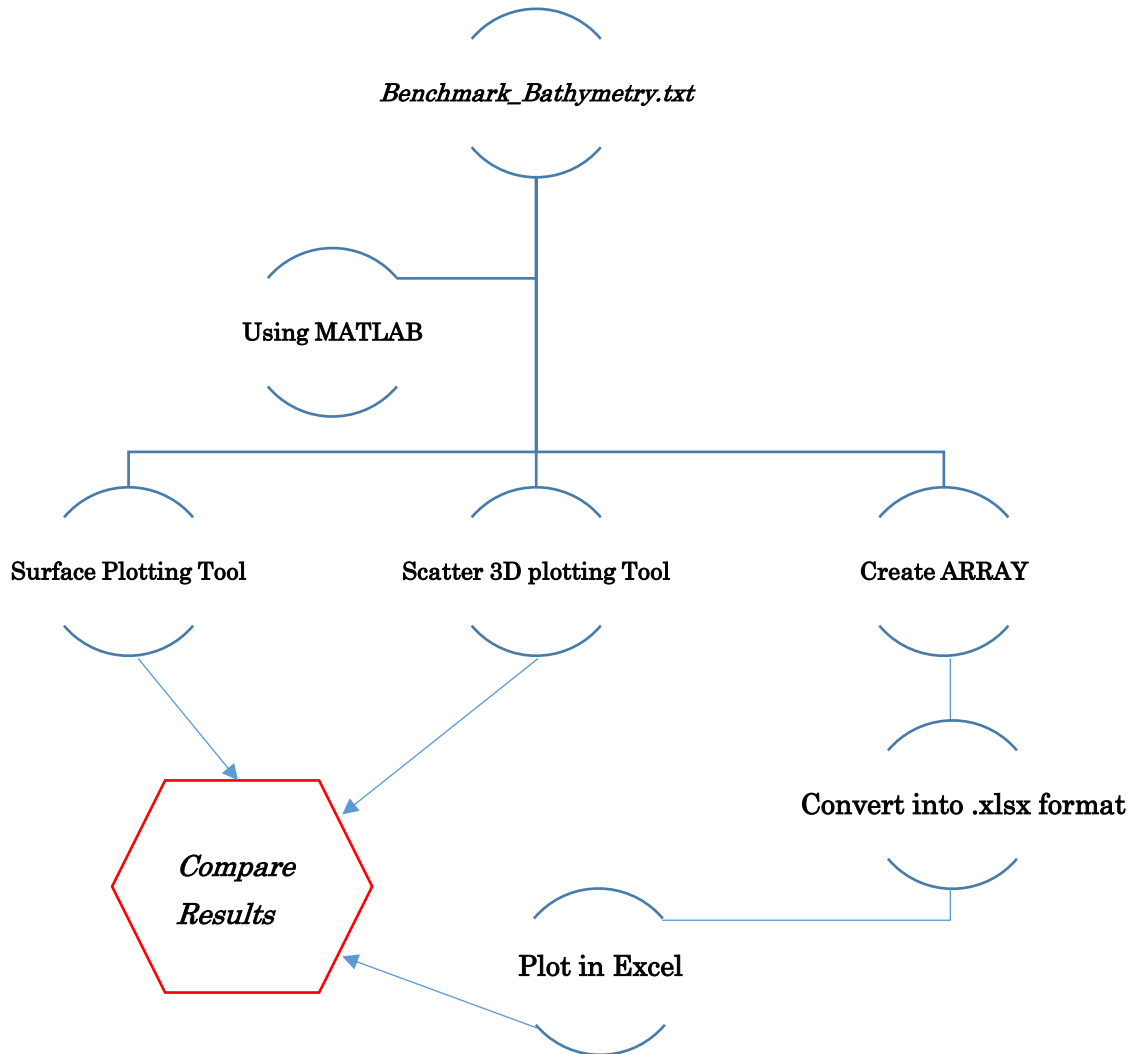


Fig 03: Inputted water surface (meters) against time (seconds) made by using simple line plot in MATLAB

3.2 Methodology

A sequence of actions has been taken by us to make topography of the inputted bathymetry data using MATLAB and Microsoft Excel. Our actions can be described in flowcharts:

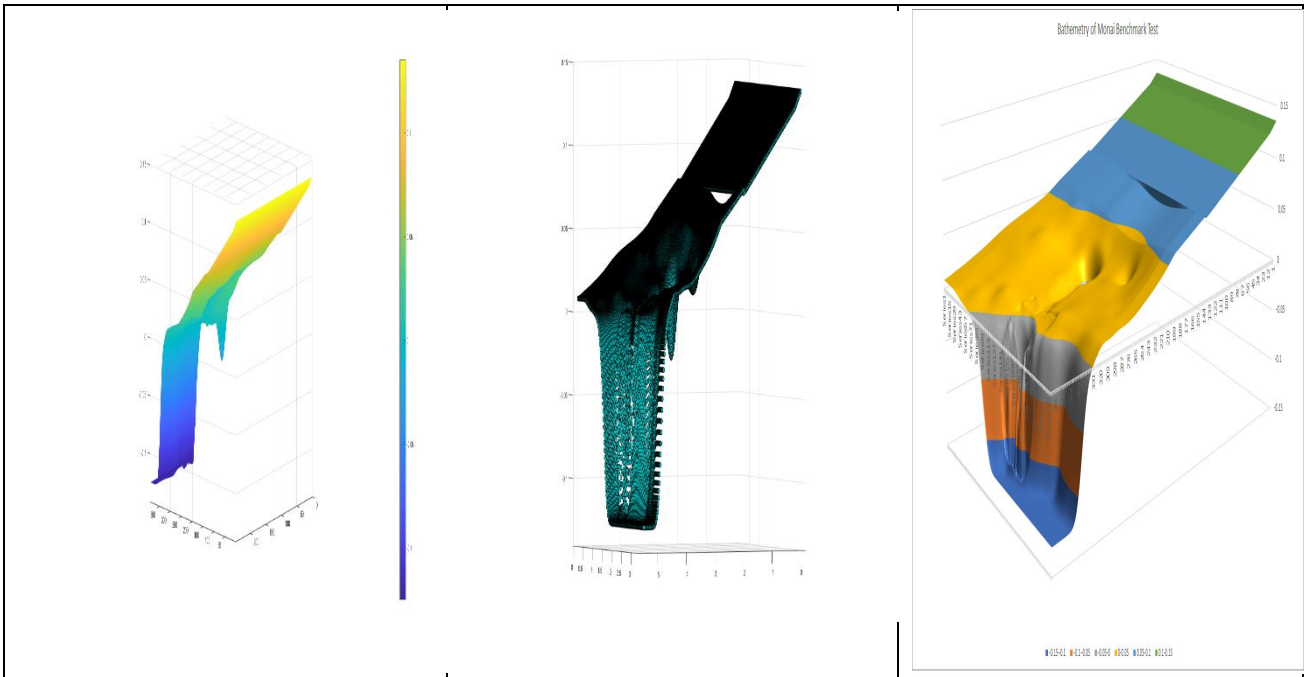


4. Results

The similar sloping trend with a certain jump of data on the above section of each result has been found (see table 01). Though Two different technology have been used, results are similar. It seems that to analysis our data we can mixed these two technologies too with many other available tools. We found that Fig 03 is similar with the picture CRIEPI has provided.

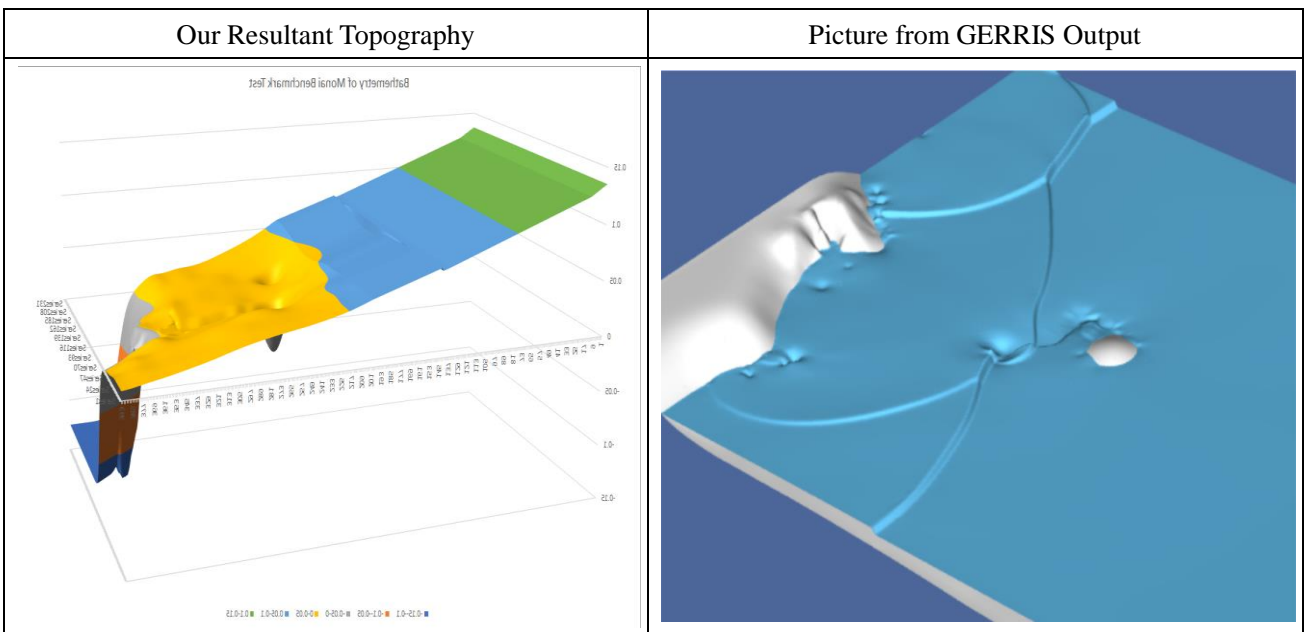
Table 01: Result Comparison

Surface Plotting Tool	Scatter 3D plotting Tool	Plot in Excel



5. Discussion and Limitation

The results of the simulation of GERRIS with our topography is looking little different considering top of the domain which is looking almost same in our resultant topography but has much difference in the same position of the picture taken from the GERRIS output. We found certain jump of data in the middle which is quite strange.



Another higher place can be easily found in the middle of the GERRIS output that is hard too find in our result.

6. Things to be done further

We should verify our inputted data using different kind of tools like MATLAB, R etc. since our domain is supposed to be built by us. We should use reasonable data to get best outputs.

References

- Lee, H. S. (2015). Impacts of tides on tsunami propagation due to potential Nankai Trough earthquakes in the Seto Inland Sea, Japan. *J. Geophys. Res. Oceans*, *120*, 6865–6883. doi:doi:10.1002/2015JC010995
- Popinet, S. (2011). Quadtree-adaptive tsunami modelling. *Ocean Dynamics*, *61*(9), 1261–1285.